Pallasitic Peridot

Vietnamese Ruby and Sapphire

CVD Synthetic Diamond and
Synthetic Amethyst Identification

Diamond Stamp Collection

JEWELS OF THE TRADE

EPHRAIM ZION of Dehres Limited handles more diamonds in a day than most people see in a lifetime. Here he discusses the power of reputation, global diamond investment and why a GIA report is vital to any business built on integrity.

What's something most people don't know about your job? It's the only business in the world conducted on trust. You sell 1 to 5 million dollars just on the telephone, without even a signature.

A diamond dealer's most valuable asset? Reputation. Yes, you need a sense of artistic value and a knack for design, but the most essential part is integrity. You can't survive without it.

What has doing business in Hong Kong taught you about the Asian market? It's one of the strongest in the world. Every day, there are new millionaires and new businesses. Asians are very investment-conscious. Diamonds are safer and more profitable than money in a bank.

All-time favorite purchase? Most recently, a 100+ ct. D FL. Incredible brilliance and scintillation. Such a beauty. People fell down when they saw it.

Did it arrive with a grading report? Ha, ha. GIA, of course. What responsible businessman, with a good reputation and name, would sell a diamond without a GIA report?

Why is a GIA evaluation so important to one's reputation? It's the most reliable, authentic, dependable gem institute in the world. People know that, especially in the Far East. Remember what I said about reputation? A GIA report is crucial.

Business words to the wise? Selling is an idea game. The more knowledge you have, the more confidence you feel.

SUBSCRIPTIONS

Copies of the current issue may be purchased for **$29.95** plus shipping. Online subscriptions are $74.95 for one year (4 issues). Combination print + online subscriptions are $139.95 in the U.S. and $160 elsewhere for one year. Canadian subscribers should add GST. Discounts are available for group subscriptions, renewals, GIA alumni, and current GIA students. For institutional rates, contact the Managing Editor. Subscriptions include *G&G's* monthly gemological e-newsletter, the *G&G eBrief*.

To purchase subscriptions and single issues (print or PDF), visit **store.gia.edu** or contact the Circulation Coordinator.

PDF versions of individual articles and sections from Spring 1981 forward can be purchased at **gia.metapress.com** for $12 each. Visit gia.edu/gandg for free online access to the 1934–2010 subject and author index and all 1934–1980 issues.

DATABASE COVERAGE

Gems & Gemology's five-year impact factor (for 2005–2009) is 1.737, according to the 2010 Thomson Reuters Journal Citation Reports (issued June 2011). *Gems & Gemology* is abstracted in Thomson Reuters products (*Current Contents: Physical, Chemical & Earth Sciences* and Science Citation Index—Expanded, including the Web of Knowledge) and other databases. For a complete list of sources abstracting *G&G*, go to gia.edu/gandg.

MANUSCRIPT SUBMISSIONS

Gems & Gemology welcomes the submission of articles on all aspects of the field. Please see the Guidelines for Authors at gia.edu/gandg or contact the Managing Editor. Letters on articles published in *Gems & Gemology* are also welcome.

COPYRIGHT AND REPRINT PERMISSIONS

ABOUT THE COVER

Pallasite is a stony iron meteorite that contains areas of gem olivine (peridot). In this issue, Dr. Andy H. Shen and coauthors demonstrate the separation of pallasitic from terrestrial peridot by LA-ICP-MS analysis. The pallasite slab is courtesy of Robert A. Haag (The MeteoriteMan, Tucson, Arizona). The 4.3-cm-tall peridot crystal from Myanmar is courtesy of William Larson (Palagems.com, Fallbrook, California). The 17.53 ct trillion and the 20.25 ct square antique cushion, both from Pakistan, were faceted and supplied by Stephen M. Avery (Colorado). The crystal and cut stones have been enlarged approximately 10% relative to the pallasite slab. Photo by Robert Weldon.

Color separations for *Gems & Gemology* are by Pacific Plus, Carlsbad, California.
Printing is by Allen Press, Lawrence, Kansas.

NEW BEGINNINGS

Thank you for the warm welcome that I've received as the new editor-in-chief of *Gems & Gemology*. I am privileged to now be a part of the gemological community and to join such a passionate industry—to be captivated not only by the beauty of the gem world, but also by its science.

Of course, the challenge for scientists today is the same as it was yesterday: to translate ongoing research into definitive answers. As you know, science doesn't always come up with absolutes; conclusions are mostly partial and incremental. It's like adding chapters to a never-ending book.

We all know that technology is always pushing the boundary of what is possible. Just look at its impact not only on gem treatments, but also on mining, stone cutting, gem identification, and so on. Gemologists now have to chase more subtle features in determining whether a gem is natural or synthetic.

In this digital age, we can brace ourselves or simply embrace the new wave of (inevitable) change. As the saying goes, change is constant. So the timeliness and the fashion in which we disseminate scientific results and information will be more important than ever to keep you abreast of these developments. As I follow in the footsteps of my esteemed predecessors, this will continue to be a part of *G&G*'s mission, particularly as new gem and jewelry markets open up and new challenges arise.

In this issue of *G&G*, we report on the geology and gemological characteristics of ruby and sapphire from Yen Bai Province, in northern Vietnam. There is an article by GIA researchers on the use of trace-element analysis to distinguish meteoritic peridot from terrestrial peridot, and a study of the origin and nature of luminescent regions in CVD-grown synthetic diamond, which distinguish them from natural material. We also feature an important collection of diamond-themed stamps, and an update on the separation of natural versus synthetic amethyst using infrared spectroscopy.

...the challenge for scientists today is the same as it was yesterday: to translate ongoing research into definitive answers.

I certainly look forward to working with all of you. We're not just in the industry—we're all a part of the industry as a whole.

I will close with Richard T. Liddicoat's words from the Spring 1981 issue of *G&G*: "It is the intention of the staff of *Gems & Gemology* to provide gemologists and gem enthusiasts everywhere with the latest developments and the most comprehensive coverage in the field." This still rings true today!

Cheers,

[signature]

Jan Iverson | Editor-in-Chief | jan.iverson@gia.edu

RUBY AND SAPPHIRE FROM THE TAN HUONG–TRUC LAU AREA, YEN BAI PROVINCE, NORTHERN VIETNAM

Nguyen Ngoc Khoi, Chakkaphan Sutthirat, Duong Anh Tuan,
Nguyen Van Nam, Nguyen Thi Minh Thuyet, and Nguy Tuyet Nhung

Primary and secondary deposits in the Tan Huong–Truc Lau area of northern Vietnam's Yen Bai Province have supplied rubies (especially star rubies) and some sapphires—mostly of cabochon quality—for more than a decade. The gems are typically translucent to semitransparent and pink to purplish or brownish red, with rare color zoning. The most distinctive features of this corundum after polishing include growth zoning and asterism. The samples contain relatively high amounts of Fe and variable Ti and Cr. The geologic origin and gemological properties of this corundum are distinct from that of the adjacent Khoan Thong–An Phu area.

For more than 20 years, Vietnam's Yen Bai Province, and the Luc Yen District in particular, have been widely known for producing high-quality rubies and sapphires. Subsequent deposits found elsewhere in Vietnam (Long et al., 2004) include Quy Chau–Quy Hop (Nghe An Province), Di Linh (Lam Dong), Dak Ton (Dak Nong), and Ma Lam and Da Ban (Binh Thuan). Still, Yen Bai remains the country's most important source of ruby and sapphire. Much of the production consists of cabochon-quality stones from the Tan Huong–Truc Lau area (e.g., figure 1), as described in this article.

Vietnamese geologists first discovered gem-quality corundum and spinel at Luc Yen in 1983 (Vinh, 1991). In early 1987, the Geological Survey of Vietnam found abundant gem material in alluvium in Luc Yen's Khoan Thong area. Mining activity soon thrived, with many companies operating in the

region (Voi, 1991). Other gem occurrences near Khoan Thong followed, such as Nuoc Ngap, Hin Om, Khau Nghien, Vang Sao, May Thuong, May Ha, An Phu, Phai Chap, Tan Lap, and Lam Dong. These

Figure 1. These star rubies (6.16–11.66 ct) are from the Tan Huong–Truc Lau area of northern Vietnam. Photo by Nuttapol Kitdee, GIA, Bangkok.
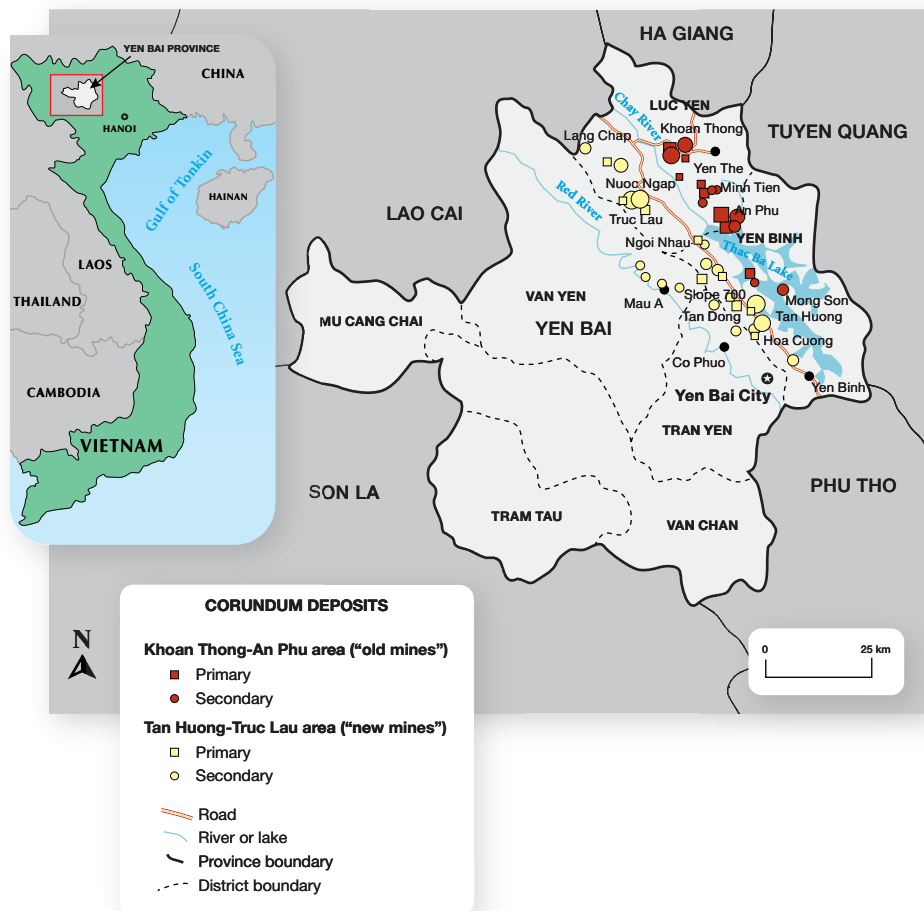
Figure 2. In northern Vietnam's Yen Bai Province, primary and secondary corundum deposits have been mined on both sides of the Chay River: the original Khoan Thong–An Phu mines on the east side and the newer Tan Huong–Truc Lau mines on the west. The size of each symbol is proportional to the importance of that mining area. Modified after Xuyen (2000) and Vinh (2005).

are located on the east side of the Chay River and have been referred to by locals as *bãi cũ*, or "old mines" (see figure 2).

In the mid-1990s, several *bãi mói* ("new mines") were established on the west side of the Chay River. These included Tan Huong, Truc Lau, kilometer 12 of National Road 70, Tan Dong, Hoa Cuong, Cam An, Bao Ai, Ngoi Nhau, and Ngoi Hop (again, see figure 2). Although corundum was discovered in this area in 1986 (Quan et al., 1998), there was no significant mining until local diggers arrived at Tan Huong

in 1994 (Thang, 1998). In 1996 the Vietnam National Gold and Gem Corporation (VIGEGO) conducted systematic assessments of Tan Huong (covering an area of 6 km²) and Truc Lau (20 km²). Official mining operations by VIGEGO started at Tan Huong the following year, yielding hundreds of kilograms of ruby and star ruby (Thang, 1998). Subsequently, other secondary (placer) and primary occurrences were discovered and mined (e.g., Quan et al., 2000). Currently, the only large-scale mechanized operation (figure 3) belongs to DOJI Gold & Gems Group

Figure 3. DOJI Gold & Gems Group currently conducts the only large-scale mining activities in the Tan Huong–Truc Lau area. These 2010 photos show open-pit mining at Truc Lau (left) and the associated processing plant (right). Photos by N. N. Khoi.

Figure 4. Local miners dig for spinel and corundum at the Lang Chap occurrence in June 2010. Photo by N. N. Khoi.

in the Truc Lau valley. Also some small-scale mining using primitive methods occurs sporadically, particularly during the dry season. Most recently, in February 2010, hundreds of local miners began operating illegally at Lang Chap, mostly for spinel (figure 4).

The mines on the west side of the Chay River typically yield cabochon-quality ruby and pink sapphire. However, some very large rubies weighing tens of kilograms have been found. Some of these contain transparent, gem-quality portions that can be faceted. A semitransparent to nearly transparent 290 ct fragment, detached from a 2.58 kg rough ruby discovered at Tan Huong in 1997, sold for US$290,000 at the Rangoon Gem Emporium (Myanmar) later that year (Nguyen Xuan An, pers. comm., 1998). Large star rubies and pink sapphires are also known. Two pieces (1.96 and 2.58 kg) now belong to the State Treasury's collection, while DOJI Gold & Gems Group has preserved an 18.8 kg specimen (figure 5).

For the sake of clarity, we will refer to the original deposits on the east side of the Chay River as *Khoan Thong–An Phu* and to the newer localities on the west side as *Tan Huong–Truc Lau* (the latter names are the main mining areas). The older deposits also have been referred to in the literature as simply *Luc Yen* (Kane et al., 1991; Long et al., 2004; Garnier et al., 2008), while the newer ones have been called *Yen Bai* (Long et al., 2004). This terminology is potentially confusing because Khoan Thong, An Phu, and Truc Lau administratively belong to the Luc Yen District, while Tan Huong is part of the Yen Binh District (again, see figure 2). Nevertheless, all of these

occurrences occupy the northeastern part of Yen Bai Province, ~250 km northwest of Hanoi. From the city of Yen Bai, it is easy to reach the new mining area by driving northwest along National Road 70, along which most of the occurrences are located.

This article describes the geology and gemological characteristics of gem corundum from Tan Huong–Truc Lau and compares it to the material from the well-known Luc Yen deposits.

GEOLOGY AND OCCURRENCE

The Khoan Thong–An Phu and Tan Huong–Truc Lau mining regions lie about 15 km from one another, but their geologic settings are clearly different. Most primary and secondary corundum occurrences in the Tan Huong–Truc Lau area are located within the Dãy Núi Con Voi mountain range, which stretches from

Figure 5. The 18.8 kg Great Star Ruby, one of many large gems mined at Tan Huong–Truc Lau, belongs to DOJI Gold & Gems Group. The stone measures approximately 32 × 24 × 17 cm and has been partly tumbled and polished to reveal its asterism. Photo by N. N. Khoi.
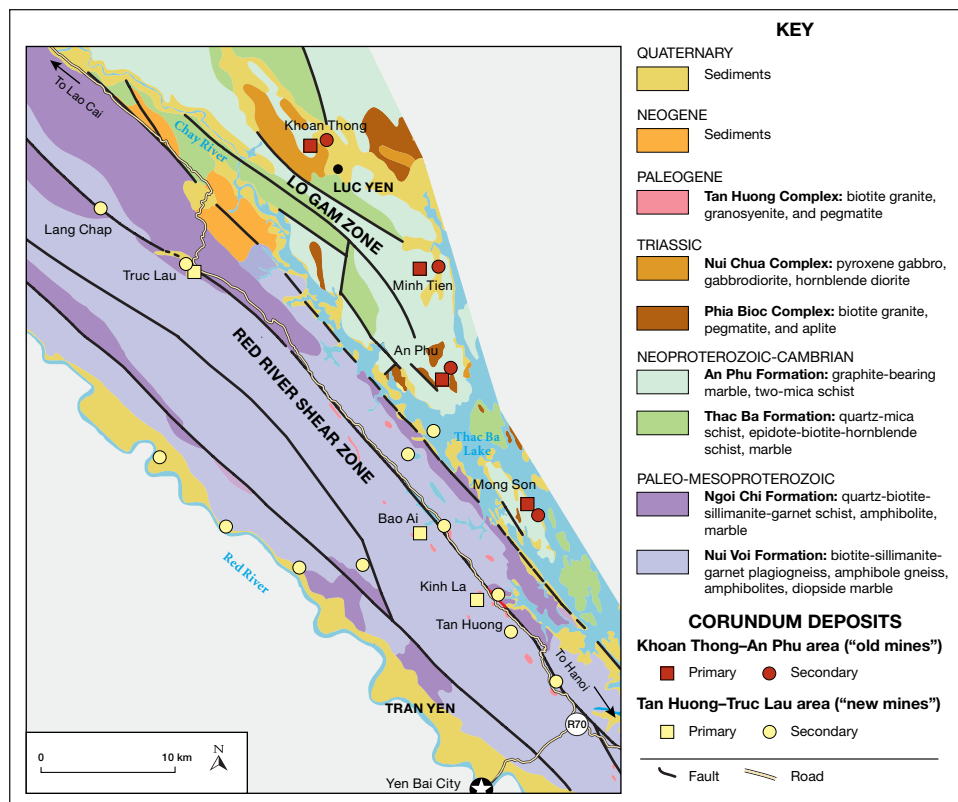
Figure 6. This simplified
geologic map shows the
locations and rock for-
mations of the corundum
occurrences at Khoan
Thong–An Phu and Tan
Huong–Truc Lau.
Modified after Vinh
(2005) and Xuyen (2000).
Smaller deposits are not
shown here.

Lao Cai Province southeast to Yen Bai Province. The
mountains are bounded by lateral strike-slip faults
(figure 6) forming a major Cenozoic geologic disconti-
nuity in Southeast Asia known as the Ailao

NEED TO KNOW

• Northern Vietnam's Yen Bai Province has pro-
  duced ruby and sapphire from adjacent geologi-
  cally distinct areas referred to as "Luc Yen" and
  "Yen Bai."

• The latter area pertains to deposits (both primary
  and secondary) located on the west side of the
  Chay River in the Tan Huong–Truc Lau area.

• Since the mid-1990s, these deposits have pro-
  duced mainly cabochon-quality rubies (especial-
  ly star rubies) and some sapphires.

• Although large pieces are known, the corundum
  is typically semitransparent to translucent, and
  most ranges from pink to purplish or brownish red.

Shan–Red River Shear Zone (Trinh et al., 1998, 1999;
Leloup et al., 2001).

Rocks in the Tan Huong–Truc Lau area mainly
consist of plagiogneiss and other gneisses intercalat-

ed with lenses of amphibolite and marble; they are
grouped as the Nui Voi Formation (Long et al., 2004;
Nam, 2007; Garnier et al., 2008; again, see figure 6).
These rocks underlie the Ngoi Chi Formation,
which comprises schist, amphibolite, and marble.
Both formations appear to have been intruded by
granite, syenite, and pegmatite of the Tan Huong
magmatic complex, which is 22–25 million years old
(Nam and Huyen, 2010).

Primary corundum deposits in the Tan
Huong–Truc Lau area can be classified into three
main types:

1. Gray, grayish white to bluish gray, and yellow-
   ish gray corundum embedded in gneisses, such
   as the Co Man outcrop in Truc Lau valley, and
   the Khe Nhan and Kinh La occurrences in the
   Tan Huong area (Nam, 2007; Thuyet, 2008).
   The corundum usually consists of large (1–3
   cm, with some over 10 cm) well-formed crys-
   tals of very low or non-gem quality (Nam, 2007;
   Thuyet, 2008; figure 7, left).

2. Dark red to pinkish red rubies of low-to-medi-
   um gem quality. These are usually also large
   and come from weathered pegmatoid feldspath-
   ic rocks (e.g., the occurrences at kilometers 12,

Figure 7. The left sample of corundum-bearing gneiss, from Co Man, contains mainly feldspar, biotite, sillimanite, and sapphire crystals up to 3 cm long. The feldspathic rock from the Slope 700 outcrop (right) typically consists of K-feldspar, biotite, and ruby. Photos by N. V. Nam.

15, and 23 along National Road 70, and also Slope 700).

3. Rubies in large marble lenses intercalated within gneiss, mica schist, and amphibolites (e.g., the Tan Huong drill core, and DOJI's Truc Lau mine). This type of ruby appears to have higher gem quality, but its distribution is limited.

These occurrences, mostly related to gneisses and schists of metasedimentary origin, are much different from the corundum deposits of Khoan Thong–An Phu, which are mainly hosted by marble formations.

The corundum-bearing host rocks in the Tan Huong–Truc Lau area appear to have originated from the metamorphism of fine-grained sediments of variable composition (Katz, 1972; Simandl and Paradis, 1999). For example, gneisses from the Co Man and Kinh La outcrops have a wide compositional range, from 50–90% feldspar, up to 40% biotite, and up to 20% sillimanite. In addition, ruby-bearing feldspathic rocks (e.g., the Slope 700 outcrop) typically consist of K-feldspar and biotite (or vermiculite; figure 7, right).

The primary host rocks are usually deeply weathered, forming numerous eluvial deposits.

The secondary (eluvial and alluvial) corundum deposits usually contain dark red ruby, pink sapphire, and red and brown spinel, as well as some garnet, trapiche-like bluish gray sapphire, sillimanite, and quartz. Of these mining areas, Truc Lau and Tan Huong are the most important. Truc Lau occupies a large valley, about 5 km long, that contains eluvial and alluvial sediments. The eluvium consists of three layers: topsoil (averaging 1 m thick); a gem-bearing layer (0.8–1 m thick) containing corundum and spinel that is composed of pebbles, gravel, and sand; and a deeply weathered gneiss layer (3 m thick) that typically contains ruby and sapphire. Compared to the eluvium, the alluvial deposits at Truc Lau are thicker (~10 m). Ruby, sapphire, and spinel are found within a gravel paleoplacer (1.2–5.0 m thick) that lies on bedrock, and is buried below 0.5–3.5 m of Quaternary sediments and 0.5–1.5 m of topsoil (figure 8). In 2002, 1–2 kg per month of pink sapphire and star ruby were produced from this paleoplacer.

At Tan Huong, the main gem occurrences are

Figure 8. Alluvial layers in the Tan Huong–Truc Lau area consist of soil, sandy and pebbly clays, and gravels containing gem corundum.

Cross-section of alluvial layers

Layer 1
(0.5-1.5 m): Soil

Layer 2
(0.5-3.5 m): Sandy and pebbly clay with small-sized corundum and spinel

Layer 3
(1.2-5.0 m): Pebbly and sandy gravel with gem-quality corundum and spinel

Layer 4
Bedrock (gneiss)
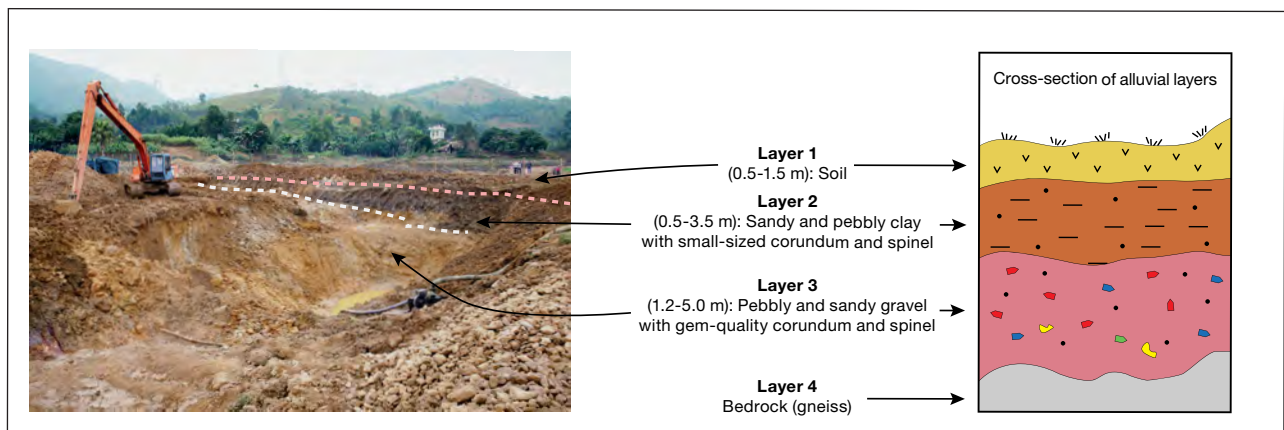
arranged in a northwesterly direction, bounded by two small lakes. The alluvial deposits consist of a topsoil layer (~0.5 m thick); a sand horizon with areas of humus (~0.5–1 m thick); and a ruby-, sapphire-, and spinel-bearing layer above the bedrock that contains mixed sand, pebbles, and boulders (~1.2–2.5 m thick). All of the alluvial deposits in the Tan Huong–Truc Lau area are quite similar to those shown in figure 8.

PRODUCTION AND DISTRIBUTION

Current production of gem material from Tan Huong–Truc Lau is about 10 kg per month. This includes approximately 20–30% ruby and some sapphire, and 70–80% spinel. Only 10–15% of the stones are of gem quality; the rest are suitable for carving material or as specimens. Most of the gems are cut and sold locally. DOJI Gold & Gems Group is the major exporter of faceted Vietnamese gemstones to the world market, either directly or through the international gem fairs in Bangkok, Hong Kong, Tokyo, and Kobe. The main markets for high-quality corundum are Japan, North America, and Hong Kong. Large, medium-quality stones are sold in the Middle East, Taiwan, and Southeast Asia, while low-quality commercial products go to India and China.

Heat treatments, including lead-glass filling, have been applied to these materials, but most appear to be unsuccessful. After heat treatment, white stripes often appear along fractures.

MATERIALS AND METHODS

A total of 57 gem samples from Tan Huong–Truc Lau, including 15 rough and 42 cut stones (12 faceted and 30 cabochons), were collected by the authors over a period of many years, and examined as summarized in table 1. Among these, 29 cut samples (nine faceted and 20 cabochons) and 10 pieces of rough were from secondary deposits (e.g., figure 9). The remaining 13 cut samples (three faceted and 10 cabochons) and five pieces of rough were from primary host rocks (e.g., figure 10) along National Road 70, at kilometers 12, 15, and 23, and at Slope 700. All of these were gem quality, although those from primary occurrences typically were of much lower quality.

We used standard gemological equipment to record optic character, refractive indices and birefringence, pleochroism, absorption spectra, and UV fluorescence (to long- and short-wave radiation). Specific gravity was measured by the hydrostatic method using an electronic balance. Various gemological microscopes (vertical and horizontal, incorporating different lighting techniques) were used to observe internal features.

Raman microspectroscopy was performed on nine observable mineral inclusions embedded in transparent hosts. The spectra were collected using a Jobin Yvon LabRam HR 800 spectrometer coupled with an Olympus BX41 optical microscope and an Si-based CCD (charge-coupled device) detector at the Institute of Geosciences, Johannes Gutenberg University (Mainz, Germany). The samples were excited by a 514 nm Ar-ion laser. The confocal mode was used to enable analysis at the micron scale (~0.2–0.5 μm).

Absorption spectra of three Tan Huong–Truc Lau rubies were collected using a Shimadzu UV-2450 UV-Vis spectrophotometer at the Center for Material Sciences, Hanoi University of Science.

Polished thin sections of 23 samples selected from primary and secondary deposits at Truc Lau and Tan Huong were prepared for quantitative chemical analysis by electron microprobe. The analyses were performed using three different instruments, as indicated in table 2. Also analyzed were 29 mineral inclusions exposed on the polished surfaces.

GEMOLOGICAL CHARACTERISTICS

Crystal Morphology. Two main crystal forms characterized the morphology of the corundum from primary deposits:

1. Prismatic crystal habits composed of the hexagonal prism a {11$\bar{2}$0} and basal pinacoid c {0001}
2. A modification of this habit, with the addition of the positive rhombohedron r {10$\bar{1}$1}

The crystals had short prismatic and sometimes tabular hexagonal shapes, with a height-to-width ratio ranging from 1 to 3.

Visual Appearance. In general, rubies and sapphires from Tan Huong–Truc Lau are only of cabochon quality. Transparent to semitransparent pieces with more marketable red to pink colors occur in secondary deposits, while those extracted from primary deposits are usually opaque to translucent and have dull to dark colors unsuitable for cutting. Corundum from the primary deposits ranges from colorless to gray, pale blue, and yellowish to dark red and violetish pink; only the latter is typically of gem quality (again, see figure 10). Corundum from

TABLE 1. Gemological characteristics of rubies and sapphires from Tan Huong–Truc Lau, Vietnam.

Property	Primary deposits		Secondary deposits	
	No. of samples	Observations	No. of samples	Observations
Color	13 polished	Colorless, gray to yellowish gray, bluish or greenish gray Dark red, red to pink, purplish pink	29 polished	Pink, pinkish to purplish and brownish red, dark red
Pleochroism	13 polished	Weak to moderate *Dark red to red, pink*: Violet to violetish red, orange to orangy red *Bluish gray*: Greenish gray to bluish gray	29 polished	Moderate to strong *Dark red to red, pink*: Violet to violetish red, orange to orangy red
Diaphaneity	5 rough, 13 polished	Poor to moderate clarity and opaque to translucent; rarely semitransparent to transparent	10 rough, 29 polished	Poor to moderate clarity, opaque to translucent and semitransparent; some parts may be transparent
Refractive Indices	3 faceted 10 cabochon	n_o = 1.762–1.763 n_e = 1.770–1.771 n = 1.76–1.77 (spot method)	9 faceted 20 cabochon	n_o = 1.762–1.763 n_e = 1.770–1.771 n = 1.76–1.77 (spot method)
Birefringence	3 faceted	0.008–0.009	9 faceted	0.008–0.009
Optic character	3 faceted	Uniaxial negative	9 faceted	Uniaxial negative
Specific gravity	5 rough, 13 polished	3.91–3.99	10 rough, 29 polished	3.92–4.07
UV fluorescence[a]	5 rough, 13 polished	*Gray to white, bluish gray*: Inert to both LW and SW *Red to pink*: • LW: Moderate to weak red • SW: Weak red	10 rough, 29 polished	*Red to pink*: • LW: Moderate to strong red • SW: Weak to moderate red
Spectroscope spectrum	5 rough, 13 polished	*Red to pink*: Chromium spectra *Bluish and greenish gray*: 450 nm (faint line)	10 rough, 29 polished	*Red to pink*: Chromium spectra
Internal features	5 rough, 13 polished	• Ilmenite, plagioclase, biotite, muscovite, apatite, zircon, rutile needles, magnetite, chlorite • Primary and secondary liquid-gas inclusions • Growth zoning, parting, fractures, lamellar twinning	10 rough, 29 polished	• Rutile (needles, silk, clouds, and stringer formations), ilmenite, zircon, apatite, spinel, diaspore, plagioclase, biotite, muscovite, chlorite, allanite(?), magnetite • Primary and secondary liquid-gas inclusions • Growth zoning, parting, fractures, lamellar twinning

[a] Abbreviations: LW = long-wave, SW = short-wave.

Figure 9. These rough and cut rubies are from secondary deposits at Truc Lau. The cabochons on the right range from 8.24 to 19.53 ct. Note the asterism in the stone on the lower right. Photos by N. N. Khoi.
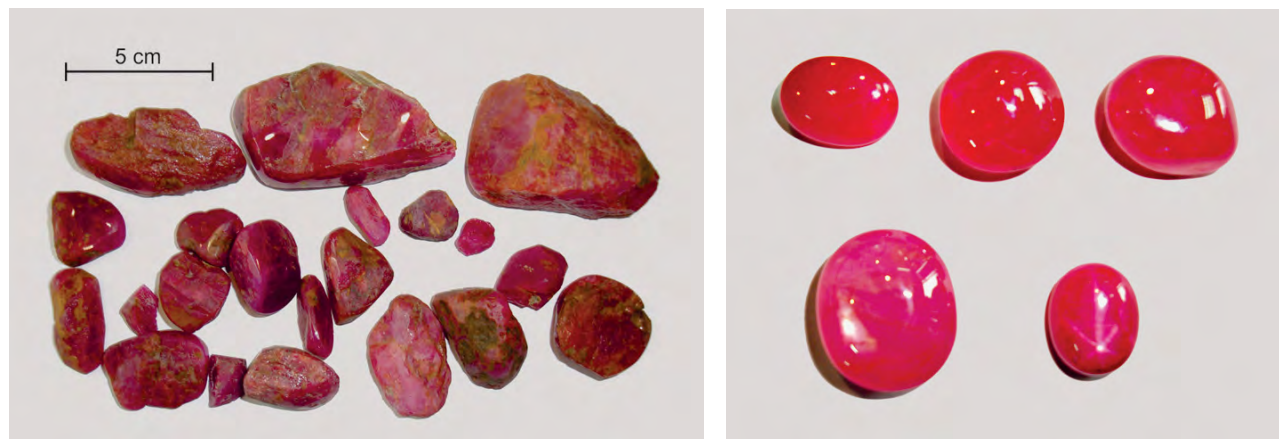
Figure 10. This ruby crystal (2.45 g) formed in feldspathic host rock (see figure 7, right). Photo by N. V. Nam.

the secondary deposits, however, has more desirable colors that commonly range from dark red, brownish red, and violetish to pinkish red (figures 1 and 11). The secondary deposits also yield sapphires that are usually colorless, yellowish gray, bluish gray, or multicolored. Blue, green, and yellow hues are very rare. Diaphaneity ranges from opaque to nearly transparent.

The corundum's dimensions vary considerably, from several millimeters to several centimeters. The most significant visual features are growth zoning (straight and angular) and asterism (figure 12); about 30% of the gem-quality stones show a star phenomenon, according to the miners. Color irregularities such as spots, streaks, and patches are uncommon in these rubies and sapphires.

Another distinct characteristic of corundum (especially ruby) from both primary and secondary deposits in Tan Huong–Truc Lau is an overgrowth of iron-stained spinel. These coated stones have an unsightly yellowish gray appearance until the spinel crust is cut away to reveal a red core of ruby (figure 13). Local gem dealers call the spinel-encrusted material *hàng mó bát* (gamble merchandise), indicating the uncertainty of dealing with these goods.

Optical Characteristics and Specific Gravity. The refractive indices, birefringence, and specific gravity values of ruby and sapphire from Tan Huong–Truc Lau fell within typical values for corundum, and there was little difference in these properties

TABLE 2. Summary of electron microprobe analyses of corundum from Tan Huong–Truc Lau, Vietnam.[a]

Oxide (wt.%)	Primary corundum		Secondary corundum		
	Bluish gray to pale blue, from Truc Lau[b] (10)	Pale pink, from Truc Lau[c] (3)	Pink to red, from Truc Lau[c] (4)	Dark red, from Tan Huong[d] (1)	Violetish red to violetish pink, from Tan Huong[d] (5)
Al_2O_3	97.12–98.95	99.00–99.30	98.90–99.30	99.76	98.90–99.98
SiO_2	nd–0.10	nd–0.10	–	–	–
TiO_2	nd–0.05	nd–0.22	nd–0.05	–	0.014–0.11
Cr_2O_3	nd–0.04	0.11–0.44	0.07–0.69	0.18	0.69–0.27
FeO	0.94–1.38	0.15–0.48	0.03–0.37	–	0.005–0.15
MnO	nd–0.02	–	–	–	–
MgO	nd–0.02	–	–	–	–
NiO	nd–0.04	–	–	–	–
CaO	nd–0.04	–	–	–	–
Na_2O	nd–0.02	–	–	–	–
K_2O	nd–0.03	–	–	–	–
V_2O_5	–	–	–	–	nd–0.12
ZnO	nd–0.23	–	–	–	–
Ga_2O_3	–	–	–	–	nd–0.04
Total	99.51	99.84	99.67	99.94	100.16

[a] *Number of samples shown in parentheses; average of 4–5 analyses per sample. Total iron is reported as FeO. Abbreviation: nd = not detected.*
[b] *Analyzed at Vietnam Institute of Geosciences and Mineral Resources, using a JEOL JXA 8800R/8900 microprobe with an accelerating voltage of 15 kV, a beam current of 1.2 nA, and a collection time of 20 seconds (major elements) or 15 kV, 50 nA, and 80 seconds (trace elements).*
[c] *Analyzed at the Institute of Geology, Russian Academy of Science, using a Camebax-Kevex microprobe with an accelerating voltage of 15 kV, beam current of 20 nA, and collection time of 20 seconds.*
[d] *Analyzed at the Earth Sciences Institute, Academia Sinica, Taiwan, using a JEOL JXA 8900-R microprobe with an accelerating voltage of 15 kV, a beam current of 20 nA, and a collection time of 20 seconds.*

Figure 11. These red to pinkish red rubies (4.26–14.58 ct) are from alluvial deposits in the Tan Huong–Truc Lau area. Note the asterism in some of the stones. Photo by N. N. Khoi.

between primary and secondary corundum (table 1). Although high-SG mineral inclusions were common in corundum from the primary deposits, some samples from the secondary deposits actually had higher SG values (up to 4.07, versus 3.99). This may be caused by a higher content of heavy inclusions such as ilmenite.

Figure 12. Growth zoning and asterism are often observed in corundum from secondary deposits in the Tan Huong–Truc Lau area. These samples range from 13.77 to 24.54 ct. Photo by N. N. Khoi.

Internal Features. The majority of the gem-quality samples were from secondary deposits, which we aimed to separate from the Khoan Thong–An Phu gem materials. Nevertheless, some samples from the primary deposits were investigated for comparison. These contained various mineral inclusions, such as ilmenite, plagioclase, biotite, muscovite, apatite, zircon, rutile, magnetite, and chlorite. Among these, ilmenite, biotite, and magnetite were the most common. Primary and secondary gas-liquid inclusions were also encountered frequently.

The most common mineral inclusions in samples from secondary deposits were rutile, ilmenite, zircon, apatite, spinel, and diaspore; some plagioclase and mica (biotite and muscovite) were also observed. The rutile usually occurred as short needles, but also seen were tiny rutile inclusions with a silk-like appearance that formed antenna-like patterns (figure 14).

In general, the range of mineral inclusions was similar between the primary and secondary samples. Ilmenite was typical, and easily recognized by its stubby crystal shape, black color (figure 15, left), and submetallic luster when exposed to the surface. Apatite (figure 15, right) and zircon were also frequently encountered in our samples, forming near-colorless euhedral crystals. In addition, we observed a wide range of fluid inclusions that often showed various stages of healing, forming negative crystals (figure 16), "fingerprints," feathers, folded patterns, and irregular fluid droplets. Iron stains were also apparent.

Figure 13. Rubies from secondary deposits at Tan Huong–Truc Lau are often coated by an iron-stained spinel aggregate. Here the spinel overgrowth has partially broken away from a ruby crystal (~2 cm across) after the specimen was sawn open. Photo by N. V. Nam.
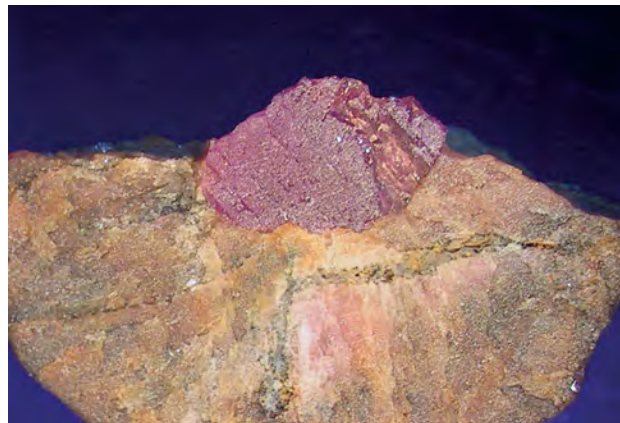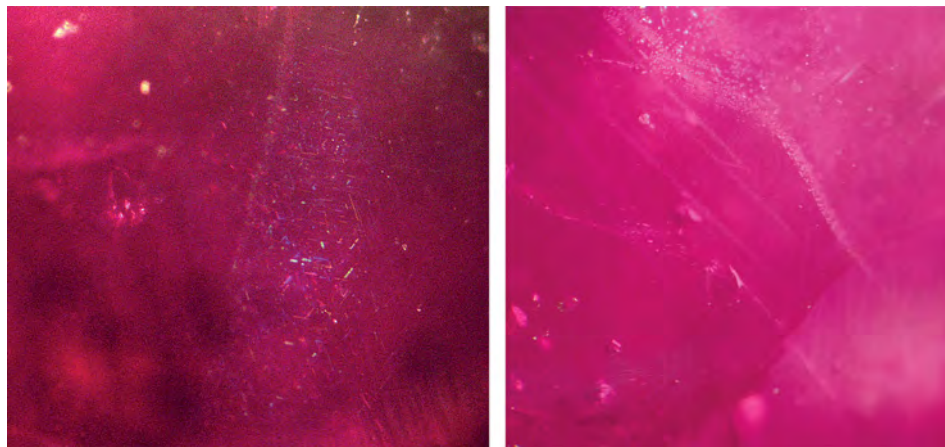
Figure 14. Rutile inclusions, usually as short needles oriented in three directions (left), may contribute to the asterism in some of the corundum. Rutile inclusions may also show a silky appearance (left) or antenna-like patterns (right). Photomicrographs by N. N. Khoi; magnified 45×.

Optical phenomena such as asterism, chatoyancy, and sheen were caused by oriented micro-inclusions, rutile needles in particular. The star effect in many of the rubies was quite sharp and attractive. Straight and angular growth zones, typically sharp and well defined, were conspicuous in most stones. Asterism and growth structures were observed together in some instances (figure 17, left). Three systems of polysynthetic lamellar twinning parallel to the positive rhombohedron r {$10\bar{1}1$} were quite common (figure 17, right). Fracturing along these twin planes yielded parallelogram-shaped rough material.

Absorption Spectra. Preliminary observation of the ruby samples with the desk-model spectroscope showed essentially the same features as the diagnostic absorption spectra described by Liddicoat (1993) for natural and synthetic rubies and purple sapphire. The strong lines at 692 and 694 nm often appeared as a single bright emission line at 693 nm. UV-Vis absorption spectroscopy (figure 18) showed peaks at ~378, 389, and 456 nm related to iron (Fe^{3+} and Fe^{2+}).

A broad band centered around 570 nm, related to Fe^{2+}/Ti^{4+}, also appeared in these spectra. Cr^{3+} features were evidently superimposed by the iron absorptions.

Chemical Analysis. Microprobe analyses of sapphires from primary deposits (table 2) showed relatively high contents of iron, especially in bluish gray stones (0.15–1.38 wt.% FeO). Chromium contents ranged from low (<0.04 wt.% Cr_2O_3) in bluish gray sapphires to moderate (0.11–0.44% Cr_2O_3) in the pink sapphires. Titanium contents ranged up to 0.22 wt.% TiO_2. In addition, some samples showed very small amounts of Si, Ca, K, Na, Ni, and Zn, probably due to tiny mineral inclusions.

The trace-element compositions of stones from placer deposits were similar to those from primary deposits. Their varying proportions clearly corresponded to differences in color. Greater contents of Cr were recorded for pink sapphires and rubies. In general, both rubies and sapphires from Tan Huong–Truc Lau had high Fe contents.
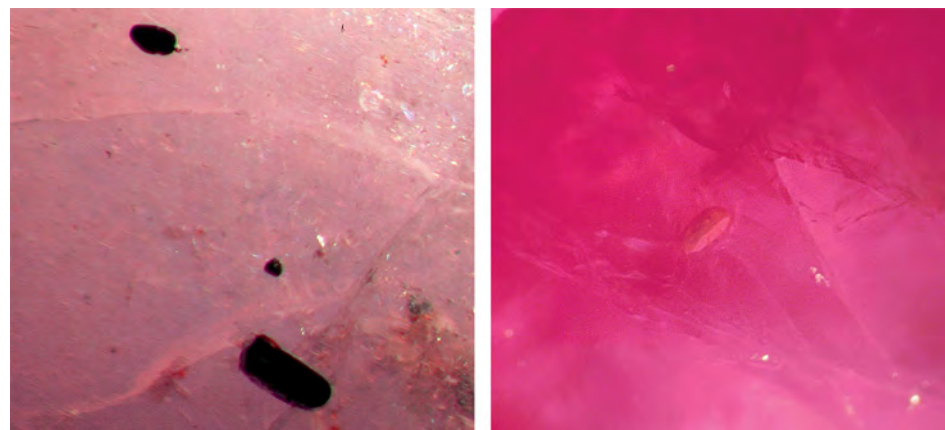
Figure 15. Ilmenite is a typical inclusion in ruby and sapphire from Tan Huong–Truc Lau, and usually shows a stubby shape and black color (left). Apatite typically occurs as colorless to light-colored euhedral crystals, as shown on the right. Photomicrographs by N. N. Khoi; magnified 45×.
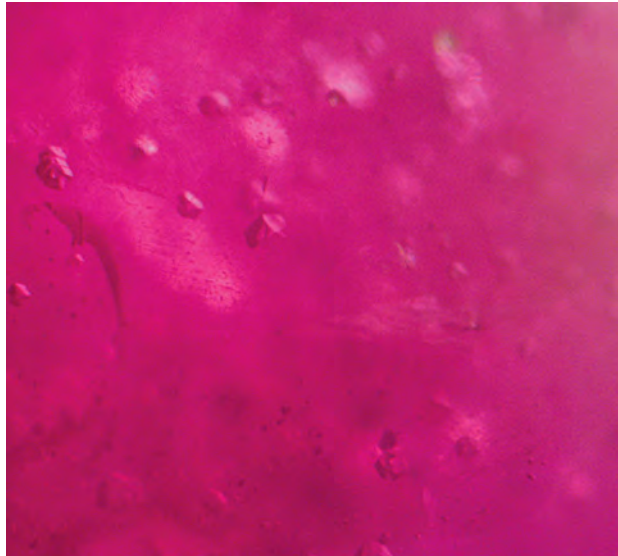
Figure 16. Negative crystals are quite common in ruby and sapphire from Tan Huong–Truc Lau, usually distributed along fractures and fissure planes. Two phases (gas and liquid) were occasionally observed in these inclusions. Photomicrograph by N. N. Khoi; magnified 45×.

DISCUSSION

Although gem corundum from Tan Huong–Truc Lau, especially star ruby, has been sold in the world market for more than 10 years, these Vietnamese deposits remain largely unknown. Many in the trade assume the stones are from Luc Yen (i.e., Khoan Thong–An Phu), but those belong to different geologic settings and consequently have distinctive gemo-

logical properties (Khoi, 2004; Khoi et al., 2010a,b), as discussed below.

Morphology and Appearance. In contrast to the short prismatic and sometimes tabular morphologies of corundum from Tan Huong–Truc Lau, crystals from Khoan Thong–An Phu typically have a barrel or spindle shape with n, z, and ω hexagonal dipyramids, r rhombohedra, and c pinacoidal faces with length-to-width ratios from 5 to 6 (Long, 2003; Nam, 2007; Thuyet, 2008). The most distinctive feature of the Tan Huong–Truc Lau corundum is its coating of granular spinel (Häger et al., 2010; Hauzenberger et al., 2010). Also, pieces of rough from Tan Huong–Truc Lau are generally much larger than those from Khoan Thong–An Phu.

The majority of cut stones from Khoan Thong–An Phu range from "pure" red or pink to purplish red or pink; other hues such as blue, orangy red, violet, or multicolored are also found with varying tones and saturations. Both rough and polished stones commonly have strong color zoning visible to the unaided eye. Diaphaneity usually ranges from transparent to translucent (Kane et al., 1991; Long, 2003; Khoi et al., 2010a). In contrast, corundum from Tan Huong–Truc Lau shows less color variation, mostly consisting of pink to purplish or brownish red hues. Color zoning is uncommon. Diaphaneity is commonly semitransparent to translucent or opaque because of fracturing and the abundance of inclusions. Interestingly, some features typical of this

Figure 17. Asterism and growth structures are seen in this 14.45 ct pink sapphire from Truc Lau (left). Polysynthetic twinning, parallel to the positive rhombohedron r $\{10\overline{1}1\}$, is a common feature of ruby and sapphire from Tan Huong–Truc Lau (right). Photomicrographs by N. N. Khoi; magnified 12×.

UV-Vis-NIR Absorption Spectrum
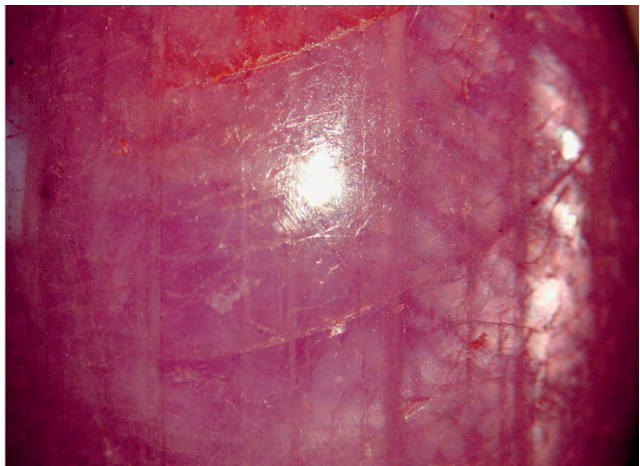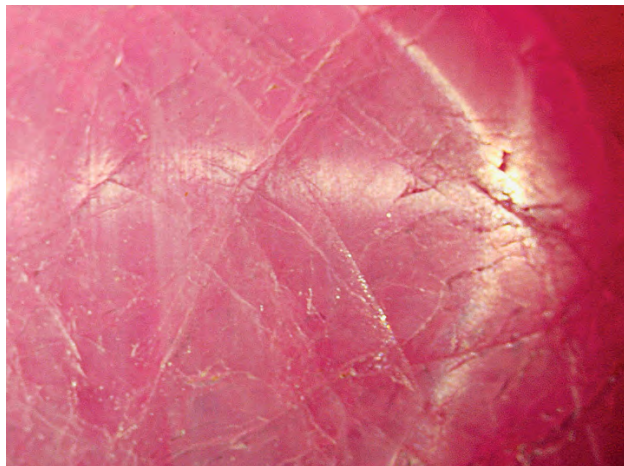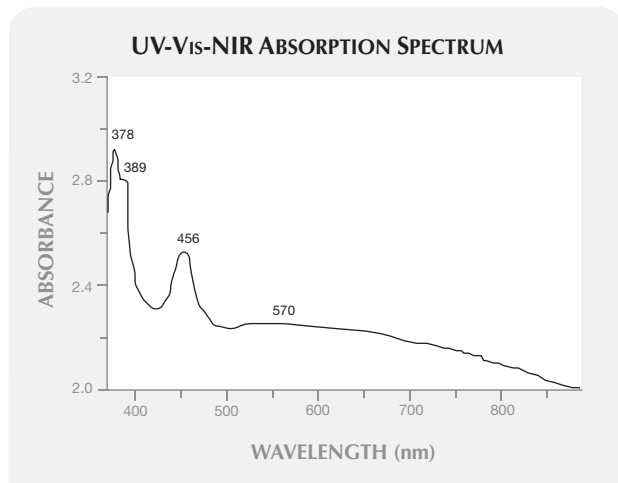
Figure 18. This UV-Vis-NIR spectrum of a ruby from a primary deposit at Truc Lau is dominated by Fe-related absorptions.

corundum (large size, asterism, and angular growth structures) are also seen in ruby crystals from Karnataka, India (Panjikar et al., 2009).

Internal Features. A summary of mineral inclusions in corundum reported from both mining areas is presented in table 3. The most common mineral inclusions in Khoan Thong–An Phu corundum are calcite, rutile, apatite, spinel, zircon, corundum, pyrrhotite, graphite, boehmite, hematite, phlogopite, muscovite, hercynite, tourmaline, and iron oxide or hydroxide (Kane et al., 1991; Long, 1999; Long et al., 2004; Khoi et al., 2010a,b). Straight, angular color zones and colored patches and spots are usually seen in the blue sapphires, and swirl growth marks are observed occasionally (see Kane et al., 1991; Long et al., 2004).

Gem corundum from Tan Huong–Truc Lau contains a diversity of mineral inclusions, most commonly ilmenite, rutile, apatite, zircon, diaspore, boehmite, magnetite, plagioclase, biotite, muscovite, and chlorite. Although straight and angular growth structures are quite common, color irregularities are rare. Trapiche rubies and pink sapphires are also known from this region (Schmetzer et al., 1996), but were not examined for this report.

The common polysynthetic twinning in corundum from the Tan Huong–Truc Lau area may be related to deformation from the Red River Shear Zone (Khoi et al., 2010b).

CONCLUSIONS

For more than two decades, Vietnam has been an important source of gem ruby and sapphire. Most of the production has come from Yen Bai Province; the original deposits in the Khoan Thong–An Phu area and the newer ones in Tan Huong–Truc Lau are con-

TABLE 3. Comparison of internal features in corundum from Tan Huong–Truc Lau and Khoan Thong–An Phu, Vietnam.[a]

Internal feature	Tan Huong–Truc Lau[b]	Khoan Thong–An Phu[c]
Solid Inclusions		
Anatase		+
Anhydrite		+
Apatite	++	++
Biotite	+	
Boehmite	+	+
Calcite		+++
Chlorite	+	
Corundum		+
Diaspore	+	+
Dolomite		+
Graphite		+
Halite		+
Hematite		+
Hercynite	+	+
Ilmenite	++	
Iron oxide or hydroxide	+++	+++
Magnetite	++	
Margarite		+
Monazite		+
Muscovite	+	+
Nepheline		+
Nordstrandite		+
Phlogopite	+	+
Plagioclase	+	
Pyrite		+
Pyrrhotite		+
Rutile (primary)	+	+
Rutile needles (silk, cloud)	++	++
Sphene		+
Spinel	+	+
Tourmaline		+
Zircon	++	+
Liquid Inclusions		
"Fingerprints"	++	++
Negative crystals	+	+
Salts (Na, Ca, K chlorides)		+
Other Features		
Color zoning	+	++
Growth structures	++	++
Twinning	+	+
Swirl growth marks		+
Wedge-shaped growth features		+

[a] Symbols: +++ = common, ++ = frequently encountered, + = encountered.
[b] From this study.
[c] References: Kane et al. (1991), Long (1999), Vinh et al. (1999), Dao and Delaigue (2001), Giuliani et al. (2003), and Long (2003).

sidered to have the most potential (see figure 19). Despite their proximity, the two areas belong to different geologic settings (marble- and gneiss-hosted, respectively). The Tan Huong–Truc Lau deposits are mostly restricted to the Dãy Núi Con Voi mountain range, which is associated with the Red River Shear Zone. Recent mining activities mostly consist of sporadic diggings by local people, though a few mechanized pits are active.

Gem corundum from Tan Huong–Truc Lau usually shows a tabular crystal form with deformed polysynthetic twinning along rhombohedral faces and sharp growth zones. Their typical colors range from pink to pinkish red. Color irregularities such as zoning and spots or patches are rare. Many stones, particularly the sapphires, have low transparency due to abundant fracturing and inclusions. The density of mineral inclusions appears crucial to differentiating these stones from those from the Khoan Thong–An Phu deposits. The most common mineral inclusions in the Tan Huong–Truc Lau stones are clusters of tiny short rutile needles, black stubby ilmenite, euhedral apatite, and assemblages of various minerals (e.g., ilmenite, rutile, and zircon), often in the same stone.

Although the vast majority of gem corundum from Tan Huong–Truc Lau is suitable for cutting cabochons (including star rubies) rather than faceted stones, some exceptionally large pieces of rough containing gem-quality areas are known. The deposits show strong potential for producing commercial quantities of gem corundum for many years. The main markets for gem material from the Tan Huong–Truc Lau area are Japan, the Middle East, and India.

Figure 19. This ring is set with a 17.50 ct star ruby from Truc Lau. The star is sharp and complete throughout the stone. Jewelry courtesy of DOJI Gold & Gems Group; photo © DOJI Gold & Gems Group and N. N. Binh.

ABOUT THE AUTHORS
Dr. Khoi is a gemologist and associate professor of geology, Dr. Thuyet is a geologist, and Dr. Nhung is a retired associate professor, at the Hanoi University of Science, Vietnam National University. Dr. Khoi is also the director of the DOJI Laboratory for Gemology and Jewelry (DOJI Gold & Gems Group, Hanoi). Dr. Sutthirat (c.sutthirat@gmail.com) is an assistant professor of geology in the Faculty of Science, Chulalongkorn University, Bangkok, and an academic advisor for the Gem and Jewelry Institute of Thailand in Bangkok. Mr. Tuan is vice general director of DOJI Gold & Gems Group. Mr. Nam holds a master's degree in geology from the Vietnam Institute of Geosciences and Mineral Resources, Hanoi.

REFERENCES

Dao N.Q., Delaigue L. (2001) Études des inclusions dans les rubis Vietnamiens par spectrometries optiques. *Proceedings of 2nd International Workshop on Material Characterization by Solid State Spectroscopy: Gems and Minerals of Vietnam*, Hanoi, April 4–10, pp. 40–78.

Garnier V., Giuliani G., Ohnenstetter D., Fallick A.E., Dubessy J., Baks D., Vinh H.Q., Lhomme T., Maluski H., Pêcher A., Bakhsh K.A., Long P.V., Trinh P.T., Schwarz D. (2008) Marble-hosted ruby deposits from Central and Southeast Asia: Towards a new genetic model. *Ore Geology Reviews*, Vol. 34, pp. 169–191, http://dx.doi.org/10.1016/j.oregeorev.2008.03.003.

Giuliani G., Dubessy J., Banks D., Vinh H.Q., Lhomme T., Pironon J., Garnier V., Trinh P.T., Long P.V., Ohnenstetter D., Schwarz D. (2003) CO_2–H_2S–COS–S_8–AlO(OH)-bearing fluid inclusions in ruby from marble-hosted deposits in Luc Yen area, north Vietnam. *Chemical Geology*, Vol. 194, No. 1–3, pp. 167–185, http://dx.doi.org/10.1016/S0009-2541(02)00276-0.

Häger T., Khoi N.N, Tuan D.A., Huong L.T.T., Hofmeister W. (2010) Ruby and sapphire rimmed by spinel from the Luc Yen–Yen Bai gem mining area, Vietnam. *20th General Meeting of the International Mineralogical Association: Abstracts*, Budapest, August 21–27, p. 27.

Hauzenberger C., Häger T., Wathanakul P., Khoi N.N., Nantasin P., Goessler W. (2010) Petrology and geochemical characteristics of ruby with associated spinel corona from Truc Lau, N-Vietnam. *Proceedings of the 5th International Conference on the Provenance and Properties of Gems and Geo-Materials*, Hanoi, October 17–24, pp. 23–28.

Kane R.E., McClure S.F., Kammerling R.C., Khoa N.D., Mora C., Repetto S., Khai N.D., Koivula J.I. (1991) Rubies and fancy sapphires from Vietnam. *G&G*, Vol. 27, No. 3, pp. 136–155.

Katz M.B. (1972) On the origin of the Ratnapura-type gem deposits of Ceylon. *Economic Geology*, Vol. 67, pp. 113–115, http://dx.doi.org/10.2113/gsecongeo.67.1.113.

Khoi N.N. (2004) Study to establish characteristic attributes of the marble-hosted type of Vietnam ruby and sapphire deposits—The basis for modeling of this type of deposit. *Journal of Earth Sciences*, Vol. 26, pp. 333–342.

Khoi N.N, Nhung N.T., Thuyet N.T.M. (2010a) Quality characteristics of rubies and sapphires from main deposit types of Vietnam. *Journal of Earth Sciences*, Vol. 32, No. 2, pp. 199–209.

Khoi N.N., Sutthirat C., Tuan D.A., Nam N.V., Thuyet N.T.M., Nhung N.T. (2010b) Comparative study of rubies and fancy sapphires from two different deposit types in Yen Bai Province, Vietnam. *Proceedings of the 5th International Conference on the Provenance and Properties of Gems and Geo-Materials*, Hanoi, October 17–24, pp. 212–223.

Leloup P.H., Arnaud N., Lacassin R., Kienast J.R., Harrison T.M., Phan Trong T., Replumaz A., Tapponnier P. (2001) New constraints on the structure, thermochronology, and timing of the Ailao Shan–Red River Shear Zone, SE Asia. *Journal of Geophysical Research—Solid Earth*, Vol. 106, No. B4, pp. 6683–6732, http://dx.doi.org/10.1029/2000JB900322.

Liddicoat R.T. (1993) *Handbook of Gem Identification*, 12th ed. Gemological Institute of America, Santa Monica, CA.

Long P.V. (1999) Characteristics of inclusions of ruby and sapphire from Luc Yen deposit. *Journal of Geology*, Series A, No. 252, pp. 21–29.

Long P.V. (2003) Gemological Characteristics and Origin of Ruby and Sapphire in Luc Yen and Quy Chau Areas. PhD thesis, Hanoi University of Science, Vietnam.

Long P.V., Vinh H.Q., Garnier V., Giuliani G., Ohnenstetter D., Lhomme T., Schwarz D., Fallick A., Dubessy J., Trinh P.T. (2004) Gem corundum deposits in Vietnam. *Journal of Gemmology*, Vol. 29, No. 3, pp. 129–147.

Nam N.V. (2007) Crystalo-Mineralogical, Gemological Characteristics and Formation Conditions of Corundums in Metasediments and Related Placer Deposits in the Area of Truc Lau. MS thesis, Hanoi University of Science [in Vietnamese].

Nam N.V., Huyen N.T. (2010) Chemical composition characteristics and forming condition of ruby and sapphire in metamorphic rocks of Red River Shear Zone. *Proceedings of the 5th International Conference on the Provenance and Properties of Gems and Geo-Materials*, Hanoi, October 17–24, pp. 224–232.

Panjikar J., Ramchandran K.T., Panjikar A. (2009) Chatoyancy and hexagonal zoning in 3.713 kg ruby from Karnataka, India. *GIT 2008: Proceedings of the 2nd International Gem and Jewelry Conference*, March 9–12, Bangkok, pp. 154–158.

Quan T.N., Nam N.V., Tien L.B., Bach V.X., Thai T.N., Hang N.B., Thao N.P. (1998) Genetic-industrial types of ruby and sapphire deposits in the Red River Shear Zone. *Geology and Mineral Resources*, Vol. 6, pp. 183–192.

Quan T.N., Bach V.X., Nam N.V., Thai T.N., Tien L.B., Tho P.D., Hang N.B., Thao N.P. (2000) Some newly discovered primary occurrences of ruby and sapphire in the Red River Shear Zone. *Journal of Geology*, Series A, Vol. 260, pp. 63–69.

Schmetzer K., Hänni H.A., Bernhardt H-J., Schwartz D. (1996) Trapiche rubies. *G&G*, Vol. 32, No. 4, pp. 242–250, http://dx.doi.org/10.5741/GEMS.32.4.242.

Simandl G.J., Paradis S. (1999) Corundum in alumina-rich metasediments. In G. J. Simandl, Z. D. Hora, and D. V. Lefebure, Eds., *Selected British Columbia Mineral Deposit Profiles*, Vol. 3, Industrial Minerals and Gemstones. British Columbia Ministry of Energy and Mines, Open File 1999-10, pp. 105–108.

Thang N.H. (1998) Report on the investigation and evaluation of gemstones in Truc Lau–Lang Chap area, Yen Bai. Archives of Vietnam National Gem and Gold Corporation (VIGEGO), Hanoi [in Vietnamese].

Thuyet N.T.M. (2008) Study on Typomorphic and Gemological Characteristics of Corundums from Some Genetic Types of Deposits in Yen Bai and Dak Nong Provinces of Vietnam. PhD thesis, Hanoi University of Science [in Vietnamese].

Trinh P.T., Leloup P.H., Arnaud N., Lacassin N. (1998) Formation of ruby in the Red River metamorphic zone. *Proceedings of the National Centre for Natural Sciences and Technology*, Vol. 10, No. 1, pp. 143–148.

Trinh P.T., Leloup P.H., Giuliani G., Vinh H.Q., Lacassin R., Long P.L. (1999) Geodynamic role in the formation of ruby in the Red River Shear Zone and surrounding area. *Journal of Geology*, Series B, Vol. 13–14, pp. 144–146.

Vinh N., Ed. (2005) Geology and Mineral Resources of Vietnam, Yen Bai Sheet, Scale 1:200.000 (F 48 XXI). Department of Geology and Minerals of Vietnam, Hanoi.

Vinh N.Q. (1991) Report on the geological prospecting for colored stones in Song Lo zone and adjacent areas. Archives of the Ministry of Heavy Industries, Hanoi [in Vietnamese].

Vinh H.Q., Giuliani V., Trinh P.T., Coget T., France-Lanord Ch., Long P.V. (1999) Origin of ruby formation in Yen Bai Province. *Journal of Geology*, Series B, Vol. 13–14, pp. 118–123.

Voi T.X. (1991) Report on the exploration and exploitation of colored gemstones at An Phu, Luc Yen, Hoang Lien Son. Archives of Vietnam National Gem and Gold Corporation (VIGEGO), Hanoi [in Vietnamese].

Xuyen T., Ed. (2000) Geology and Mineral Resources Map of Vietnam, Bac Quang Sheet, Scale 1:200.000 (F 48 XV). Department of Geology and Minerals of Vietnam, Hanoi.

INFRARED SPECTROSCOPY OF NATURAL VS. SYNTHETIC AMETHYST: AN UPDATE

Stefanos Karampelas, Emmanuel Fritsch, Triantafillia Zorba, and Konstantinos M. Paraskevopoulos

When microscopic identification is not feasible, FTIR spectra at high resolution (0.5 cm^{-1}) can distinguish natural and synthetic amethyst. The 3595 cm^{-1} band is characteristic of natural amethyst and has a full width at half maximum (FWHM) of 3.3 ± 0.6 cm^{-1}. In synthetic amethyst, this band is either absent or (very rarely) about twice as broad. Exceptions to this criterion include natural amethyst with pronounced near-colorless zones, which do not always display this band, and natural specimens that either have an intense, unusually broad 3595 cm^{-1} band or show total absorption in the X-OH region (3800–3000 cm^{-1}) of the spectrum.

Gem-quality amethyst is found on all continents and in various geologic environments (figure 1). Some contemporary sources are Brazil, Uruguay, Zambia, Namibia, Mexico, Russia, Arizona, Canada, Bolivia, and Sri Lanka (Shigley et al., 2010). Synthetic amethyst crystals are grown in either a near-neutral NH$_4$F solution (see figure DD-1 in the *G&G* Data Depository at gia.edu/gandg) or an alkaline K$_2$CO$_3$ solution (figure 2). The identification of NH$_4$F-grown synthetic amethyst is straightforward with standard microscopy (observation of color zoning; figure DD-2) or infrared spectroscopy (Balitsky et al., 2004b; figure DD-3). However, most

synthetics in the market today are grown in K$_2$CO$_3$ solution (cited below simply as "synthetic" amethyst). Classical gemological techniques (observation of twinning, color zoning, and inclusions) can distinguish only some of these synthetics (Crowningshield et al., 1986; Notari et al., 2001, and references therein). The highest-quality products are free of inclusions, distinct color zoning, and in many cases twinning, which makes their identification more challenging.

Recent investigations have demonstrated the effectiveness of laser ablation–inductively coupled plasma–mass spectrometry (LA-ICP-MS) in separating natural and synthetic quartz. Plots of Ti+Cr vs. Ga are reportedly the most useful (Breeding and Shen, 2010). Unfortunately, this technique is not widely available and is too expensive to use for the identification of a common gem such as amethyst. Furthermore, overheating from the ablation laser may cause cracks in the samples (L. Klemm, pers. comm., 2011).

Infrared absorption spectroscopy in the region of X-OH stretching vibrations (i.e., 3800–3000 cm^{-1}) has long been considered useful for distinguishing natural and synthetic amethyst (Smaali, 1998; Zecchini and Smaali, 1999; Notari et al., 2001; Balitsky et al., 2004a,b; Karampelas et al., 2006, and references therein). In this region, the infrared spectra of natural and synthetic amethyst are largely similar, though they have some important differences. The specific range of interest is from 3640 to 3500 cm^{-1}, where both show absorptions at approximately 3612 and 3585 cm^{-1}. These two absorptions are probably due to vibrations caused by Al substitutions (Kats, 1962).

Earlier studies used bands at 3595 and 3543 cm^{-1}

Figure 1. Determining the natural or synthetic origin of some amethyst remains a challenge for gemologists. Shown here are three natural samples weighing 22.00–43.79 ct (at left; GIA Collection nos. 13143, 37216, and 31971) and a 4.89 ct synthetic (the emerald cut at lower right, GIA Collection no. 17239) in front of various samples of undetermined origin. Photo by Robert Weldon.

to separate natural and synthetic amethyst. The band at 3543 cm^{-1}, observed in the vast majority of lab-grown amethyst, was considered indicative of synthesis (Fritsch and Koivula, 1988). However, stones from a number of natural deposits can also show this absorption (Kitawaki, 2002), which is related to the negative rhombohedron growth sector rather than synthesis (Balitsky et al., 2004a,b). Likewise, the 3595 cm^{-1} band observed in most natural amethyst was once considered indicative of nat-

ural origin (Zecchini and Smaali, 1999, and references therein), but this band was subsequently noted in the spectra of some synthetic amethyst (Notari et al., 2001; Karampelas et al., 2005, 2006), and was reported to be absent from some natural samples (Balitsky et al., 2004a,b). FTIR measurements at high resolution (0.5 cm^{-1}) found that this band is present in all natural amethyst, but can be missed with standard 4 cm^{-1} resolution. In synthetic amethyst, this band is either absent or (rarely) when present has a

Figure 2. These K_2CO_3-grown synthetic amethysts include an unusual Russian prismatic cluster (left; 10 cm tall) and a crystal weighing more than 1 kg (right; 15 cm tall). The vast majority of synthetic amethyst in the gem market is K_2CO_3 grown. Photos by Franck Notari.

TABLE 1. Comparison of the 3595 cm^{-1} band in natural and synthetic (K$_2$CO$_3$ grown) amethyst.

Sample no.	Origin	Type	Weight (ct)	No. scans[a]	FWHM (cm^{-1})
		Natural			
Am008	Bolivia (Anahí)	Rough	0.4	128 or 512	2.7
Am082	Bolivia (Anahí)	Rough	4.1	128 or 1024	3.2
Am106	Brazil (Marabá)	Rough	5.3	128 or 1024	3.3
Am016	Brazil (Pau d'Arco)	Rough	0.8	200 or 300	3.5
Am448	France (St. Raphael)	Rough	1.0	128 or 512	3.0
Q022	Japan (Ishikawa)	Faceted	2.3	512 or 512	3.0
Am060	Mexico (Veracruz)	Faceted	3.0	128 or 1024	3.3
Ru007	Russia (Urals)	Rough	1.0	128 or 512	3.0
Uru007	Uruguay (Artigas)	Rough	0.4	128 or 512	3.9
Am068	USA (Four Peaks, Arizona)	Rough	3.4	128 or 1024	3.0
Am075	Zambia (Solwezi)	Rough	3.8	150 or 300	3.5
Am080	Zambia (Solwezi)	Faceted	4.0	128 or 512	3.5
Am023	Unknown	Faceted	1.2	200 or 700	5.0
Am057	Unknown	Faceted	2.9	200 or 700	5.0
		Synthetic			
Q198	Japan	Faceted	3.1	300 or 900	–
Am169	Russia	Faceted	8.5	128 or 1024	–
Am004	Russia (prismatic)	Rough	0.2	256 or 1024	–
Am585	Russia	Faceted	29.3	128 or 1024	–
Am4	Russia	Faceted	16.0	128 or 1024	–
Am1612	Russia	Faceted	8060.0	128 or 1024	–
Am177	Russia	Faceted	8.9	128 or 1024	–

[a] At 4 or 0.5 cm^{-1} resolution, respectively.

FWHM value approximately two times larger than that of natural specimens (Karampelas et al., 2005, 2006).

MATERIALS AND METHODS

This study was carried out on 21 samples, 14 natural and seven synthetic. Several geographic localities were represented, including some that did not satisfy the proposed IR separation criteria given in previous studies. The natural identity of two samples of unknown origin was confirmed microscopically. All the synthetic amethyst samples in this study were grown in alkaline K$_2$CO$_3$ solutions, including rare and unusual prismatic material (figure 2, left). Nine samples were faceted and 12 were rough (for details on their size and origin, see table 1). All were obtained from reputable sources (see Acknowledgments), and none contained near-colorless zones.

Infrared absorption spectra of the faceted and some of the rough samples were acquired with a Bruker Vertex 70 FTIR spectrometer (under vacuum) at the University of Nantes, and a Varian 640 FTIR spectrometer at the Gübelin Gem Lab, both using a diffuse reflectance accessory as a beam condenser.

A Bruker 113v FTIR spectrometer (under vacuum) in the Physics Department of Aristotle University was used for measurements on some of the rough samples. The spectra were taken in random crystallographic orientation, as the bands of interest are little-affected by direction (see Karampelas et al., 2005).

Previous studies found that the true shape of the 3595 cm^{-1} band is obtained at a resolution of 0.5 cm^{-1} (Karampelas et al., 2005; figure DD-4). Thus, we measured the samples at 0.5 cm^{-1}, as well as at the standard 4 cm^{-1} resolution. To obtain a high signal-to-noise ratio, multiple scans were collected (again, see table 1). When the 3595 cm^{-1} band was present, we measured its FWHM (see figure DD-5 for more information on this process).

RESULTS AND DISCUSSION

IR absorption spectra in the 3640–3500 cm^{-1} range are presented in figures 3–5 (and DD-6 through DD-

NEED TO KNOW

- Standard gemological testing is not always sufficient to identify synthetic amethyst.
- High-resolution (0.5 cm^{-1}) FTIR analysis has shown that the band at 3595 cm^{-1} is present in the vast majority of natural amethyst.
- While the 3595 cm^{-1} band can occur in synthetic amethyst, it has a much larger FWHM value than in natural specimens.

10). The spectra corresponding to the two different resolutions are stacked and offset in absorbance for clarity. In these figures, the upper spectra are taken at a resolution of 0.5 cm^{-1}, and the lower ones with a 4 cm^{-1} resolution. The expected absorption bands at 3614 and 3585 cm^{-1} were observed in all samples, natural and synthetic. The 3543 cm^{-1} band was observed in five of the natural and all of the synthetic amethyst (see figure 3 and also figures DD-6 and DD-7).

The 3595 cm^{-1} band was visible in some natural amethyst at 4 cm^{-1} resolution and in all of them at 0.5 cm^{-1} resolution (see figure 4 and also figures DD-8 and DD-9). In some samples, this band was very intense (figures 5 and DD-10). The band did not appear in the spectra of any of the synthetic

IR Absorption Spectra
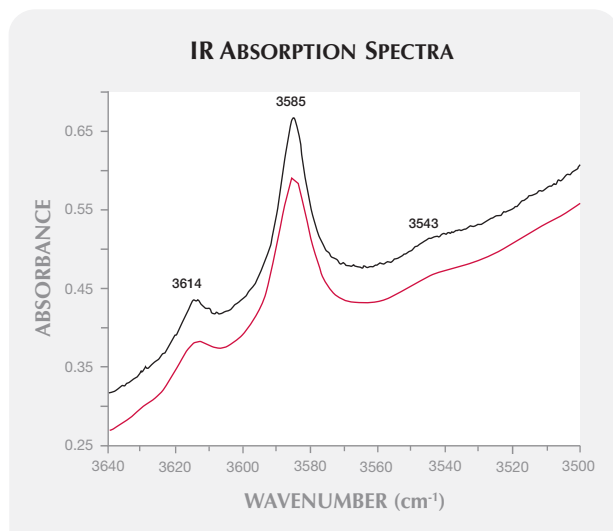
Figure 3. The infrared absorption spectra of a rare 0.2 ct rough "prismatic" synthetic amethyst from Russia (Am004; see figure 2, left) are shown at resolutions of 4 cm⁻¹ (red) and 0.5 cm⁻¹ (black). The 3595 cm⁻¹ band is not observed, but a shoulder is present at 3543 cm⁻¹.

amethyst studied here, though it did in a sample from a previous study (Karampelas et al., 2005). Some natural material from (Marabá) Brazil shows total absorption in the ~3600 to 3000 cm⁻¹ region, but this has been documented as being characteristic of natural amethyst (Smaali, 1998). In a previous

Figure 4. The infrared absorption spectra of a 3.8 ct rough amethyst from Zambia (Am075) are shown at resolutions of 4 cm⁻¹ (red) and 0.5 cm⁻¹ (black). The 3595 cm⁻¹ band is barely visible at 4 cm⁻¹ but well resolved at 0.5 cm⁻¹ (FWHM of 3.5 cm⁻¹).

IR Absorption Spectra

IR Absorption Spectra
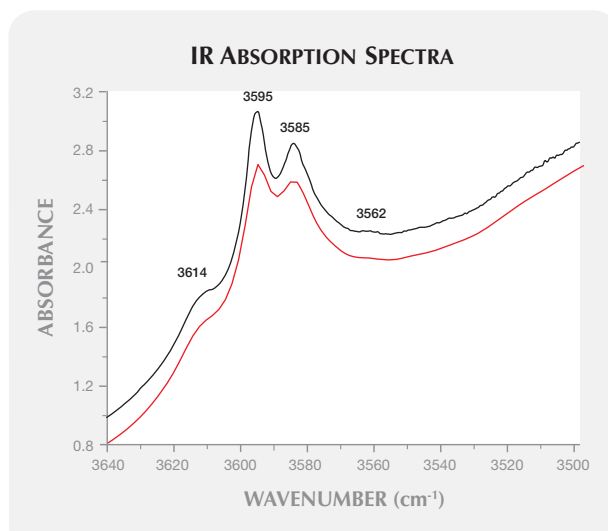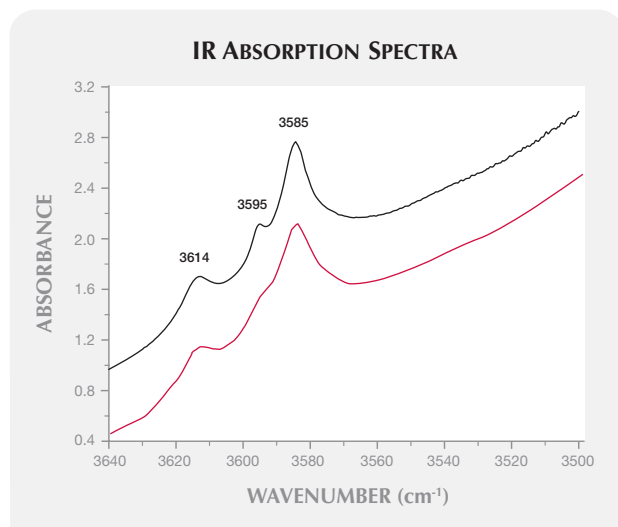
Figure 5. The infrared absorption spectra of a 2.9 ct rough amethyst of unknown origin with natural inclusions (Am057) are shown at resolutions of 4 cm⁻¹ (red) and 0.5 cm⁻¹ (black). The 3595 cm⁻¹ band is more intense than the one at 3585 cm⁻¹ in both spectra, with an FWHM of 5 cm⁻¹ at 0.5 cm⁻¹ resolution. A shoulder at about 3562 cm⁻¹ is observed at both resolutions.

study, a sample that presented total absorption in this region was cut into two halves, which both displayed the 3595 cm⁻¹ band (as well as those at 3585 and 3614 cm⁻¹; Karampelas, 2002). Some natural amethyst from other localities (e.g., Solwezi, Zambia) also shows strong absorption (i.e., a high absorption coefficient) in this region. Relatively small pieces (<10 ct) of natural amethyst with a high absorption coefficient can show total absorption in the ~3600 to 3000 cm⁻¹ region. To date, no known synthetic amethyst (even large samples; figure DD-7) presents total absorption in this region. However, more samples of synthetic amethyst need to be studied to strengthen these findings.

The natural amethyst FWHM values of the 3595 cm⁻¹ band at 0.5 cm⁻¹ resolution are similar to those previously published (3.3 ± 0.6 cm⁻¹; Karampelas et al., 2006). Some larger 3595 cm⁻¹ bands recorded in this study (FWHM: 5.0 cm⁻¹) were obtained from samples in which the 3595 cm⁻¹ band was more intense than the 3585 cm⁻¹ band (again, see figures 5 and DD-10). Very intense bands at 3595 cm⁻¹ have also been measured in rock crystal quartzes from Norway and Japan (Nimi et al., 1999; Müller and Koch-Müller, 2009). Although some natural samples with colorless bands do not show absorption at 3595 cm⁻¹, most of those can be identified with classical gemology (e.g.,

observations of twinning and color zoning).

The exact cause of the 3595 cm⁻¹ band in amethyst is unknown (Staats and Kopp, 1974; Nimi et al., 1999; Miyoshi et al., 2005; Lameiras et al., 2009; Thomas et al., 2009; Müller and Koch-Müller, 2009). This OH⁻ band has been linked to the presence of boron in synthetic quartz (Staats and Kopp, 1974), and more recently it was observed in the spectra of B-doped synthetic quartz with an FWHM of about 7 cm⁻¹ (at 2 cm⁻¹ resolution; Thomas et al., 2009). The same OH⁻ band was attributed to structural B-related defects in the lattice of natural quartz (Müller and Koch-Müller, 2009). To the best of our knowledge, however, B-doped synthetic amethyst is not present in the gem market. Additional research is needed to find the exact cause of the slight differences in the FWHM of the 3595 cm⁻¹ band in natural and synthetic amethyst.

CONCLUSION

When classical gemological techniques are inconclusive, FTIR spectroscopy at high resolution (0.5 cm⁻¹) can provide a criterion of demonstrated validity in separating the material currently on the market (figure 6), including some rare and unusual synthetics. If there is no 3595 cm⁻¹ absorption, or if it has an FWHM of 7 cm⁻¹ or more, the sample is synthetic. If the 3595 cm⁻¹ band has a width of 3.3 ± 0.6 cm⁻¹, the sample is natural. If the 3595 cm⁻¹ band is more prominent than the 3585 cm⁻¹ band, its FWHM can be larger. Total absorption in the X-OH region (3800–3000 cm⁻¹) occurs only in natural amethyst and has not been observed to date in synthetic mate-
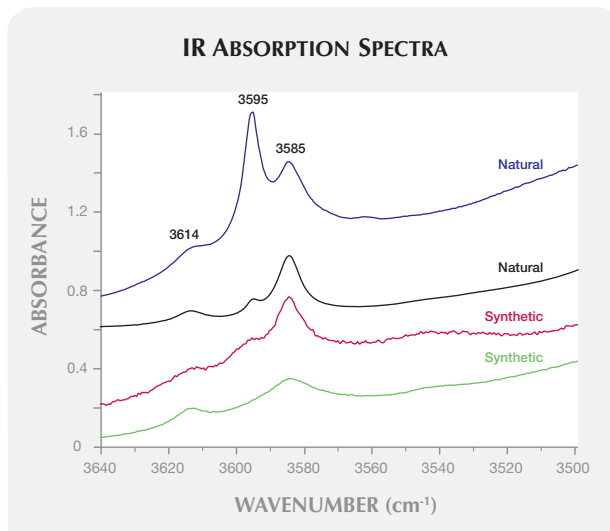
Figure 6. Shown here are infrared absorption spectra at 0.5 cm⁻¹ resolution of two synthetic amethysts (green: Am006, and red: K_2CO_3-grown from Russia, not presented in table 1 but published in Karampelas et al., 2005) and two natural specimens (black: Am060, and blue: Am023). In the synthetics, the 3595 cm⁻¹ band is either absent (green) or has an FWHM of 7 cm⁻¹ (red). Natural amethyst typically has the 3595 cm⁻¹ band with an FWHM of 3.3 ± 0.6 cm⁻¹ (black). However, some natural samples have a 3595 cm⁻¹ band that is more intense than the one at 3585 cm⁻¹, with an FWHM of 5 cm⁻¹ at 0.5 cm⁻¹ resolution (blue).

rial. The IR criteria cited above are only valid for amethyst that does not have large near-colorless zones. The 3595 cm⁻¹ band may be due to a boron-related defect in the amethyst lattice.

ABOUT THE AUTHORS

Dr. Karampelas (s.karampelas@gubelingemlab.ch) is a research scientist at the Gübelin Gem Lab, Lucerne, Switzerland. Dr. Fritsch is professor of physics at the Institut des Matériaux Jean Rouxel (IMN)-CNRS, Team 6205, University of Nantes, France. Mrs. Zorba is a research analyst, and Dr. Paraskevopoulos is professor of physics, at the Aristotle University of Thessaloniki, Greece.

REFERENCES

Balitsky V.S., Bondarenko G.V., Balitskaya O.V., Balitsky D.V. (2004a) IR spectroscopy of natural and synthetic amethysts in the 3000–3700 cm⁻¹ region and problem of their identification. *Doklady Earth Sciences*, Vol. 394, No. 1, pp. 120–123.

Balitsky V.S., Balitsky D.V., Bondarenko G.V., Balitskaya O.V. (2004b) The 3543 cm⁻¹ infrared absorption band in natural and synthetic amethyst and its value in identification. *G&G*, Vol. 40, No. 2, pp. 146–161, http://dx.doi.org/10.5741/GEMS.40.2.146.

Breeding C.M., Shen A.H. (2010) Separation of natural and synthetic gemstones using LA-ICP-MS: Amethyst, citrine, and malachite. *Goldschmidt 2010*, Knoxville, TN, June 13–18, p. A120.

Crowningshield R., Hurlbut C., Fryer C.W. (1986) A simple procedure to separate natural from synthetic amethyst on the basis of twinning. *G&G*, Vol. 22, No. 3, pp. 130–139, http://dx.doi.org/10.5741/GEMS.22.3.130.

Fritsch E., Koivula J.I. (1988) How to tell natural amethyst. *Jewelers Circular Keystone*, Vol. 158, No. 10, pp. 244–248.

Karampelas S. (2002) Absorption infrarouge de l'améthyste. MS thesis, University of Nantes, France, 21 pp.

Karampelas S., Fritsch E., Zorba T., Paraskevopoulos K.M., Sklavounos S. (2005) Distinguishing natural from synthetic amethyst: The presence and shape of the 3595 cm⁻¹ peak. *Mineralogy and Petrology*, Vol. 85, No. 1–2, pp. 45–52, http://dx.doi.org/10.1007/s00710-005-0101-9.

——— (2006) A refined infrared-based criterion for successfully separating natural from synthetic amethyst. *G&G*, Vol. 42, No. 3, p. 155, http://dx.doi.org/10.5741/GEMS.42.3.i.

Kats A. (1962) Hydrogen in alpha-quartz. *Philips Research Report*, Vol. 17, 279 pp.

Kitawaki H. (2002) Natural amethyst from Caxarai mine, Brazil, with a spectrum containing an absorption peak at 3543 cm⁻¹. *Journal of Gemmology*, Vol. 28, No. 1, pp. 101–108.

Lameiras F.S., Nunes E.H.M., Vasconcelos W.L. (2009) Infrared and chemical characterizations of natural amethysts and prasiolites colored by irradiation. *Materials Research*, Vol. 12, No. 3, pp. 315–320, http://dx.doi.org/10.1590/S1516-14392009000300011.

Miyoshi N., Yamaguchi Y., Makino K. (2005) Successive zoning of Al and H in hydrothermal vein quartz. *American Mineralogist*, Vol. 90, No. 2–3, pp. 310–315.

Müller A., Koch-Müller M. (2009) Hydrogen speciation and trace element contents of igneous, hydrothermal and metamorphic quartz from Norway. *Mineralogical Magazine*, Vol. 73, No. 4, pp. 569–583.

Nimi N., Aikawa N., Shinoda K. (1999) The infrared absorption band at 3596 cm⁻¹ of the recrystallized quartz from Mt. Takamiyama, southwest Japan. *Mineralogical Magazine*, Vol. 63, No. 5, pp. 693–701.

Notari F., Boillat P.Y., Grobon C. (2001) Discrimination des améthystes et des citrines naturelles et synthétiques. *Revue de Gemmologie a.f.g.*, Vol. 141/142, pp. 75–80.

Shigley J.E., Laurs B.M., Janse A.J.A., Elen S., Dirlam D.M. (2010) Gem localities of the 2000s. *G&G*, Vol. 46, No. 3, pp. 188–216, http://dx.doi.org/10.5741/GEMS.46.3.188.

Smaali M. (1998) Hétérodiffusion et Irradiation Gamma du Quartz Alpha. PhD thesis, University of Franche-Comté, Besançon, France, 134 pp.

Staats P.A., Kopp O.C. (1974) Studies on the origin of the 3400 cm⁻¹ region infrared bands of synthetic and natural α-quartz. *Journal of Physics and Chemistry of Solids*, Vol. 35, No. 9, pp. 1029–1033, http://dx.doi.org/10.1016/S0022-3697(74)80118-6.

Thomas S-M., Koch-Müller M., Reichart P., Rhede D., Thomas R., Wirth R., Matsyuk S. (2009) IR calibrations for water determination in olivine, r-GeO₂, and SiO₂ polymorphs. *Physics and Chemistry of Minerals*, Vol. 36, No. 9, pp. 489–509, http://dx.doi.org/10.1007/s00269-009-0295-1.

Zecchini P., Smaali M. (1999) Identification de l'origine naturelle ou artificielle des quartz. *Revue de Gemmologie a.f.g.*, Vol. 138–139, pp. 74–83.

EXPLORING THE ORIGIN AND NATURE OF LUMINESCENT REGIONS IN CVD SYNTHETIC DIAMOND

Bert Willems, Alexandre Tallaire, and Julien Barjon

In the DiamondView instrument, blue to blue-green luminescent zones may be seen in CVD synthetic diamond when the growth run has been interrupted and resumed, a well-known practice in the production of gem-quality CVD synthetics. DiamondView, photoluminescence (PL), and cathodoluminescence (CL) imaging were applied to study the origin and nature of these luminescent regions in two samples of high-purity single-crystal CVD synthetic diamond. DiamondView and PL measurements showed a correlation with silicon-related centers. In addition, CL analysis confirmed the presence of boron. Both silicon and boron showed preferential incorporation at the interface between CVD layers, where a higher uptake of impurities lead to the observed luminescence. Although the growth interruptions cannot be detected with the naked eye, the growth history can be determined accurately using luminescence imaging and spectroscopy techniques.

L uminescence spectroscopy and imaging are important techniques for characterizing optical defects in diamond. The luminescence characteristics of diamond have been studied extensively and have provided insight into associated optical defect centers (see, e.g., Walker, 1979; Collins, 1992).

The Laboratoire des Sciences des Procédés et des Matériaux (LSPM; formerly known as Laboratoire d'Ingénierie des Matériaux et des Hautes Pressions, LIMHP) near Paris grows high-purity, unintentionally doped single-crystal chemical vapor deposition (CVD) synthetic diamond for high-power electronic devices (Kone et al., 2010). As part of the fabrication process for such applications, several active layers may be grown in different CVD reactors (Denisenko and Kohn, 2005), which requires that the growth run be interrupted and resumed in cycles. Although the CVD synthetic diamond samples studied here were thin plates rather than faceted gems, the same approach is applicable to the production of gem-quality CVD synthetic diamonds (figure 1), as it enables the growth of thick single crystals in three dimensions (Ho et al., 2006) and offers a method to control the bulk crystalline quality (Friel et al., 2009). The present study focuses on the luminescence generated by optical defect centers occurring in the process of these growth interruptions and resumptions (with pre- or intermediate etching steps). As such, gemologists can acquire in-depth information about the origin and growth history of these synthetic diamonds, which is crucial in differentiating them from natural material.

MATERIALS AND METHODS

The two synthetic diamond samples investigated here were grown at LSPM-CNRS using the plasma-assisted CVD method (Achard et al., 2005). Sample A was synthesized in a microwave plasma reactor operating at 2.45 GHz. A previously etched HPHT-grown type Ib (100)-oriented synthetic diamond was

used as the substrate. The growth was performed in two runs under high-power conditions (3 kW, 200 millibars, 850°C, 4% CH_4). The thickness of material deposited was 190 μm in the first growth run, and 330 μm in the second. Before deposition took place in the second run, a high-power pure hydrogen plasma was applied for 45 minutes. This step is necessary to clean and prepare the surface prior to growth. Figure 2 shows the schematics of the growth layers (left) and DiamondView images (right) taken from the cross-sectional {100} side of the sample. The HPHT-grown substrate was subsequently removed by laser cutting. After polishing, the final thickness of the sample was about 465 μm and the lateral dimensions were 4.49 × 4.52 mm.

Sample B was grown for cathodoluminescence (CL) study under similar conditions. The initial lateral dimensions before laser cutting were 4.32 × 4.32 mm. Three CVD layers were grown with thicknesses of 190, 175, and 220 μm, corresponding to two growth interruptions resulting in a final thickness of 585 μm. Before the growth was resumed, the crystal was submitted to H_2/O_2 (98%/2%) etching in high-power conditions for about 30 minutes. This ensured the surface was clean prior to growth, but it also induced a slight roughening. To access the phosphorescent region of the sample, a cross-sectional slice was prepared by laser cutting and polishing along two opposite corners. The schematics of the cross-sectional slice of sample B are illustrated in figure 3 (left). The corresponding DiamondView (center) and CL (right) images show the interfaces between the successive synthetic diamond layers.

Sample A was examined by optical microscopy combined with luminescence spectroscopy and imaging techniques. Optical micrographs were recorded using the D-Scope stereomicroscope. This microscope (with magnifications of 0.7–40×) was equipped with an illumination system consisting of

Figure 1. Colorless gem-quality CVD-grown synthetic diamonds such as these (0.22–0.31 ct) are now commercially available, making proper identification important. Photo by Robert Weldon.

darkfield, overhead daylight, and fluorescence modes. A specially designed vacuum sample manipulator allowed easy handling. Crossed-polarized images were acquired with a Leica DFC digital camera attached to a Leica DL LM microscope.

Luminescence patterns generated by the intense ultra short-wave UV illumination of the Diamond-View instrument were recorded with the maximum illumination power (100%), full aperture (100%), and integration times of 4–10 seconds.

Photoluminescence (PL) measurements were performed on sample A using a Renishaw inVia Raman microscope at 77 K. The system was equipped with an Ar-ion laser operating at an excitation wavelength of 514.5 nm. Highly localized PL information was acquired using a Leica Fluotar L 50× objective (NA = 0.55) in the high-confocal mode using a 2D increment of 5 μm depth × 25 μm across, with a slit width of 20 μm and a CCD area of 2 pixels (image

Figure 2. The schematics of the growth layers in sample A are shown for a cross-section across {100}. At right, the Diamond-View luminescence (top) and phosphorescence (bottom) images show the two CVD layers and the HPHT-grown substrate.
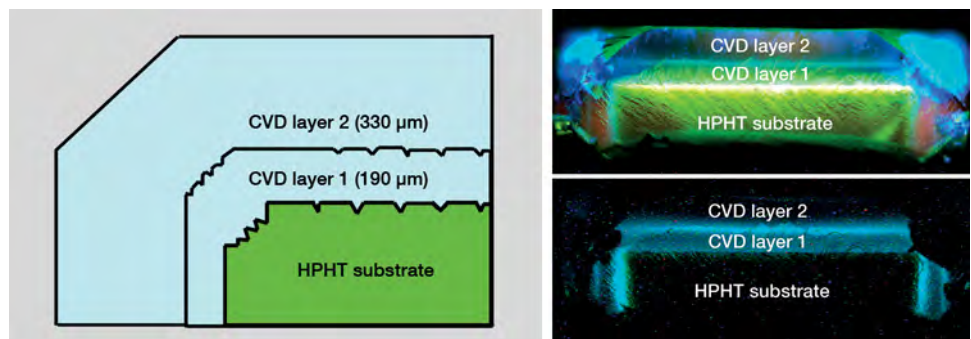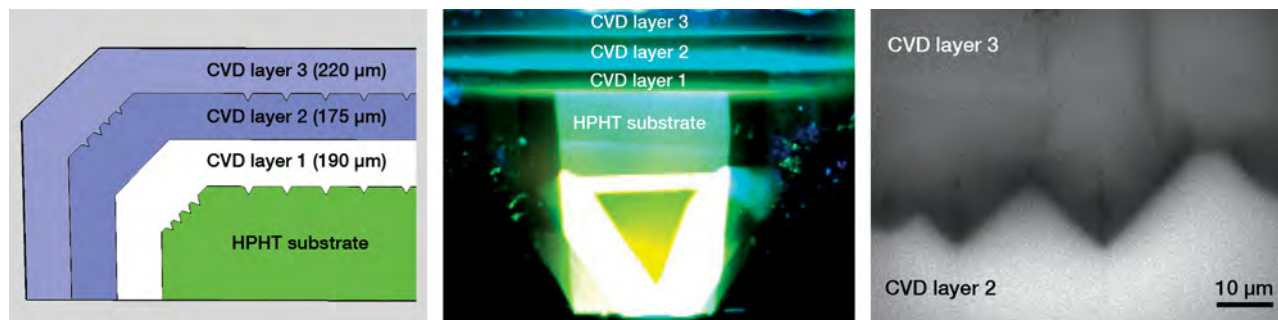
Figure 3. The schematics of the growth layers in sample B are also shown for a cross-sectional slice (across {100}, left). The DiamondView luminescence image (center) shows the successive CVD layers and the HPHT-grown substrate. The cathodoluminescence image (right) depicts the roughened interface between the CVD layers, which exhibits typical etching features and dark lines due to threading dislocations (Tallaire et al., 2011).

height) × 576 pixels (spectrometer range), resulting in an axial resolution of ~5 μm. Applying an automated xyz sample stage, we recorded detailed line and depth profiles and 2D mapping.

CL imaging of sample B was performed using a 10 kV electron beam produced in a JEOL 7001F scanning electron microscope. Monochromatic CL images were taken by filtering the excitonic signal through the monochromator, which was also equipped with a photomultiplier detector synchronized with the beam scanning.

RESULTS AND DISCUSSION

Optical Microscopy and DiamondView Imaging. Strain-related birefringence in sample A is shown in figure 4 (top left). Typical four-petal patterns related to dislocation bundles also were clearly observed. Their density was higher at the boundary with the HPHT-grown substrate, but they were also visible throughout the interior of the sample. Two examples of dislocation bundles are indicated with white arrows. Such threading dislocations in CVD synthetic diamond are usually formed at the substrate/layer interface and penetrate through the overgrowth by propagating along the [001] growth direction (Friel et al., 2009; Pinto and Jones, 2009).

The DiamondView images in figure 4 were taken from the top (growth side; upper right) and from the bottom (substrate side; lower left) of sample A, and showed a blue to blue-green "picture frame" corresponding to the interface between the subsequent CVD layers but also above the substrate imprint. In addition to the "picture frame," numerous sharp violetish blue linear features were observed; these are related to the dislocation bundles.

From the substrate side, sample A also showed a weak-to-strong red luminescence. This red luminescence originates from NV^0 and NV^- centers at 575

and 637 nm and is characteristic of trace nitrogen incorporation in this particular region of the sample. Previous measurements have shown that when no nitrogen is intentionally added to the gas phase, the

NEED TO KNOW

- Production of large single-crystal CVD synthetic diamonds typically involves multiple growth runs.

- Blue to blue-green luminescent zones may be created when the growth run is interrupted and resumed.

- DiamondView, photoluminescence, and cathodoluminescence imaging were applied to study the origin and nature of these luminescent zones.

- Both silicon and boron showed preferential incorporation at the interface between CVD layers, though the exact cause of the luminescence is still under investigation.

nitrogen content in the synthetic diamond crystal is below 10 ppb (Tallaire et al., 2006), which is believed to be the case here. The incorporation of nitrogen impurities in the crystal was not uniform, however, since no red luminescence was observed on the other side of the sample.

Blue to blue-green phosphorescence lasting up to several seconds was observed (figure 4; lower right). Similar phosphorescence has been documented in HPHT-grown synthetic and treated blue type IIb diamond crystals (Watanabe et al., 1997; Lu and Eaton-Magaña, 2009). Boron-doped blue type IIb synthetic diamonds exhibit a blue to blue-green phosores-

cence peak with a maximum at ~500 nm. In contrast, virtually all natural blue type IIb gem diamonds exhibit two phosphorescence peaks, one at ~500 nm (blue-green) and the other at ~660 nm (orange-red). In addition, it was reported that an HPHT-treated blue diamond only exhibited a peak at 500 nm (Eaton-Magana et al., 2008). These results suggest that phosphorescence spectroscopy might be an effective tool for discriminating synthetic from natural blue diamonds. In this study we report for the first time the observation of this blue to blue-green phosphorescence in (near-)colorless CVD synthetic diamond crystals where boron is present as a background impurity, as no boron was intentionally added during the growth process.

The origin of this phosphorescence has been attributed to the generally accepted donor-acceptor recombination mechanism (Dean et al., 1965), where holes bound to boron acceptors recombine with electrons that are bound to donors and emit luminescence with energy equal to the difference in energy between the donor and acceptor. The identity of the donor impurities is still under debate.

Cathodoluminescence Imaging. As shown in figure 3 (right), the interface between two successive CVD layers was clearly visible with CL imaging. The interface was slightly roughened and showed the appearance of typical etching features.

CL spectroscopy of sample B was performed in a previous study (Tallaire et al., 2011), and clearly showed the presence of boron impurities. However, it was not possible to draw conclusions about nitrogen incorporation from the CL observations.

Photoluminescence Spectroscopy and Imaging. The normalized PL emission intensity profiles of selected optical defects (NV^0 at 575.0 nm, NV^- at 637.2 nm, and a $[Si-V]^-$ doublet at 736.6–736.9 nm) on the substrate side are shown in figure 5 (right). The analyzed area is marked with an arrow in the DiamondView image in figure 5 (left). The NV luminescence decreased progressively from the edge of the layer toward the interior. The most striking feature was a sharp increase in the $[Si-V]^-$ doublet emission near the blue luminescence band. (Note: Features in the PL line scan do not reflect the strong red/orange band visible in the DiamondView image. PL measurements in the confocal mode used in this study analyze a restricted volume, and the data in figure 5 were obtained from the near-surface. Based on PL depth profile measurements [see below], there is a
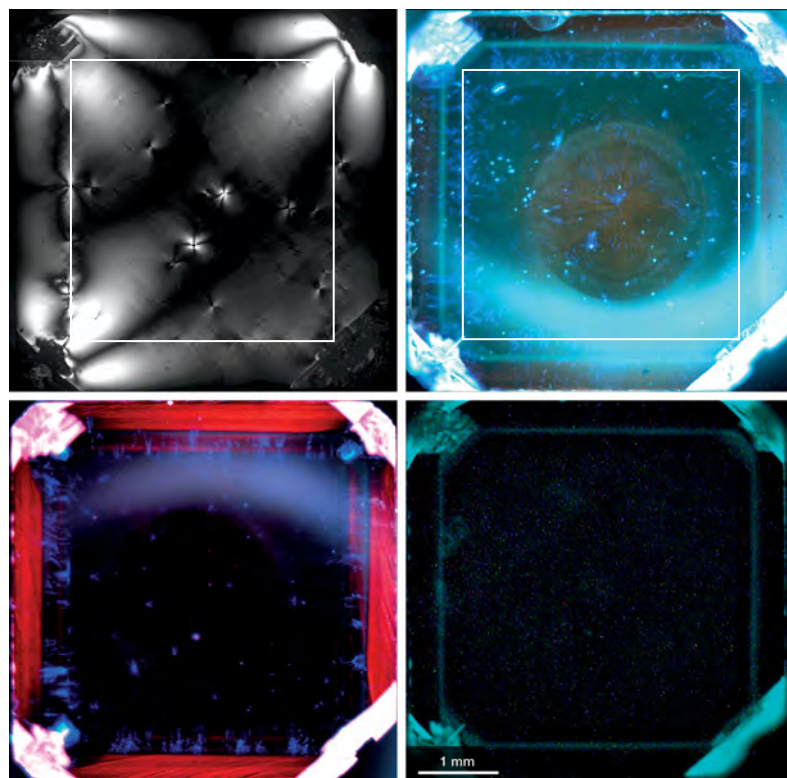
Figure 4. Strain-related birefringence (top left) was observed between crossed polarizing filters in sample A. The substrate's imprint is indicated (white square), as are two examples of dislocation bundles (arrows). In DiamondView images of the growth side (top right) and the substrate side (bottom left), a square "picture frame" corresponds to the interface between the subsequent CVD layers. The dark circular outline indicates the position of the vacuum sample manipulator. The corresponding phosphorescence image of sample A (bottom right) was recorded with a delay time of 1 millisecond. The "picture frame" is clearly presented in the phosphorescence image.
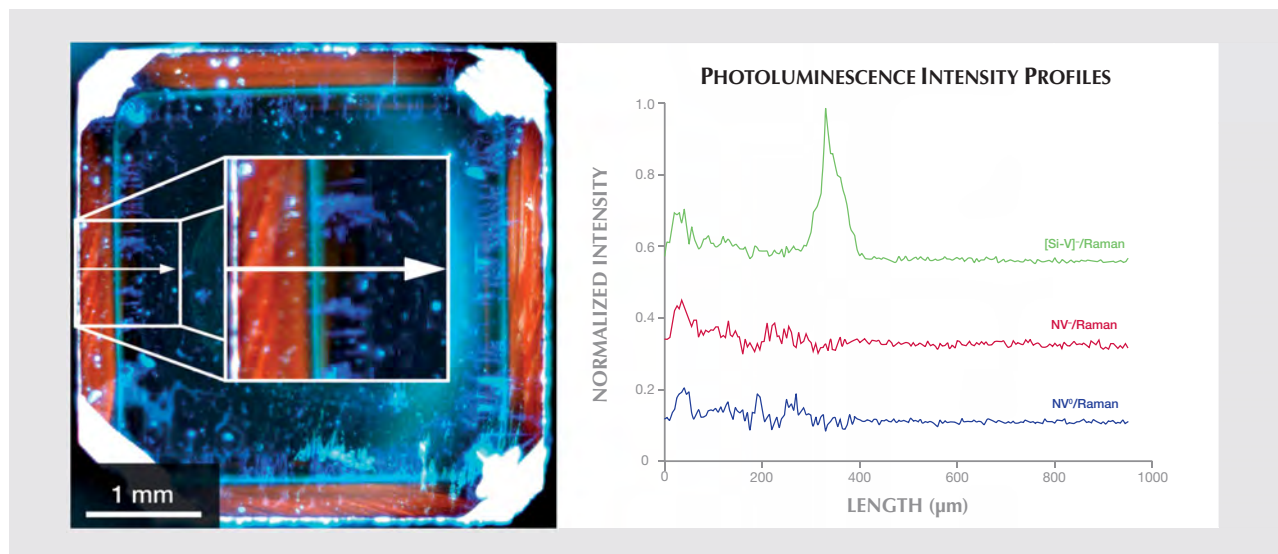
Figure 5. DiamondView imaging (left) and normalized photoluminescence intensity profiles (right) of NV^0 (575.0 nm), NV^- (637.2 nm), and $[Si\text{-}V]^-$ (736.6–736.9 nm) from the substrate side of sample A show a decrease in NV luminescence from the edge to the interior, and a sharp increase in the $[Si\text{-}V]^-$ doublet emission near the blue luminescence band.

great amount of NV luminescence centers present at depth. Also, the DiamondView image shows both fluorescence and phosphorescence; the blue to blue-green phosphorescence is much stronger and overwhelms the red-orange fluorescence.)

A combination of line and depth profiles generates 2D images reflecting the PL intensity of the diamond Raman line and the luminescence associated with the NV^0, NV^-, and $[Si\text{-}V]^-$ centers, as shown in figure 6. The $[Si\text{-}V]^-$ associated luminescence is clearly localized in a well-defined zone, and extends vertically over several tens of micrometers. Its location is consistent with the interface between the two CVD layers, suggesting preferential incorporation, as with boron. In contrast, nitrogen does not show clearly preferential incorporation.

Boron, one of the main impurities reported to cause phosphorescence, was clearly detected in both samples (see also Tallaire et al., 2011). In addition, silicon was found to be incorporated at the interrupted interface where new dislocations were formed. Although NV centers were absent, nitrogen could still be present as isolated single substitutional impurities not causing direct luminescence. The cause of the phosphorescence at the growth interruption cannot be fully determined at this time, and further studies will be required to identify the contribution of silicon, nitrogen, and dislocations.

CONCLUSIONS

Analysis using complementary luminescence spectroscopy and imaging techniques identified preferential incorporation of trace impurities in the CVD synthetic diamond crystals, especially at the interface between successive layers. CL analysis confirmed that boron is present at the interrupted inter-

Figure 6. Photoluminescence depth profiles of the substrate side of sample B were used to create the two-dimensional maps on the right, which reflect the PL intensities of the Raman line and NV^0, NV^-, and $[Si\text{-}V]^-$ centers. The $[Si\text{-}V]^-$ luminescence is clearly localized along the interface between the two growth layers.
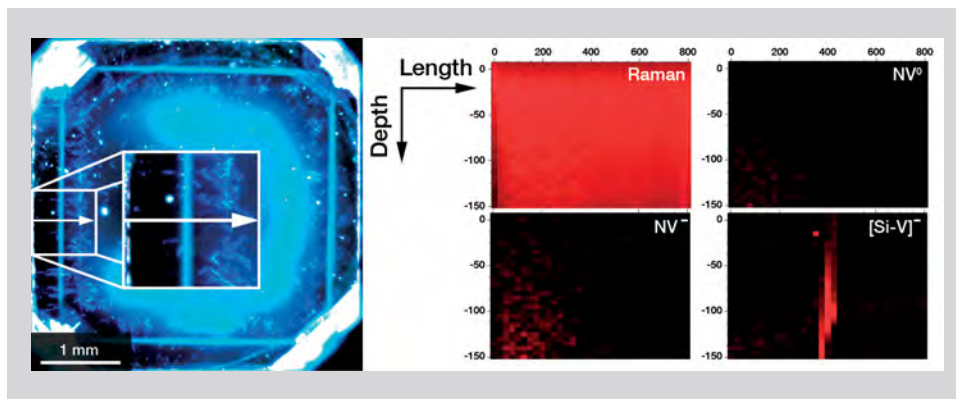
face, while PL showed the presence of silicon-related defects. All these impurities are present at background levels in the CVD reactor chamber. We propose that the uptake of these impurities is enhanced at the growth resumption of the crystal, leading to the appearance of a distinct luminescent pattern. On the microscopic level, the surface is roughened by the formation of etch pits that decorate threading dislocations. The surface roughening enhances the uptake of these impurities and also the generation of new threading dislocations.

The samples in this study were too thin to be cut into gemstones, but larger samples are technologically feasible. It is likely that CVD growth techniques will continue to improve, resulting in purer and larger CVD synthetic diamonds entering the gem market. The spatial distribution of spectroscopic features is important for CVD synthetic diamond identification, as they can provide evidence of the growth history and, in particular, growth interruptions that are commonly used for the synthesis of large crystals. Moreover, typical luminescence features associated with CVD synthetic diamonds (such as NV^0, NV^-, and $[Si-V]^-$), as reported in the literature (Martineau et al., 2004), were also clearly detected in this study.

The identification of CVD synthetic diamonds depends on a combination of various gemological and spectroscopic features, as no single feature will ensure proper identification. The observations obtained in this study by DiamondView, cathodoluminescence, and photoluminescence spectroscopy and imaging showed typical CVD-related optical centers. The discrete growth interruptions between subsequent CVD layers can be monitored and visualized. As such, the observations unambiguously confirmed the synthetic origin of these samples. The combination of these techniques is fully applicable in the detection and identification of natural and synthetic gem diamonds.

ABOUT THE AUTHORS
Dr. Willems (bert.willems@hrdantwerp.be) is a research scientist in the Research department of HRD Antwerp, Belgium. Dr. Tallaire is a research associate at Centre National de la Recherche Scientifique (CNRS), within the Laboratoire des Sciences des Procédés et des Matériaux (LSPM), Villetaneuse, France. Dr. Barjon is a lecturer at the Université de Versailles Saint-Quentin en Yvelines (Groupe d'Etude de la Matière Condensée, GEMaC), Meudon, France.

REFERENCES

Achard J., Tallaire A., Sussmann R., Silva F., Gicquel A. (2005) The control of growth parameters in the synthesis of high-quality single crystalline diamond by CVD. *Journal of Crystal Growth*, Vol. 284, pp. 396–405, http://dx.doi.org/10.1016/j.jcrysgro.2005.07.046.

Collins A.T. (1992) The characterization of point defects in diamond by luminescence spectroscopy. *Diamond and Related Materials*, Vol. 1, pp. 457–469, http://dx.doi.org/10.1016/0925-9635(92)90146-F.

Dean P.J., Lightowlers E.C., Wight D.R. (1965) Intrinsic and extrinsic recombination from natural and synthetic aluminum-doped diamond. *Physical Review*, Vol. 140, No. 1A, pp. A352–A368, http://dx.doi.org/10.1103/PhysRev.140.A352.

Denisenko A., Kohn E. (2005) Diamond power devices. Concepts and limits. *Diamond and Related Materials*, Vol. 14, No. 3–7, pp. 491–498, http://dx.doi.org/10.1016/j.diamond.2004.12.043.

Eaton-Magaña S., Post J.E., Heaney P.J., Freitas J., Klein P., Walters R., Butler J.E. (2008) Using phosphorescence as a fingerprint for the Hope and other blue diamonds. *Geology*, Vol. 36, pp. 83–86, http://dx.doi.org/10.1130/G24170A.1.

Friel I., Clewes S.L., Dhillon H.K., Perkins N., Twitchen D.J., Scarsbrook G.A. (2009) Control of surface and bulk crystalline quality in single crystal diamond grown by chemical vapour deposition. *Diamond and Related Materials*, Vol. 18, pp. 808–815, http://dx.doi.org/10.1016/j.diamond.2009.01.013.

Ho S.S., Yan C.S, Liu Z., Mao H.K., Hemley R.J. (2006) Prospects for large single crystal CVD diamond. *Industrial Diamond Review*, Vol. 66, pp. 28–32.

Kone S., Civrac G., Schneider H., Isoird K., Issaoui R., Achard J., Gicquel A. (2010) CVD diamond Schottky barrier diode, carrying out and characterization. *Diamond and Related Materials*, Vol. 19, pp. 792–795, http://dx.doi.org/10.1016/j.diamond.2010.01.036.

Lu R., Eaton-Magaña S. (2009) Lab Notes: Fancy Intense blue type IIb synthetic diamond. *G&G*, Vol. 45, No. 4, pp. 291–292, http://dx.doi.org/10.5741/GEMS.45.4.288.

Martineau P.M., Lawson S.L., Taylor A.J., Quinn S.J., Evans D.J.F., Crowder M.J. (2004) Identification of synthetic diamond grown using chemical vapor deposition. *G&G*, Vol. 40, No. 1, pp. 2–25, http://dx.doi.org/10.5741/GEMS.40.1.2.

Pinto H., Jones R. (2009) Theory of the birefringence due to dislocations in single crystal CVD diamond. *Journal of Physics: Condensed Matter*, Vol. 21, Art. 364220 (7 pp.), http://dx.doi.org/10.1088/0953-8984/21/36/364220.

Tallaire A., Collins A.T., Charles D., Achard J., Sussmann R., Gicquel A., Newton M.E., Edmonds A.M., Cruddace R.J. (2006) Characterisation of high-quality thick single-crystal diamond grown by CVD with a low nitrogen addition. *Diamond and Related Materials*, Vol. 15, pp. 1700–1707, http://dx.doi.org/10.1016/j.diamond.2006.02.005.

Tallaire A., Barjon J., Brinza O., Achard J., Silva F., Mille V., Issaoui R., Tardieu A., Gicquel A. (2011) Dislocations and impurities from etch-pits at the epitaxial growth resumption of diamond. *Diamond and Related Materials*, Vol. 20, pp. 875–881, http://dx.doi.org/10.1016/j.diamond.2011.04.015.

Walker J. (1979) Optical absorption and luminescence in diamond. *Reports of Progress in Physics*, Vol. 42, pp. 1605–1659, http://dx.doi.org/10.1088/0034-4885/42/10/001.

Watanabe K., Lawson S.C., Isoya J., Kanda H., Sato Y. (1997) Phosphorescence in high-pressure synthetic diamond. *Diamond and Related Materials*, Vol. 6, pp. 99–106, http://dx.doi.org/10.1016/S0925-9635(96)00764-9.

IDENTIFICATION OF EXTRATERRESTRIAL PERIDOT BY TRACE ELEMENTS

Andy H. Shen, John I. Koivula, and James E. Shigley

Twenty-six peridot samples from the Esquel pallasite meteorite and 27 samples from 10 terrestrial sources were studied by laser ablation–inductively coupled plasma–mass spectrometry (LA-ICP-MS). Among the 32 elements analyzed, six of them—Li, V, Mn, Co, Ni, and Zn—provided an excellent separation between pallasitic and terrestrial peridot.

Peridot, known by the ancient Egyptians as "the gem of the sun," has long been valued as a gemstone. It was mined on Zabargad (now St. John's Island) in the Red Sea some 3,500 years ago, making it one of the earliest known gemstones (Gübelin, 1981; Ogden, 1992). Peridot is the gem-quality green variety of olivine, an important mineral found in ultramafic igneous rocks such as dunite and in mafic rocks such as basalt. Among the major modern productive localities, the main sources of peridot are peridotite xenoliths in alkali basalts (U.S., Myanmar, China) and serpentinized dunites (Pakistan).

Olivine is believed to be one of the major minerals in the earth's mantle and in many rocky planets and smaller bodies in the solar system. Pallasite is a rare type of stony iron meteorite that contains gem-quality crystalline olivine in an iron-nickel matrix (figure 1). It is believed to have formed in asteroids composed of an iron-nickel core and a silicate mantle (Dodd, 1981). The olivine crystals can be extracted from some of these meteorites to make beautiful—although typically small—faceted gems (Koivula et al., 1993a,b, 1994). Pallasitic peridot gemstones were first characterized in 1991, and the subsequent report by Sinkankas et al. (1992) found that their optical and physical properties, such as refractive index and specific gravity, were very similar to and overlapped those of their terrestrial counterparts, negating any useful separation through standard gemological testing.

Nevertheless, the inclusion suites of pallasitic peridot can be quite telling, allowing relatively easy separation from terrestrial material (e.g., Koivula, 1981; Koivula and Fryer, 1986; Milisenda et al., 1996; figures 2 and 3) by means of magnification. In addition, due to pallasite's fiery descent through earth's atmosphere, inclusion-free extraterrestrial olivine of significant size (>1 ct) is virtually unheard of. Olivine is generally heat- and impact-sensitive and is prone to cracking, so any peridot pieces extracted from such meteorites are typically fractured, and any gems fashioned from them usually weigh less than half a carat.

Because pallasitic peridot is a commercially available extraterrestrial gem, there is sufficient interest to make its identification worthwhile. A peridot without diagnostic inclusion features requires chemical analysis to make the determination. We used LA-ICP-MS to study the trace-element chemistry because of the wide range of elements this technique can analyze, as well as its superior sensitivity.

Figure 1. These polished pallasitic peridot specimens (50.00 and 25.66 ct) are from the Esquel meteorite, which was found in Argentina in 1951. Photo by Maha Smith.

In terms of chemical composition, olivine is among the most extensively studied minerals, with scores of published studies on major and trace-element chemistry of samples from many natural occurrences. In the GEOROC database maintained by the Max Planck Institute for Chemistry in Mainz, Germany (http://georoc.mpch-mainz.gwdg.de/georoc), more than 40,000 records are dedicated to olivine. Yet geochemical studies focusing on gem-quality peridot are very limited, and not all trace elements are included in GEOROC's data. The gemological literature contains very few papers on pallasitic peridot (see Sinkankas et al., 1992; Pearson, 2009), let alone detailed studies of its trace-element composition. To our knowledge, though much research has been published on the trace-element composition of olivine in pallasite (see Hsu, 2003 and the references therein), most of the literature is focused on deducing the parent body or the thermal history of the pallasites, and very few articles have mentioned terrestrial olivine at all. One recent study (Leelawatanasuk et al., 2011) specifically focused on comparing gem peridots from terrestrial and extra-terrestrial sources, though using EDXRF rather than LA-ICP-MS. In this article, we present our chemical analysis results comparing pallasitic peridots to

Figure 2. Cruciform acicular dislocations have been observed in pallasitic peridot. Such features have not been seen in terrestrial material. Photomicrograph by J. I. Koivula; magnified 15×.
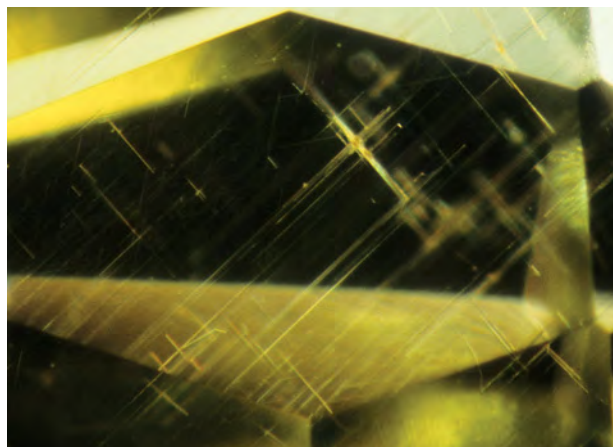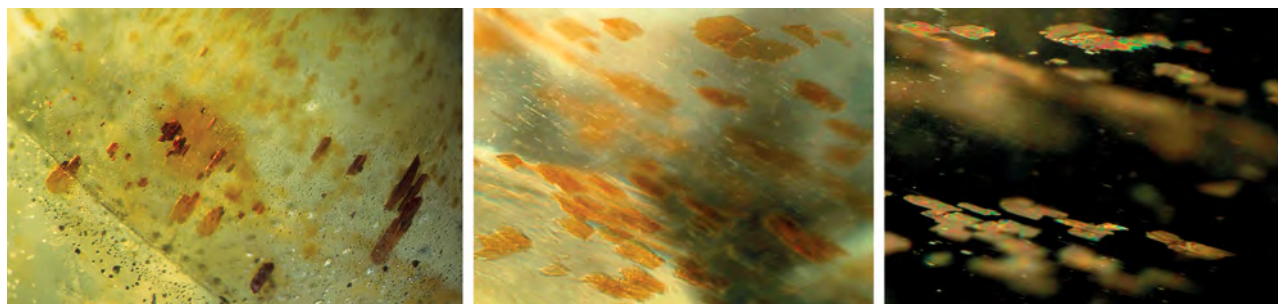
Figure 3. Other internal features distinctive of pallasitic peridot are striated brownish red plates (left) and thin transparent reddish brown platy inclusions (center); the platy inclusions also showed iridescence (right). Neither type of inclusion could be identified with Raman analysis. Photomicrographs by J. I. Koivula; magnified 80× (left) and field of view 1.2 mm (center and right).

natural samples from several known terrestrial localities.

MATERIALS AND METHODS

Twenty-six samples of pallasitic peridot and 27 terrestrial samples were examined as part of this study. The latter consisted of 22 pieces of rough, four faceted stones, and one cabochon (table 1). Three of the pallasitic peridot samples were faceted stones, but the remainder were still in matrix as part of three polished slabs from the Esquel meteorite (e.g., figure 1).

We performed chemical analyses with a Thermo X Series II ICP-MS. A New Wave Research UP-213 laser ablation unit with a frequency-quintupled Nd:YAG laser (213 nm wavelength) running at 4 ns

pulse width was chosen to ablate the samples. We used 55 μm diameter laser spots, a fluence of around 10 J/cm^2, and a 7 Hz repetition rate. For most of the terrestrial samples, we selected three spots for analysis, though some of the rough was tested on up to six spots. The faceted pallasitic samples received three analysis spots and the pieces in the slabs only two. For the ICP operations, the forward power was set at 1300 W and the typical nebulizer gas flow was ~0.90 l/min. The carrier gas used in the laser ablation unit was He, set at 0.78 l/min. The actual nebulizer flow rate varied somewhat from run to run. The criteria for the alignment and tuning sequence were to maximize Be counts and keep the ThO/Th ratio below 2%. We used National Institute of Standards and Technology SRM (standard reference

TABLE 1. Terrestrial peridot samples used in this study.

Locality	No. samples	Weight (ct)	Description	Source[a]	References
China	2	2.98–4.51	Emerald and triangular cut	GIA	Huang and Xu (2010)
Hawaii, USA	1	0.48	Rough	JIK	Baker et al. (1996)
Kilbourne Hole, Texas, USA	2	2.06–2.88	Rough	GIA	Bussod and Williams (1991), Fuhrbach (1992)
San Carlos, Arizona, USA	3	1.17–10.85	Rough and oval cut	GIA, JIK	Frey and Prinz (1978)
Mogok, Myanmar	2	0.93–1.90	Rough	GIA	Webb (1993)
Norway	2	9.53–17.11	Oval cut	GIA	Kostenko et al. (2002)
Pakistan	3	0.64–15.11	Rough and cabochon	GIA	Kane (2004), Bouilhol et al. (2009)
Saudi Arabia	4	1.60–2.88	Rough	JR	McGuire (1988), Camp et al. (1992)
Tanzania	2	2.49–2.79	Rough	GIA	Furman (2007)
Zabargad (St. John's Island), Egypt	6	2.33–5.17	Rough	LT, JH	Kurat et al. (1993), Brooker et al. (2004)

[a] *Initials other than GIA refer to authors or those listed in the Acknowledgments.*

material) 610 and 612 glasses for calibration. We analyzed three spots apiece on the standards at the beginning of the experiment; after every four to five sample runs, three additional spots were measured. This process allowed us to correct the drift of the instrument.

To obtain accurate and precise trace-element chemistry, we selected ^{29}Si as our internal standard. To determine the accurate concentration of Si, we used the method developed by Breeding and Shen (2008), renormalizing each experimental run into a model molecular formula of $(Mg,Fe,Mn,Ni)_2SiO_4$ and then calculating the Si concentration from that formula. The calculated Si concentrations were used as internal standard values for experimental runs, and the concentrations of the other 27 trace elements were then calculated.

RESULTS AND DISCUSSION

Table 2 shows the chemical elements that can be used to separate pallasitic and terrestrial peridot. Most olivines belong to a complete solid-solution series between forsterite (Mg_2SiO_4) and fayalite (Fe_2SiO_4). Tephroite (Mn_2SiO_4) and Ni-olivine (Ni_2SiO_4) have the same olivine structure and can form a solid solution—typically in small amounts—with forsterite and fayalite. Most peridot falls toward the forsterite end of the solid solution. The major-element composition of our samples is given in table 2 as molar percent forsterite. This limited range of compositional variation accounts for the restricted variability of the gemological properties (Phillips and Griffen, 1981; Deer, et al., 1982).

TABLE 2. Concentration ranges of diagnostic trace elements, and gemological properties, of tested peridot samples.

Element (ppm)	Terrestrial	Extraterrestrial
Li	1.10–14.5	0.21–0.96
V	0.11–4.46	9.18–23.4
Mn	772–1410	1920–2490
Co	84.8–147	4.37–19.6
Ni	1770–4070	8.53–112
Zn	9.04–67.4	5.20–9.98
Molar fraction (forsterite%)	$Fo_{96.0}$–$Fo_{88.6}$	$Fo_{90.0}$–$Fo_{85.5}$
SG[a]	3.27–3.36	3.35–3.40
RI (n_α)[a]	1.640–1.655	1.652–1.662
RI (n_β)[a]	1.657–1.675	1.670–1.683
RI (n_γ)[a]	1.680–1.693	1.690–1.703

[a] Values estimated (RI) or calculated (SG) from Deer et al. (1982).
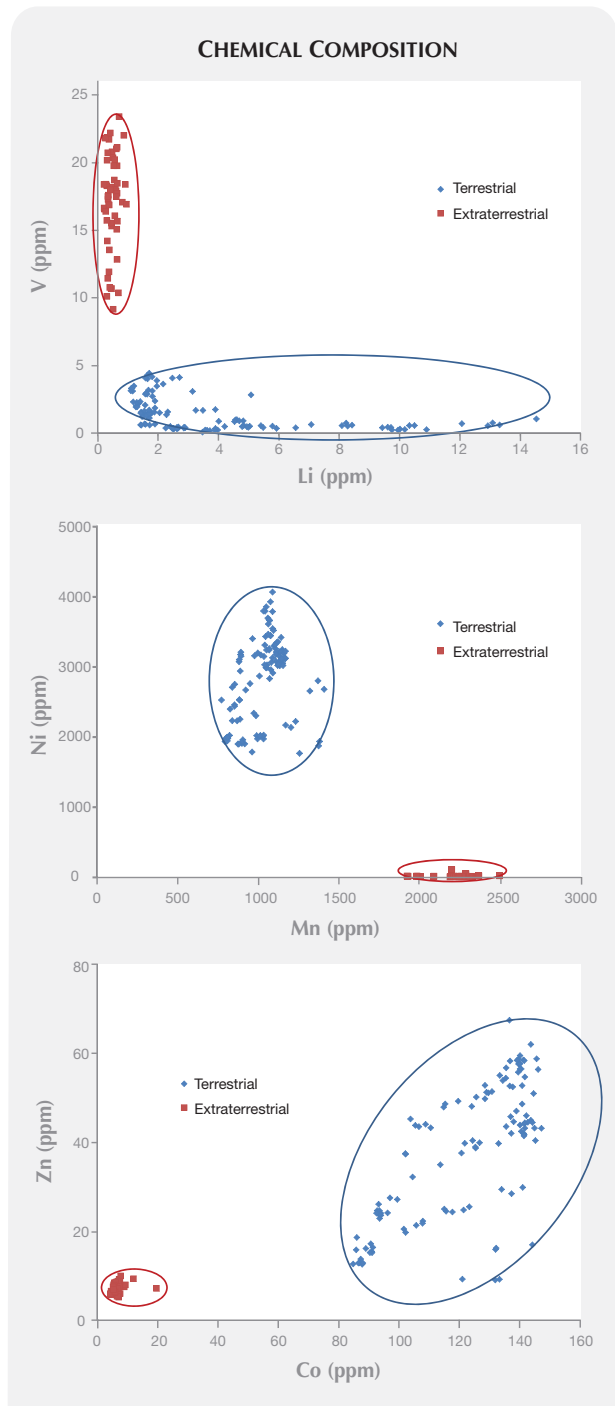
Figure 4. Chemical plots of vanadium vs. lithium (top), nickel vs. manganese (middle), and zinc vs. cobalt (bottom) all show an obvious separation between the extraterrestrial and terrestrial peridot groups. The concentration ranges of these elements are listed in table 2.

Of the 32 elements studied, six—Li, V, Mn, Co, Ni, and Zn—were diagnostic. Figure 4 (top) is a plot of V vs. Li, which displays an obvious separation between pallasitic and terrestrial peridot. The same observations are seen in the plots of Ni vs. Mn (figure 4, middle) and Zn vs. Co (figure 4, bottom). In all three of these plots, the data points for the samples of pallasitic and terrestrial origin are clearly segregated. When we compared our extraterrestrial data set with published pallasitic olivine chemical data, our Ni, Co, and Mn concentrations agreed with the results in Hsu (2003) almost perfectly. All but one of these six elements, Li, can also be determined using EDXRF, but the concentrations of V in terrestrial peridot and those of Co and Zn in pallasitic peridot may be difficult to detect or determine accurately with EDXRF because they are so low. However, if an EDXRF instrument can accurately determine Mn and Ni, then it is possible to perform the separation based on these two elements alone (Leelawathanasuk et al., 2011).

Although we analyzed a limited number of peridot samples from a single pallasite and various terrestrial sources, each group showed remarkable consistency. Leelawatanasuk et al. (2011) studied four different pallasite meteorites, and their results also showed good consistency among those samples. In addition, our major-element compositional data agreed well with the chemistry of most pallasitic olivines (from over 40 fall locations) listed in Wasson and Choi (2003). This consistency in major-element chemistry has been noted in the literature.

Figure 5. Though its rarity limits its commercial significance, pallasite can make an attractive gemstone. This faceted stone (1.12 ct) from the Esquel pallasite is resting on a polished slab that was cut from the same meteorite. Courtesy of Robert A. Haag; photo by Robert Weldon.

CONCLUSION

Twenty-six samples of pallasitic peridot and 27 representative samples from 10 world localities were analyzed by LA-ICP-MS. The results showed that six elements—Li, V, Mn, Co, Ni, and Zn—provided excellent separation between pallasitic (figure 5) and terrestrial origin. The collection of additional data on pallasitic and terrestrial peridot is ongoing.

REFERENCES

Baker M.B., Alves S., Stolper E.M. (1996) Petrography and petrology of the Hawaii Scientific Drilling Project lavas: Inferences from olivine phenocryst abundances and compositions. *Journal of Geophysical Research–Solid Earth*, Vol. 101, No. B5, pp. 11751–11727, http://dx.doi.org/10.1029/96JB00180.

Bouilhol P., Burg J.P., Bodinier J.L., Schmidt M.W., Dawood H., Hussain S. (2009) Magma and fluid percolation in arc and forearc mantle: Evidence from Sapat (Kohistan, northern Pakistan). *Lithos*, Vol. 107, No. 1/2, pp. 17–37, http://dx.doi.org/10.1016/j.lithos.2008.07.004.

Breeding C.M., Shen A.H. (2008) Quantitative major element chemical analysis using LA-ICP-MS: Gem feldspar and tourmaline. *Winter Conference on Plasma Spectrochemistry*, Temecula, CA, January 7–12, Abstract WP21.

Brooker R.A., James R.H., Blundy J.D. (2004) Trace elements and Li isotope systematics in Zabargad peridotites: Evidence of ancient subduction processes in the Red Sea mantle. *Chemical Geology*, Vol. 212, No. 1/2, pp. 179–204, http://dx.doi.org/10.1016/j.chemgeo.2004.08.007.

Bussod G.Y.A., Williams D.R. (1991) Thermal and kinematic model of the southern Rio Grande Rift: Inferences from crustal and mantle xenoliths from Kilbourne Hole, New Mexico. *Tectonophysics*, Vol. 197, No. 2/4, pp. 373–389, http://dx.doi.org/10.1016/0040-1951(91)90051-S.

Camp V.E., Roobol M.J., Hooper P.R. (1992) The Arabian continental alkali basalt province: Part III. Evolution of Harrat Kishb, Kingdom of Saudi Arabia. *Geological Society of America Bulletin*, Vol. 104, No. 4, pp. 379–396, http://dx.doi.org/10.1130/0016-7606(1992)104<0379:TACABP>2.3.CO;2.

Deer W.A., Howie R.A., Zussman J. (1982) *Rock-Forming Minerals*, Vol. 1a—Orthosilicates, Longman, London, 919 pp.

Dodd R.T. (1981) *Meteorites: A Petrologic-Chemical Synthesis*. Cambridge University Press, Cambridge, UK, 368 pp.

Frey F.A., Prinz M. (1978) Ultramafic inclusions from San Carlos, Arizona: Petrological and geochemical data bearing on their petrogenesis. *Earth and Planetary Science Letters*, Vol. 38, No. 1, pp. 129–176, http://dx.doi.org/10.1016/0012-821X(78)90130-9.

Fuhrbach J.R. (1992) Kilbourne Hole peridot. *G&G*, Vol. 28, No. 1, pp. 16–27, http://dx.doi.org/10.5741/GEMS.28.1.16.

Furman T. (2007) Geochemistry of the East African Rift basalts: An overview. *Journal of African Earth Sciences*, Vol. 48, No. 2/3, pp. 147–160, http://dx.doi.org/10.1016/j.jafrearsci.2006.06.009.

Gübelin E. (1981) Zabargad: The ancient peridot island in the Red Sea. *G&G*, Vol. 17, No. 1, pp. 2–8, http://dx.doi.org/10.5741/GEMS.17.1.2.

Hsu W. (2003) Minor element zoning and trace element geochemistry of pallasites. *Meteoritics & Planetary Sciences*, Vol. 38, No. 8, pp. 1217–1241, http://dx.doi.org/10.1111/j.1945-5100.2003.tb00309.x.

Huang X.L., Xu Y.G. (2010) Thermal state and structure of the lithosphere beneath eastern China: A synthesis on basalt-borne xenoliths. *Journal of Earth Science*, Vol. 21, No. 5, pp. 711–730, http://dx.doi.org/10.1007/s12583-010-0111-3.

Kane R.E. (2004) The creation of a magnificent suite of peridot jewelry: From the Himalayas to Fifth Avenue. *G&G*, Vol. 40, No. 4, pp. 288–302, http://dx.doi.org/10.5741/GEMS.40.4.288.

Koivula J.I. (1981) San Carlos peridot. *G&G*, Vol. 17, No. 4, pp. 205–214, http://dx.doi.org/10.5741/GEMS.17.4.205.

Koivula J.I., Fryer C.W. (1986) The gemological characteristics of Chinese peridot. *G&G*, Vol. 22, No. 1, pp. 38–40, http://dx.doi.org/10.5741/GEMS.22.1.38.

Koivula J.I., Kammerling R.C., Fritsch E., Eds. (1993a) Gem News: Extraterrestrial gem materials. *G&G*, Vol. 29, No. 1, pp. 55–56, http://dx.doi.org/10.5741/GEMS.29.1.52.

Koivula J.I., Kammerling R.C., Fritsch E., Eds. (1993b) Gem News: Meteorites with gems. *G&G*, Vol. 29, No. 4, p. 293, http://dx.doi.org/10.5741/GEMS.29.4.285.

Koivula J.I., Kammerling R.C., Fritsch E., Eds. (1994) Gem News: Miscellaneous notes on peridot. *G&G*, Vol. 30, No. 1, p. 53, http://dx.doi.org/10.5741/GEMS.30.1.47.

Kostenko O., Jamtveit B., Austrheim H., Pollok K., Putnis C. (2002) The mechanism of fluid infiltration in peridotites at Almklovdalen, western Norway. *Geofluids*, Vol. 2, No. 3, pp. 203–215, http://dx.doi.org/10.1046/j.1468-8123.2002.00038.x.

Kurat G., Palme H., Embey-Isztin A., Touret J., Ntaflos T., Spettel B., Brandstätten F., Palme C., Dreibus G., Prinz M. (1993) Petrology and geochemistry of peridotites and associated vein rocks of Zabargad Island, Red Sea, Egypt. *Mineralogy and Petrology*, Vol. 48, No. 2/4, pp. 309–341, http://dx.doi.org/10.1007/BF01163106.

Leelawatanasuk T., Atichat W., Sutthirat C., Wathanakul P., Sriprasert B., Naruedeesombat N., Srithunayothin P., Davies S. (2011) Pallasitic peridot: The gemstone from outer space. *Proceedings of the 32nd International Gemmological Conference*, Interlaken, Switzerland, July 13–17, pp. 110–113.

McGuire A.V. (1988a) Petrology of mantle xenoliths from Harrat al Kishb: The mantle beneath western Saudi Arabia. *Journal of Petrology*, Vol. 29, No. 1, pp. 73–92.

Milisenda C.C., Bank H., Henn A. (1995) Peridot aus Pakistan. *Gemmologie: Zeitschrift der Deutschen Gemmologischen Gesellschaft*, Vol. 44, No. 2/3, pp. 33–42.

Ogden J. (1992) *Ancient Jewellery*. University of California Press, Berkeley, CA, 64 pp.

Pearson G. (2009) Meteorites: Origins, properties and gemological significance. *Australian Gemmologist*, Vol. 23, No. 10, pp. 457–472.

Phillips W.R., Griffen D.T. (1981) *Optical Mineralogy: The Nonopaque Minerals*. W.H. Freeman and Company, San Francisco, CA, 677 pp.

Sinkankas J., Koivula J.I., Becker G. (1992) Peridot as an interplanetary gemstone. *G&G*, Vol. 28, No. 1, pp. 43–51, http://dx.doi.org/10.5741/GEMS.28.1.43.

Wasson J.T., Choi B.-G. (2003) Main-group pallasites: Chemical composition, relationship to IIIAB irons, and origin. *Geochimica et Cosmochimica Acta*, Vol. 67, No. 16, pp. 3079–3096, http://dx.doi.org/10.1016/S0016-7037(03)00306-5.

Webb G. (1993) An important peridot. *Australian Gemmologist*, Vol. 18, No. 6, pp. 191–193.

A HISTORY OF DIAMONDS THROUGH PHILATELY: THE FRANK FRIEDMAN COLLECTION

Stuart D. Overlin

South African jeweler Frank Friedman's collection of diamond-themed stamps and other postal material offers an illuminating visual record of diamond history. Comprising approximately 2,000 pieces, these items chronicle diamond formation, the history of mining and manufacturing, and the evolution of a science and an industry built around this remarkable gemstone.

Philately, the collecting of stamps and other postal material, first became popular with the introduction of the British penny and two-penny adhesive stamps in 1840. Much of the hobby's attraction lies in the range of fascinating subjects that have been documented. Diamonds have appeared in postage stamps, special cancellation marks, and postcards issued by numerous countries, especially those with ties to the industry (figure 1). The present article reviews one important collection of such material.

Frank Friedman (figure 2) has spent much of his life in the South African gem and jewelry industry. He joined the family enterprise, J. Friedman Jewellers, as an apprentice goldsmith in 1959 and helped build it into one of the country's top retailers. In 1985 he established F. Friedman Jewellers, which was rebranded as Frankli Wild in 1999.

Mr. Friedman began collecting stamps in 1961, inspired by a jewelry magazine article that described

the hobby as "the poor man's way to collect gems" (Friedman, 2007). He joined the Johannesburg Philatelic Society to learn more and began to acquire pieces. His collection now totals approximately 2,000 items from more than 36 countries. In addition to stamps, it contains rare postcards, cancellation marks, historical letters, and original artists' renderings of stamp and cancellation designs.

Mr. Friedman has displayed his collection internationally on several occasions. In 1989 it was showcased in the Harry Oppenheimer Museum at the Israeli Diamond Center in Ramat Gan. In June 1997, it was the keynote exhibit at the Vicenza Trade Fair (Weil, 1997). Awards include a gold medal at the 2006 World Philatelic Exhibition in Washington ("Stamp of approval," 2006), a 2008 silver medal at the World Stamp Championship in Israel, and a large vermeil medal at the 26th Asian International Stamp Exhibition (Joburg 2010).

HIGHLIGHTS FROM THE COLLECTION

Selected items from the Friedman collection, arranged thematically, are described below. These were chosen for their historical and educational value.

Diamond Origins. The pair of stamps in figure 3 depicts the eruptive emplacement of diamonds on the earth's surface. The 1973 Lesotho stamp provides a cross-section of a diamond-bearing kimberlite pipe. The artist's rendering for a 1993 stamp from the Tongan island of Niuafo'ou shows an erupting volcano juxtaposed with diamond crystals and a polished stone.

History of Prospecting and Mining. Throughout much of recorded history, India was the world's sole diamond source. After alluvial diamonds began to

Figure 1. These diamond-themed stamps issued by various countries are shown with seven rough crystals (1.24–22.32 ct). The diamonds were donated to GIA by De Beers chairman Ernest Oppenheimer in 1955. Photo by Robert Weldon.

Figure 2. Jeweler Frank Friedman examines some of the prized stamps from his collection. "Through stamps you learn so much about the different countries and glean a lot of information about the diamond trade in those countries," he says. Photo by Merle Friedman.

NEED TO KNOW

- Jeweler Frank Friedman's diamond-themed collection of stamps and other postal material contains ~2,000 pieces, representing more than 36 countries.

- The pieces date back to the early 19th century and illustrate diamond formation, the growth of the global trade, the cutting and polishing processes, important diamonds, and distinguished scientists.

emerge from Brazil in the mid-1700s, the Portuguese crown controlled the market for the next hundred years. The Friedman collection's earliest *cover*, an envelope or postcard sent through the mail system, is an 1807 specimen with a postmark from the Brazilian mining town of Diamantina (figure 4).

The discovery of diamonds in South Africa in late 1866 marked the birth of the modern industry. Although the country did not issue stamps featuring diamonds until 1960, other postal items show early South African mining. Examples are an 1873 cover with a "De Beers NR" (New Rush) cancellation mark and turn-of-the-century postcards from the Jagersfontein and Kimberley mines (again, see figure 4).

Figure 3. The Lesotho stamp on the left and the artist's rendering for a stamp from the Tongan island of Niuafo'ou illustrate the process of diamond emplacement in kimberlite.

Twentieth-century mining developments elsewhere in Africa are represented in figure 5. In 1964, three decades after it began producing diamonds, Sierra Leone issued the world's first self-adhesive stamps, bearing the inscription "Land of Iron & Diamonds." Subsequent stamps featuring diamonds
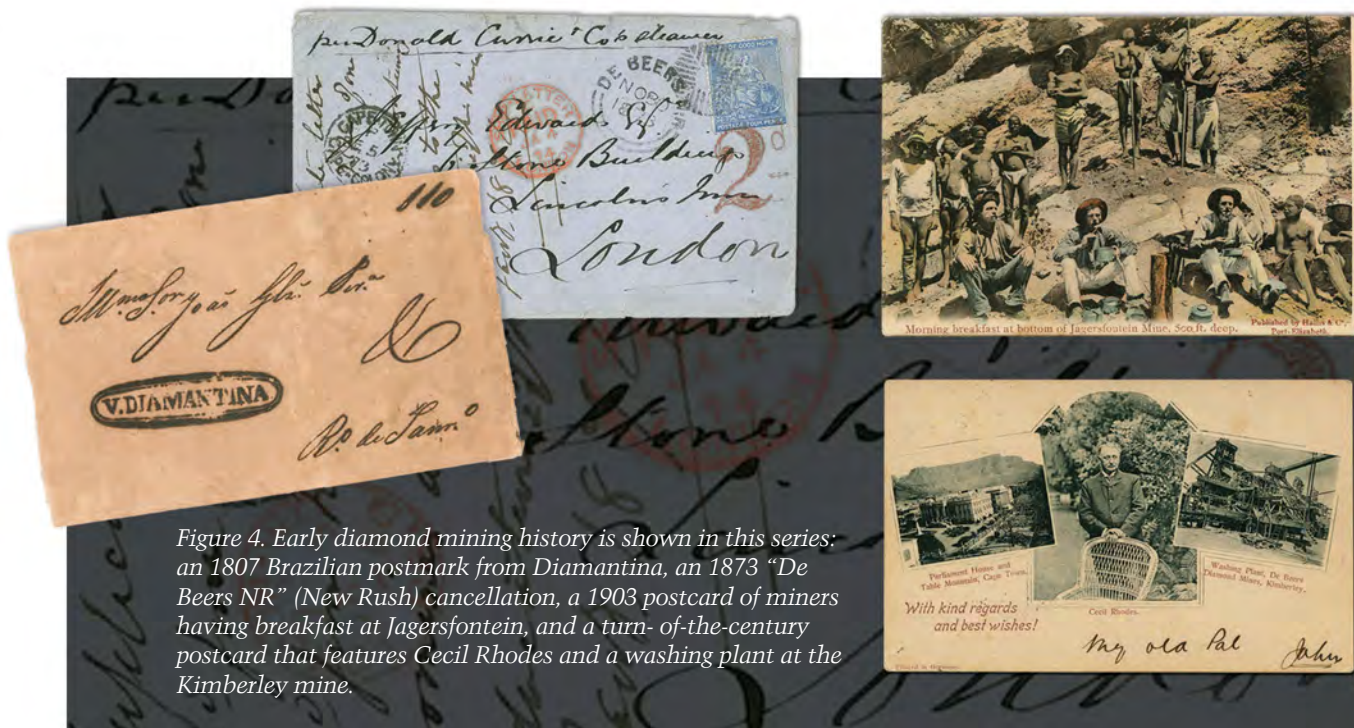
Figure 4. Early diamond mining history is shown in this series: an 1807 Brazilian postmark from Diamantina, an 1873 "De Beers NR" (New Rush) cancellation, a 1903 postcard of miners having breakfast at Jagersfontein, and a turn-of-the-century postcard that features Cecil Rhodes and a washing plant at the Kimberley mine.

had advertisements for Harry Winston on the paper backing. Other pieces from this set recognize diamond mining in South-West Africa (now Namibia). An original artist's rendering for a 1974 stamp shows marine mining along the coastline, while a 1983 issue marks the 75th anniversary of Namibian diamond mining. In the latter scene, prospectors are literally scratching the surface of the desert at Kolmanskop (near Lüderitz). A 1987 stamp shows Kolmanskop after it was abandoned in 1950, while a 2008 set of four commemorates the country's diamond mining centennial.

The Global Diamond Industry. Pioneers of the African diamond industry appear in figure 6, beginning with a 1940 stamp from Southern Rhodesia (now Zimbabwe) bearing a likeness of De Beers founder Cecil Rhodes (1853–1902). A 75th anniversary stamp commemorates August Stauch, the railroad supervisor who secured the prospecting rights near Lüderitz in 1908 after his employees brought

Figure 5. Items related to 20th century diamond mining include (clockwise from top left) a diamond-shaped stamp and a Harry Winston advertisement from the backing of a self-adhesive stamp, both from Sierra Leone; an original rendering of coastal mining in South-West Africa; four stamps marking the 100th anniversary of diamond mining in South-West Africa (now Namibia); and a pair of stamps showing the desert mining town of Kolmanskop.

Figure 6. Captured in the top row are early diamond magnates Cecil Rhodes, August Stauch, and Ernest Oppenheimer. The bottom row shows an Israeli cancellation mark for the 1956 World Congress of Diamond Bourses, a printer's proof of a 1992 Belgian stamp issued on the Antwerp Diamond Club's centennial, and a 1997 German stamp celebrating Idar-Oberstein's 500 years as a gem cutting center.

Figure 7. The individual stamps below depict the transformation of rough diamonds. On the left, clockwise from top left: a sorter examining a crystal, a processing plant in Ivory Coast, the five stages of diamond cutting, a worker at a diamond polishing wheel, and a pair of Belgian stamps commemorating Antwerp's role as a world diamond cutting center. Diamonds were once routinely shipped by regular mail, as seen on the right in a 1940 package containing 1,410 carats sent from the Williamson mine in Tanganyika.

Figure 8. Famous diamonds appear in these items from the Friedman collection (top to bottom): a 1953 telegram from the Indian parliament regarding ownership of the Koh-i-Noor, a 1971 Soviet stamp depicting the Shah diamond, South African stamps of Cullinans I and II, and an original artist's rendering for a 1976 stamp of the Lesotho Brown.

the Antwerp Diamond Club's centennial, and a 1997 German stamp celebrating 500 years of the diamond and colored stone industry in Idar-Oberstein.

Cutting and Polishing. Figure 7 follows the transformation of diamonds from rough to polished gems, starting with a signed proof of a 1972 Ivory Coast stamp of a diamond processing plant. In a 2001 stamp issued by Botswana, a sorter uses her loupe visor to examine a crystal. A printer's proof of an Ivory Coast stamp from 1972 shows a processing plant, while a 1970 Botswanan stamp illustrates the five stages of diamond cutting: rough octahedron, sawn crystal, fashioned girdle, polished top, and brilliant cut. A signed proof of a 1966 Central African Republic stamp shows a worker at a polishing wheel. Belgian-issued stamps from 1960 and 1983 celebrate Antwerp's role as a world diamond cutting center. Diamonds all along the distribution chain were once routinely shipped by regular mail, as indicated by the parcel carrying 1,410 carats of diamonds from the Williamson mine in Tanganyika (now Tanzania) in 1940, the year it opened.

Famous Diamonds. The Friedman collection also portrays some of the world's most exceptional diamonds (figure 8). The first is the legendary Koh-i-Noor, the ancient Indian diamond that was handed over to the British Empire in 1850. Evidence of a postcolonial dispute over the Koh-i-Noor emerges in a 1953 telegram from the Indian parliament that mentions the diamond's ownership. A 1971 Soviet stamp shows the 88.7 ct table-cut Shah, including the engraved inscriptions. This diamond was offered by Persian ruler Fath Ali Shah to placate Czar Nicholas I after the 1829 assassination of a Russian diplomat (Balfour, 2000). Cullinans I and II, cut from a 3,106 ct piece of rough discovered at South Africa's Premier mine, became the centerpiece of the Crown Jewels of England. They are seen in a pair of 1980 South African stamps issued on the 75th anniversary of the discovery of the rough. Rounding out this group is a hand-painted proof of a 1976 stamp featuring the Lesotho Brown. This 603.1 ct diamond was discovered in 1967 and later cut into 18 stones, one of which was set in an engagement ring for Jacqueline Kennedy Onassis (Balfour, 2000).

Scientific Breakthroughs. Figure 9 shows a selection of stamps commemorating scientists who advanced our understanding of diamonds. A 1980 German stamp recognizes naturalist Albertus Magnus

him handfuls of shiny stones. A 1983 stamp from South-West Africa honors Sir Ernest Oppenheimer (1880–1957), who led De Beers for 30 years and established its Central Selling Organisation in 1934.

The collection also offers a glimpse into the diamond trade's impact elsewhere. These pieces include an Israeli cancellation mark created for Tel Aviv's hosting of the 1956 World Congress of Diamond Bourses, a 1992 Belgian stamp printed for

Figure 9. These stamps featuring Albertus Magnus, Antoine Lavoisier, Pierre and Marie Curie, Henri Moissan (far left in the group illustration), and Alexander Du Toit recognize pioneers of diamond research.

(1193–1280), a medieval writer on diamonds and one of the first to document the gem's extraordinary hardness. The famed chemist Antoine Lavoisier (1743–1794), whose research demonstrated that diamond consists of pure carbon, is featured in a 1943 French stamp. A 1977 stamp issued by the Central African Republic pays tribute to Marie and Pierre Curie, who received the 1903 Nobel Prize in physics for their early studies of radiation and tested its effects on diamond. Fellow Nobel Prize winner Henri Moissan, seen in a 1966 Swedish stamp, per-

formed early experiments on diamond synthesis. In 1991, South Africa issued a stamp in honor of Alexander Du Toit, the chief geological consultant to De Beers from 1927 to 1941. Dr. Du Toit mapped the geology of his native country and produced influential work supporting the continental drift theory, which asserts that South Africa and South America were once connected.

CONCLUSION

Fifty years after starting his collection, Mr. Friedman still adds to it regularly. "One of the thrills of collecting is filling that gap that has eluded me for years, or finding an unusual variety in an unexpected way," he says. "For instance, I've just acquired a Namibian stamp of a diamond-barren kimberlite pipe. It enhances the Namibian content."

Even in the age of digital communication, philately remains a powerful educational medium, a form of visual history in miniature. The portraits, scenes, and other information capture illuminating details and foster greater appreciation of the subject. Frank Friedman's philatelic collection, which preserves several aspects of diamond history, represents an important contribution to gemology's scholarship and heritage.
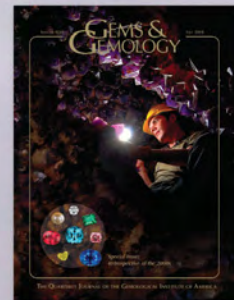
REFERENCES

Balfour I. (2000) Famous Diamonds, 4th ed. Christie, Manson and Woods Ltd., London, 320 pp.
Friedman F. (2007) Diamonds and philately. The SA Philatelist, April, pp. 263–264.
Stamp of approval (2006) SA Jewellery News, August, p. 55.
Weil A. (1997) Keystone exhibit honours SA jeweler. Diamond News & SA Jeweller, August, p. 11.

GEMS & GEMOLOGY 2011

CONGRATULATIONS

G&G CHALLENGE WINNERS

This year, hundreds of readers participated in the 2011 GEMS & GEMOLOGY Challenge. Entries arrived from around the world, as readers tested their gemological knowledge by answering questions listed in the Spring 2011 issue. Those who earned a score of 75% or better received a GIA Letter of Completion recognizing their achievement. The participants who scored a perfect 100% are listed here.

AUSTRALIA **Queensland,** *Elanora:* Bert J. Last. *Warwick:* Elizabeth Cassidy. **Victoria,** *Ringwood:* Paulina Holmer. **Western Australia,** *Coogee:* Helen Judith Haddy. **South Australia,** *Grange:* Barbara Wodecki • **BELGIUM** **Flemish Brabant,** *Brussels:* Brigitte Revol MacDonald. **West Flanders,** *Ruiselede:* Lucette Nols. *Egenhoven:* Guy Lalous. *Hemiksem:* Daniel De Maeght • **CANADA** **British Columbia,** *Delta:* Barbara Mui • **INDONESIA** *Jakarta:* Warli Latumena • **IRELAND** *Galway:* Simon Zaletel • **ITALY** **Varese,** *Malnate:* Gabriele Tralli. *Naples:* Stefano Montemurro. **Udine,** *Tarvisio:* Chiara Piussi • **LITHUA-NIA** *Vilnius:* Saulius Fokas • **NETHERLANDS** *Rotterdam:* E. van Velzen • **NEW ZEALAND** *Tauranga:* Graeme Petersen. *Wellington:* Thomas Brent Layton • **SPAIN** *Las Palma De Gran Canaria:* Robert Ernst. *Valencia:* Monika P. Bergel Becker • **SWITZERLAND** *Zurich:* Doris C. Gerber, Eva Mettler • **UNITED KINGDOM** **Devon,** *Okehampton:* Damian J. Miles • **USA** **Arkansas,** *Greenbrier:* Beverly A. Brannan. **California,** *Anaheim:* Nalini Pattni. *Carlsbad:* Brenda Harwick, Abba Steinfeld. *Hidden Hills:* Bradley Partington. *Rancho Cucamonga:* Sandy MacLeane. *Redwood City:* Starla Turner. **Connecticut,** *Wilton:* Susan DiGeorgio. **Florida,** *Clearwater:* Tim Schuler. *Deland:* Sue Angevine Guess. *Longwood:* David Hermann. *Riverview:* Kenneth S. Fee. *Tampa:* R. Fred Ingram. **Georgia,** *Roswell:* Gary Braun. **Hawaii,** *Makawao:* Alison Fahland. **Iowa,** *West Des Moines:* Franklin Herman. **Illinois,** *Bloomington:* William Lyddon. *Downers Grove:* Sakina Bharani. **Indiana,** *Carmel:* Wendy Wright Feng. **Louisiana,** *Baton Rouge:* Cynthia Gestring-Blumberg. *Lake Charles:* Cynthia McCown. **Massachusetts,** *Littleton:* Jane L. Millard. *Millbury:* Bernard M. Stachura. **Maryland,** *Chevy Chase:* Andrea R. Blake. **Missouri,** *Saint Ann:* Bruce S. Hoffmann. **Minnesota,** *Minneapolis:* Andy Stevens. **Montana,** *Billings:* Onna Stene. **New Jersey,** *Monmouth Beach:* Michele Kelley. *West Orange:* Jessica M. Craig. **Nevada,** *Las Vegas:* Colleen Walsh. *Reno:* Terence E. Terras. **New York,** *City Island:* Marjorie Kos. *Hawthorne:* Lorraine Bennett. *Tarrytown:* Ronnie Xu. **Ohio,** *Dayton:* Michael Williams. *Medina:* Charles Perkins. **Pennsylvania,** *State College:* Dennis Zwigart. **Rhode Island,** *Rumford:* Sarah Horst. **South Carolina,** *Sumter:* James S. Markides. **Texas,** *Amarillo:* Daniel Novak. *Livingston:* Janet S. Mayou. **Virginia,** *Hampton:* Edward A. Goodman. **Washington,** *Bellevue:* Thomas Charles Estervog. *Bothell:* Kathryn Howe. *Freeland:* Warren Carrow. *Seattle:* Janet Suzanne Holmes. **Wisconsin,** *Beaver Dam:* Thomas G. Wendt. *Pulaski:* Stephen Kientop.
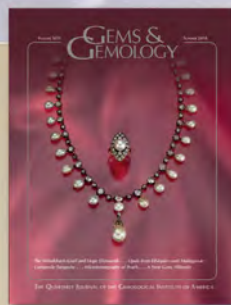
Answers

See pages 75–76 of the Spring 2011 issue for the questions.
1 (a), 2 (b), 3(c), 4 (c), 5 (d), 6 (a), 7 (d), 8 (c), 9 (c), 10 (b), 11 (b), 12 (c), 13 (a), 14 (d), 15 (b), 16 (b), 17 (c), 18 (d), 19 (c), 20 (b), 21 (d), 22 (b), 23 (d), 24 (b), 25 (a)

The information you need... at a glance!
Perfect for home or office use.

LAMINATED REFERENCE CHARTS

NEW!

- World Gem Localities **NEW!**
- HPHT-Grown Synthetic Diamonds
- Gem Treatments
- GIA Diamond Cut Grading System
- Recognizing Be-Diffused Rubies and Sapphires
- Pink Diamond Color Chart

Also available:
- Separation of Natural and Synthetic Diamonds
- Identification of Filled Diamonds

Only $16.95 (plus shipping)
Buy two or more and SAVE!
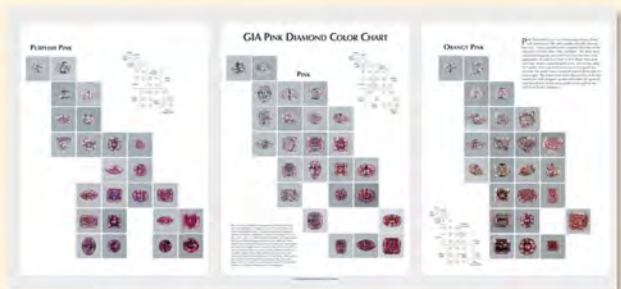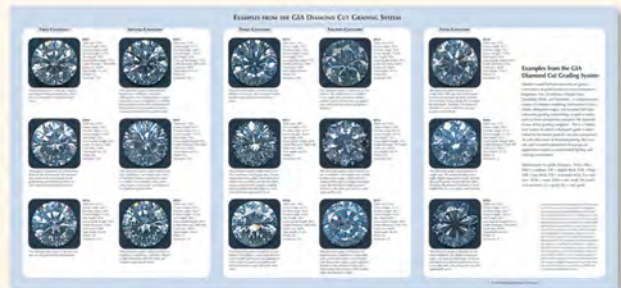
GEMS & GEMOLOGY®

Order Yours Today!

Visit store.gia.edu

Or call 800-421-7250, ext. 7142
(outside the U.S., 760-603-4000, ext. 7142)

G&G Lab Notes

EDITORS

Thomas M. Moses | Shane F. McClure

Unusually Large CLINOHUMITE

Clinohumite, $(Mg,Fe^{2+})_9(SiO_4)_4(F,OH)_2$, is a fairly rare collectors' stone with orangy yellow to brownish orange coloration. Faceted stones typically weigh <2 ct, but a few much larger stones have been cut (e.g., 36.56 ct, see L. Massi, "AIGS Bangkok inspects exceptional clinohumite from Tajikistan," *InColor*, Summer 2007, pp. 30–31). In the present report, we document the properties of an exceptionally large clinohumite weighing 84.23 ct (32.6 × 24.79 × 17.77 mm). For background information on the cutting of this stone, see Y. Zhukov, "Clinohumite—The mountain fire,"

Figure 1. This faceted clinohumite weighs an impressive 84.23 ct.

InColor, Spring 2011, pp. 48–51.

The stone was faceted into a pear brilliant and was brownish orange (figure 1). Internal features consisted of numerous two-phase inclusions (figure 2, left) and "fingerprints," as well as distinct angular brownish orange growth lines (figure 2, center), as documented previously in clinohumite (e.g., U. Henn et al., "Gem-quality clinohumite from Tajikistan and the Taymyr region, northern Siberia," *Journal of Gemmology*, Vol. 27, No. 6, 2001, pp. 335–339; and Winter 2004 GNI, pp. 337–338). Abundant twin planes were also seen with cross-polarized light (figure 2, right). The stone was inert to long-wave UV radiation, whereas short-wave UV produced moderate orange to strong chalky yellow fluorescence along the growth lines. Its Raman spectrum, along with gemological properties such as RI (1.635–1.670) and SG (3.21) values, confirmed that it was clinohumite. IR spectroscopy recorded typical absorptions for clinohumite, including a broad band centered at 3560 cm^{-1} due to OH stretching and additional bands at 4100 and 4510 cm^{-1} caused by MgOH units and Si-OH bonding,

Figure 2. Microscopic observation of the clinohumite revealed two-phase (fluid-gas) inclusions, (left, magnified 35×), distinct angular brownish orange growth lines (center, 12×), and numerous twin planes (right, cross-polarized light, 75×).
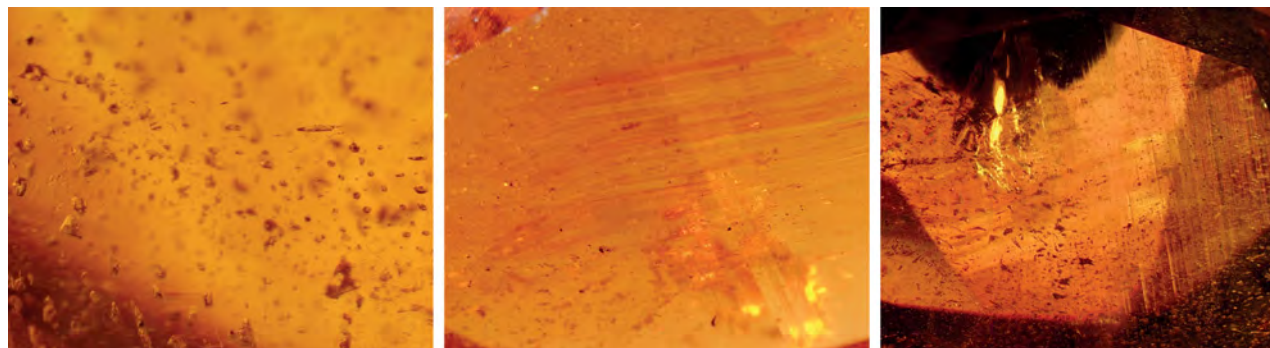
respectively (R. L. Frost et al., "Near-infrared and mid-IR spectroscopy of selected humite minerals," *Vibrational Spectroscopy*, Vol. 44, 2007, pp. 154–161, http://dx.doi.org/10.1016/j.vibspec.2006.11.002). The FTIR and Raman spectra of this stone are available in the *G&G* Data Depository (gia.edu/gandg). Energy-dispersive X-ray fluorescence (EDXRF) spectroscopy detected major amounts of Mg, Fe, and Si, and traces of Ti and Mn, as expected for clinohumite.

There are two main localities that produce gem-quality clinohumite—the Pamir Mountains of Tajikistan and the Taymyr region of northern Siberia (Massi, 2007). Unfortunately, the geographic origin of the present clinohumite is unknown. It is the largest gem-quality clinohumite ever tested at GIA.

Kyaw Soe Moe and Wai Win

DIAMOND

Black Diamond, Colored by Strong Plastic Deformation

Black color in diamonds can have various natural or artificial causes, from inclusions (abundant graphite or pinpoints, or dense clouds) to heating or extremely strong irradiation. The New York laboratory recently examined a black diamond colored by another mechanism.

This round-cut diamond weighed

Figure 3. The black color of this 0.85 ct diamond is attributed to very strong plastic deformation.

Figure 4. With magnification and very strong lighting, the diamond in figure 3 showed a dark brown color with banded linear distribution. Magnified 70×.

0.85 ct (5.70 × 5.78 × 3.87 mm) and was color graded as Fancy black (figure 3). Viewed with magnification and very strong fiber-optic illumination, it revealed fractures and mineral inclusions, as well as a dark brown color with banded linear distribution (figure 4). Strong plastic deformation and the related linear banding were also clearly revealed in the DiamondView. Its mid-infrared spectrum showed strong N-related absorption in the one-phonon region and a weak H-related feature at 3107 cm^{-1}. Also recorded were very strong absorptions from amber centers at ~4170 and 4070 cm^{-1}, with intensities of 2.0 and 1.1 cm^{-1}, respectively.

The vacancy cluster, a diamond lattice defect closely related to plastic deformation, usually absorbs visible light from ~600 nm to lower wavelengths. When its concentration is very high, such as in this diamond, its absorption extends across the entire visible light region and blocks the vast majority of light. It is very rare to see a natural gem diamond with such strong plastic deformation that it causes a black appearance. This stone demonstrates yet another cause of natural black color in diamond.

Wuyi Wang

Coated Black Diamond

Gems & Gemology has reported on a number of interesting black diamonds in recent years (see the Spring 2007, Winter 2007, Fall 2008, and Summer
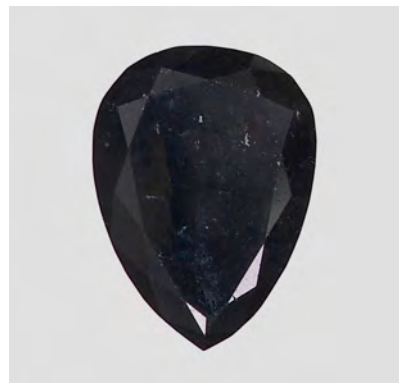
Figure 5. This 1.29 ct diamond proved to be coated to enhance its black color appearance.

2010 Lab Notes sections and S. V. Titkov et al., "An investigation into the cause of color in natural black diamonds from Siberia," Fall 2003, pp. 200–209). This color, when natural, is typically caused by dark/intense mineral or cloud inclusions. It can also be induced by artificial irradiation or graphitization along fractures due to heating (naturally or in the laboratory).

Recently, the New York laboratory received a 1.29 ct black pear shape (figure 5) for color origin determination. Infrared absorption spectroscopy confirmed it was a type Ia diamond with hydrogen impurities. As expected, it was inert to both long- and short-wave UV radiation. However, microscopic examination revealed a distinctly lighter color along the facet junctions (figure 6), and these areas showed contrasting luminescence in the

Figure 6. In reflected light, the 1.29 ct diamond displays a distinctly lighter color along the facet junctions. Magnified 30×.
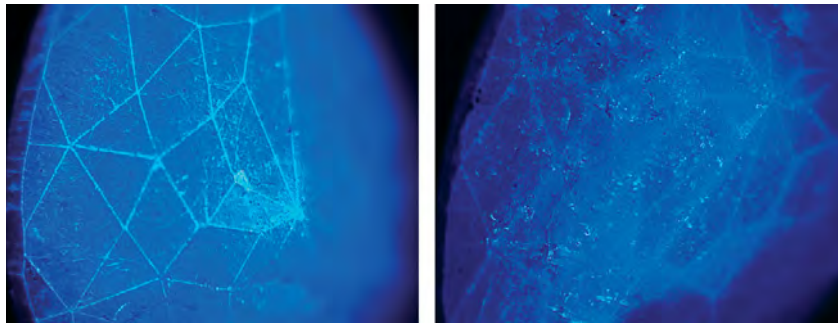
Figure 7. In the DiamondView, the coating on the black diamond was apparent from the different luminescence of the facet junctions, where it had apparently worn off (left). After cleaning with acetone and corundum powder (with client permission), the coating appeared smeared and the junctions were less distinct (right).

DiamondView (figure 7). The girdle also showed uneven concentrations of dark color, and there were scratches on the pavilion that were lighter than the black bodycolor; both of these could be easily observed with the microscope. Feathers within the diamond were dark colored due to black natural inclusions. It was obvious that this diamond, though rather dark, had been coated to further enhance its color.

This was our first encounter with a coated black diamond. Because of the coating, we did not issue a color grade. In this case, the black coating made the stone appear a deeper, more even black. Although coating a black diamond can improve its overall appearance or color distribution, in this case the treatment was detectable with a microscope.

Erica Emerson
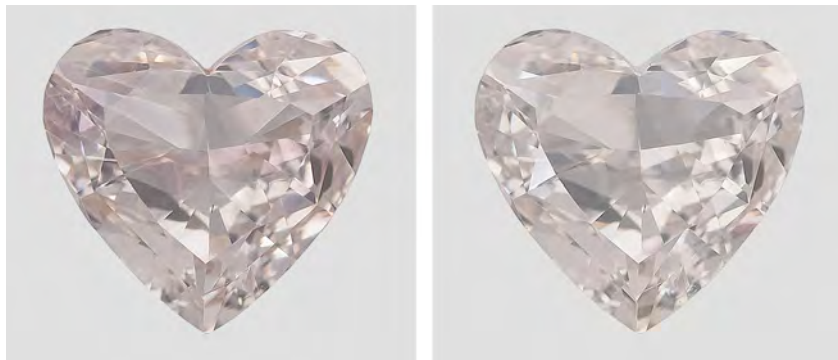
Coated Diamond with Spectroscopic Features of a Natural-Color Pink

Coated diamonds are fairly commonly encountered, both in the trade and the grading lab. Most coatings consist of a thin film applied to one or more pavilion facets, often at or near the girdle edge, though sometimes the coating will completely cover the diamond's surface. Because of the value of natural-color pink diamonds, pink is a common choice for such coatings, which are intended to deepen a weak bodycolor or to mask an undesired one (e.g., Winter 2010 Lab Notes, pp. 299–300). This treatment can be identified through microscopic observation and UV-Vis spectroscopic features. In the case of pink-coated diamonds, the typical absorption band at ~520 nm (see A. H. Shen et al.,

"Serenity coated colored diamonds: Detection and durability," Spring 2007 *G&G*, pp. 16–34, http://dx.doi.org/10.5741/GEMS.43.1.16) is easily distinguished from the ~550 nm band in natural-color stones.

The 1.05 ct heart-shaped diamond in figure 8, recently submitted for color grading, initially received a grade of Fancy Light brown-pink. Its UV-Vis spectrum showed the broad ~550 nm absorption band (figure 9) typical of naturally colored pink diamonds. With magnification, however, a coating was clearly visible on the pavilion facets (figure 10). After the coating was removed by boiling the stone in acid, the color grade was revised to J (figure 8, right).

Because the normally diagnostic absorption band for a pink coating was shifted from 520 to 550 nm, spectroscopy alone would not have detected this coating. This reinforces the essential role of conventional observation in gem identification.

Sally Chan

Colorless Untreated Diamonds with High Levels of Strain

Diamonds form under enormous heat and pressure deep in the earth, and endure additional stresses during their journey to the surface. Such stresses can cause irregularities in their lattice structure, which can impart color to a diamond in a variety of ways. For example, brown color in type IIa diamonds is believed to be caused by vacancy clusters, and the depth of color generally corresponds to the degree of strain (D. Fisher et al., "The vacancy as a probe of the strain in type IIa diamonds," *Diamond and Related Materials*, Vol. 15, 2006, pp. 1636–1642, http://dx.doi.org/10.1016/j.diamond.2006.01.020; D. Fisher, "Brown diamonds and high pressure high temperature treatment," *Lithos*, Vol. 112S, 2009, pp. 619–624, http://dx.doi.org/10.1016/j.lithos.2009.03.005). Since high-pressure, high-temperature (HPHT) treatment can remove brown color from type IIa diamonds but has a minimal effect

Figure 8. This 1.05 ct diamond owed its apparent Fancy Light brown-pink color (left) to a coating. After the coating was removed by acid cleaning, the diamond was given a color grade of J (right).

VISIBLE ABSORPTION SPECTRA
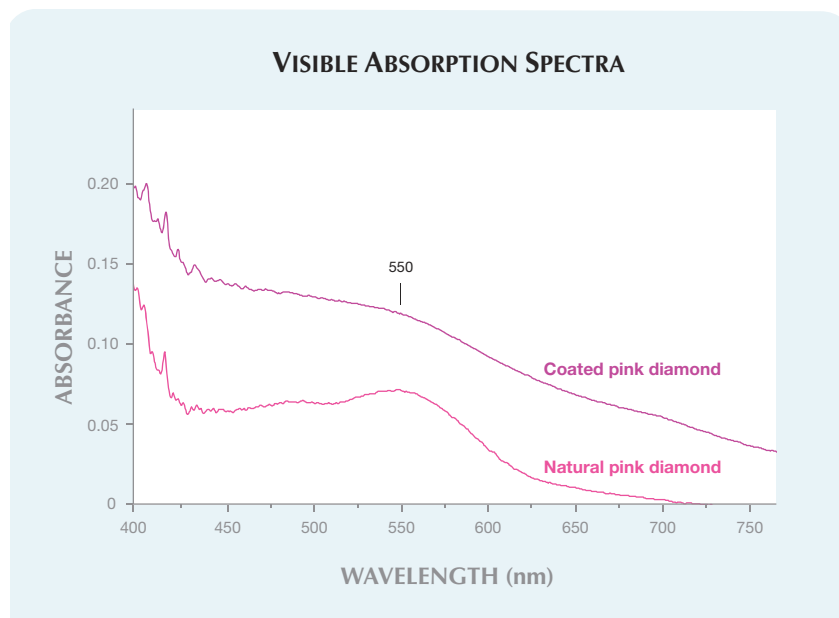
Figure 9. The coated diamond's absorption band at ~550 nm was very similar to that of a naturally colored pink diamond. Both spectra were collected at liquid-nitrogen temperature.

on strain, the presence of strain can be an important criterion for identifying HPHT-annealed stones.

Recently, the Carlsbad laboratory received two colorless type IIa diamonds for identification: a 0.90 ct E-color marquise and a 0.73 ct D-color round brilliant. Based on gemological and spectroscopic features, these diamonds were found to be natural and untreated. However, in the course of this determination, we also noticed that both showed an unusually high degree of "tatami" strain (figure 11) when viewed with cross-polarized light. The strong strain patterns were more consistent with those seen in brown diamonds. Typically, type IIa colorless diamonds show a tatami pattern, but with a lower concentration of strain laminations.

In addition to visual assessment using crossed polarizers, an indirect but relatively reliable indicator of strain is the peak width of certain defects determined from photoluminescence (PL) spectra taken at liquid nitrogen temperature. The PL spectrum of the 0.90 ct diamond showed both the neutral (575 nm) and negatively charged (637 nm) NV centers; the full width at half maximum (FWHM) for these centers was 0.89 and 1.56 nm, respectively. As with the observed strain, these values were much higher than is commonly seen in untreated colorless diamonds. A compilation of calculated FWHM values for 250 untreated diamonds in the D–E range showed that the NV^0 center had an average width of 0.29 nm with a standard deviation of 0.07 nm; the highest value was 0.65 nm. For the NV^- center, the average width was 0.30 nm with a standard deviation of 0.10 nm; the maximum was 0.79 nm. These values are far lower than those for the 0.90 ct diamond.

It is unusual to find natural-color diamonds that endured such a high amount of stress during their history and yet remained colorless. One possible explanation is that the associated brown coloration was naturally annealed out during their geologic history.

Sally Eaton-Magaña

HPHT Treatment for Subtle Color Enhancement of Diamond

It is well known that HPHT annealing can remove brown coloration from natural type IIa diamonds, making them colorless to near-colorless. While a significant number of HPHT-

Figure 11. These untreated natural type IIa diamonds (0.90 ct E color, left; 0.73 ct D color, right) experienced a high amount of stress, as evidenced by the extensive "tatami" strain seen in cross-polarized light. They are unusual since they do not show any of the brown color that typically correlates with such strain. (The apparent brown color in these images is an artifact of the lighting.)

Figure 10. A pink coating on the diamond's pavilion facets was clearly visible with magnification (here, 40×).

Figure 12. Shown here after HPHT treatment (E–F color, 1.74–2.57 ct), these type IIa diamonds originally had color grades of J–M. This demonstrates that HPHT annealing is being used to make subtle color improvements in such diamonds.

treated type IIa diamonds have been seen in gem laboratories over the past decade, little has been published on the characteristics of the starting materials. Recently, however, the New York laboratory had the opportunity to follow four diamonds through the HPHT treatment process.

When they were first received, three of the four round diamonds (1.8–2.6 ct) were color graded in the J–K range, with the fourth being M color. Photoluminescence spectroscopy confirmed that they were naturally colored. Infrared spectroscopy showed they were very pure type IIa; only one stone had an extremely weak hydrogen-related absorption, at 3107 cm^{-1}. When the diamonds reappeared in the lab very recently, their color ranged from E to F (figure 12). They also showed a 2–5% weight loss, consistent with the necessary repolishing after treatment. Their

photoluminescence spectra revealed the exact changes that were expected as a result of HPHT annealing.
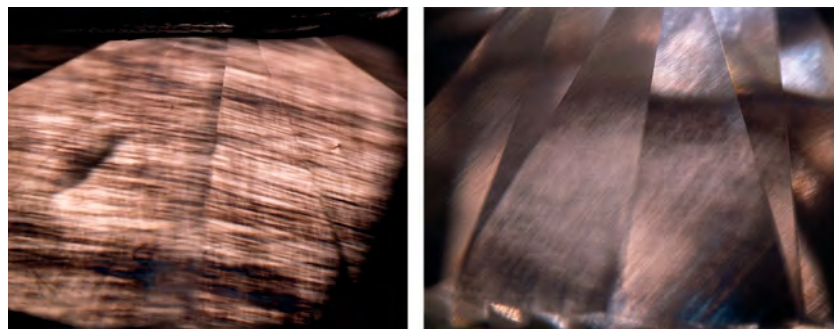
Though the general impression of HPHT treatment in the trade is that it is used to turn obviously brown diamonds colorless, this experience suggests that such treatment may also be used to achieve more subtle improvements in diamond color.

Wuyi Wang

An Interesting Luminescent Cleavage in Diamond

Although diamond is the hardest natural substance, it still is susceptible to breakage along its cleavage directions. Often mistakenly described as a "fracture," cleavage is one of the most common clarity characteristics in gem-quality diamonds, and generally is of little interest to gemologists. However,

the Carlsbad laboratory recently graded a type Ia colorless round brilliant with a remarkable cleavage-related feature. The cleavage showed prominent brown radiation staining, suggesting that radioactive fluids had been present in the post-growth environment (figure 13). When the diamond was viewed face-up in the microscope with darkfield illumination, the cleavage also exhibited pronounced green luminescence to visible light (figure 14, left); fiber-optic illumination made the green luminescence even more dramatic. Radiation stains are well documented in the gemological literature (e.g., J. I. Koivula, *The MicroWorld of Diamonds*, Gemworld International, Northbrook, Illinois, 2000).

Green luminescence in diamond is known to be produced by the H3 lattice defect (503.2 nm), which consists of two nitrogen atoms separated by a vacancy (N-V-N)^0. When examined in the DiamondView, the stone showed clear green fluorescence along the cleavage (figure 14, right). Using this image as a map, we collected photoluminescence data from the cleavage area. In addition to the H3 defects, analysis also revealed high concentrations of the 3H interstitial defect (503.4 nm). An interstitial defect occurs when a carbon atom is displaced from its original lattice position, typically by radiation. Thus, the occurrence of 3H with the green luminescing H3 defects is consistent

Figure 13. The brown coloration confined to the cleavage area of this diamond resulted from the interaction of radioactive fluids in the post-growth environment. Magnified 20×.
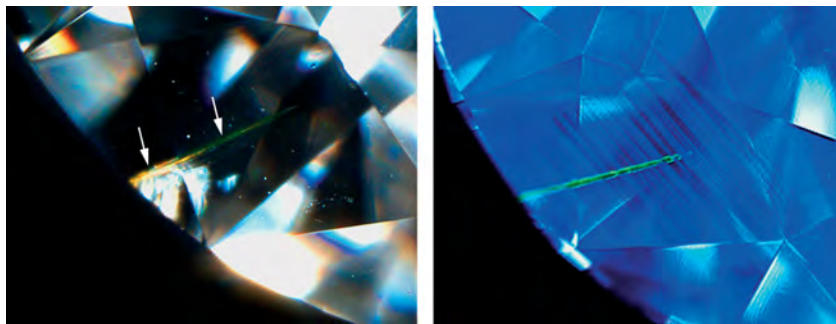
Figure 14. Darkfield illumination revealed green luminescence along the cleavage shown in figure 13 (left, see arrows; magnified 20x). In the DiamondView (right), green luminescence from the H3 defect was clearly visible. Magnified 30×.

with the microscopic evidence of radiation staining.

This is one of the more unusual examples of cleavage we have seen in the Carlsbad laboratory. The diamond's cleavage, radiation staining, and green luminescence all reveal important information about its history and indicate that radiation exposure occurred naturally.

Nathan Renfro and
Christopher M. Breeding

A Large HPHT-Annealed Pink Diamond

Unlike irradiation treatment, which usually adds additional color, annealing a natural diamond under HPHT

Figure 15. This 21.73 ct Light pink diamond proved to be HPHT annealed.

conditions can remove preexisting colors as well as create new ones. When a suitable type IIa brown diamond is HPHT annealed at temperatures appropriate for removing brown but not pink coloration, then the preexisting pink color can be enhanced. Such HPHT-treated type IIa pink diamonds have been available for more than 10 years (e.g., Fall 2000 Lab Notes, pp. 254–255).

The New York laboratory recently received the large pink diamond in figure 15 for identification. This marquise brilliant (28.15 × 15.41 × 7.71 mm) weighed 21.73 ct and was color graded Light pink. The color was distributed evenly throughout the stone with no detectable pink graining, and it showed typical blue fluorescence when examined in the DiamondView. The mid-IR spectrum showed type IIa features with no detectable hydrogen-related absorption at 3107 cm^{-1}. A weak band centered at ~550 nm was present in the UV-Vis absorption spectrum at liquid nitrogen temperature. This band is very common in naturally colored pink-to-red diamonds and can be made more visible by removing other unwanted colors. Photoluminescence spectra collected at liquid nitrogen temperature with varying laser excitations confirmed that this diamond was HPHT annealed.

HPHT annealing has become a very common type of diamond color treatment. With advances in processing techniques, a substantial number of large diamonds can now be treated successfully, though these can still be identified by gem labs. This 21.73 ct pink diamond is one of the largest HPHT-treated pink diamonds identified in GIA's laboratories.

Wuyi Wang

SYNTHETIC DIAMOND

Gem-Quality CVD Synthetic Diamonds from Gemesis

In recent years, limited quantities of gem-quality synthetic diamonds produced by chemical vapor deposition (CVD) have reached the market. Most of these have come from Apollo Diamond Inc. (Boston, Massachusetts). We recently examined similar products introduced by Florida-based Gemesis Corp., better known for its HPHT-grown synthetic diamonds (J. E. Shigley et al., "Gemesis laboratory-created diamonds," Winter 2002 *G&G*, pp. 301–309). In November 2010, the company announced plans to market CVD-grown synthetics.

GIA examined 16 CVD synthetic diamonds (e.g., figure 16) that were faceted as round brilliants with the exception of one rectangular cut. They ranged from 0.24 to 0.90 ct, with an average weight of 0.46 ct. They were colorless (3 samples), near-colorless (11), and lightly colored (2). For the most part, clarity grades fell between IF and VVS, due to internal graining and a few pinpoint inclusions. Only four of the 16 samples had VS clarity.

Infrared absorption spectroscopy revealed that all of the CVD synthetic diamonds were type IIa. Unlike typical as-grown CVD products, no defect-related absorptions were recorded in either the mid- or near-infrared regions. Photoluminescence analysis of all samples showed moderately strong emission from the H3 optical center (zero-phonon line at 503.2 nm), moderately strong emissions from NV centers (575.0 and 637.0 nm), and moderate to strong emissions from the [Si-V]$^-$ center (doublet at 736.6 and 736.9

Figure 16. These CVD synthetic diamonds were produced by Gemesis. The 0.39 ct round brilliant on the left was graded F color and VVS$_2$ clarity; the 0.83 ct sample on the right was graded J-VVS$_2$.

nm). In four samples, the [Si-V]$^-$ concentrations were relatively high and could even be detected in the UV-Vis absorption spectra. A notable feature of these synthetic diamonds was their weak to moderate green fluorescence to short-wave UV radiation. Most were inert to long-wave UV radiation, with only five samples showing very weak green fluorescence. In the Diamond-View, they exhibited strong green fluorescence and noticeable blue phosphorescence; characteristic growth striations also were easily seen.

Gemological and spectroscopic observations strongly suggested that these CVD synthetic diamonds were annealed after their growth, presumably to improve their color and transparency. This study confirms that the quality of CVD synthetic diamonds continues to improve. Nevertheless, gemological and spectroscopic features can clearly separate Gemesis CVD synthetics from natural diamonds.

Wuyi Wang and Thomas M. Moses

Treated Synthetic Diamonds with Pink Color Intensified by Fluorescence

A combination of irradiation and HPHT annealing can create pink to red colors in both natural and synthetic diamonds. We have reported on a number of these treated stones over the past few years (see, e.g., Lab Notes: Winter 2005, pp. 341–343; Spring 2010, pp. 51–52 and 52–54; and Winter 2010, pp. 300–301). Two more examples recently submitted (on separate occasions) to the New York laboratory showed an unusual fluorescence effect.

The two round brilliants (0.47 and 0.63 ct; figure 17) were color graded Fancy Vivid purplish pink and Fancy Deep purple-pink, respectively. Their mid-IR spectra indicated they were type Ib, with a very low concentration of isolated nitrogen. However, they did not display the "tatami" strain pattern expected for such diamonds, so we tested them using the DiamondView. The 0.47 ct round brilliant showed the cuboctahedral pattern typical of HPHT synthetic growth, while the 0.63 ct sample had a CVD growth pattern; both displayed strong orange luminescence (figure 17, bottom). Microscopic examination revealed strong color zoning along growth sectors in the 0.47 ct synthetic, but this effect was very subtle in the 0.63 ct sample

Figure 17. These treated-color synthetic diamonds (0.47 and 0.63 ct) have an evenly distributed face-up color. Their DiamondView images (bottom) display the patterns typical of HPHT (left) and CVD growth (right).
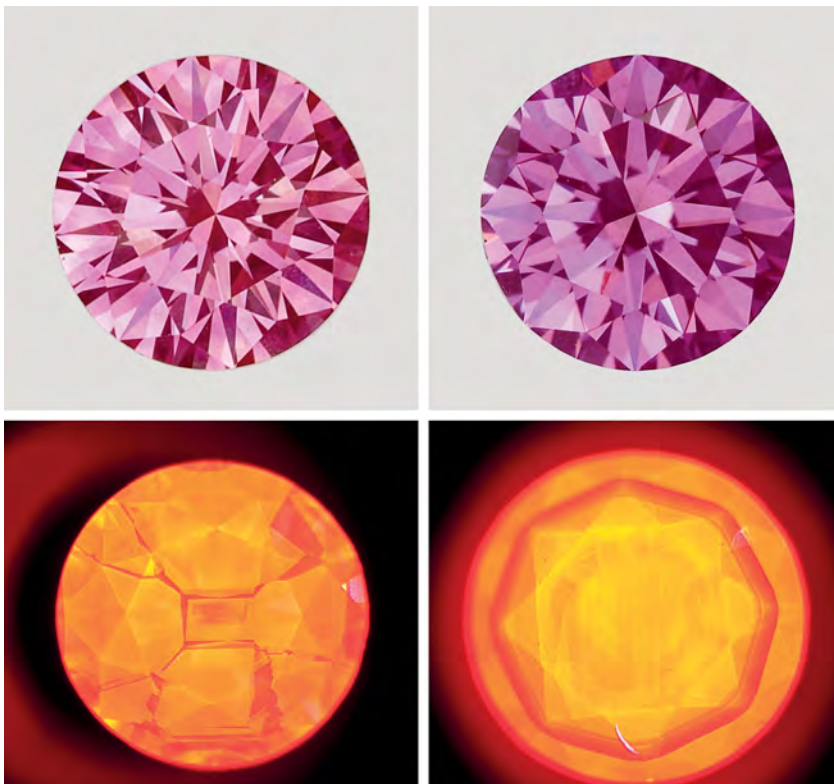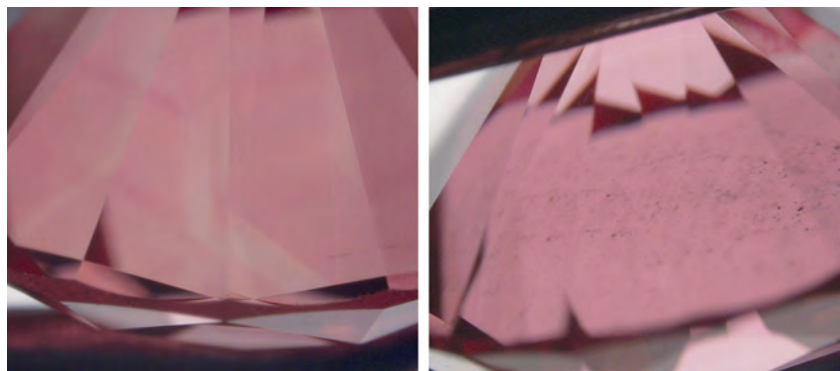
Figure 18. In diffused light, the 0.47 ct pink synthetic diamond displayed strong, uneven color zoning along growth sectors (left, magnified 45×). The 0.63 ct sample only showed subtle color zoning (right, 35×).

(figure 18). The former had only a VVS$_1$-grade feather in the lower girdle facet, while the latter contained graphitized feathers and tiny black particles (possibly graphite).

The diamonds' UV-Vis-NIR absorption spectra were collected at liquid-nitrogen temperature with broadband illumination (Avantes AvaLight-HAL-S) and a CCD detector (Ocean Optics HR-4000). This light source has significant emission in the visible-light region (>400 nm) but very little in the UV region. The 575 nm feature (zero-phonon line of NV^0) appeared as a negative peak (figure 19), caused by fluorescence. Strong fluorescence was also present in the ~650–825 nm region from the NV$^-$ center (637 nm). In addition, a sharp peak at 595 nm was recorded in the absorption spectra, and this peak, together with the strong NV features at 575 and 637 nm, were also detected in low-temperature photoluminescence spectra. These features suggest that both pink synthetic diamonds had undergone post-growth treatments, such as irradiation and annealing. These treatments caused the vacancies to migrate and combine with preexisting isolated nitrogen atoms, forming the NV centers that produce the strong purplish pink color.

The absorption spectra of most pink diamonds that are naturally colored by NV centers show a transmission window in the red region with a smooth, gentle slope (indicated by the blue dotted line in figure 19). These samples had a more pronounced window (represented by the shaded region) due to the emission from NV$^-$ centers. Fluorescence from the NV$^-$ center, activated by visible light, strongly enhances pink to red color in diamond. This phenomenon is not as obvious in natural-color pink diamonds that are colored by NV centers, due to their much lower concentrations.

Kyaw Soe Moe

PEARL

Cultured Pearls from *Pteria Sterna* With Plastic Bead Nuclei

It is generally agreed that freshwater mother-of-pearl shell nuclei produce the best results for both saltwater and freshwater beaded cultured pearls. Occasionally, other materials such as saltwater shell, ceramic, plastic, or wax have been used, but these are not common due to high rejection and mortality rates (P. C. Southgate and J. S. Lucas, Eds., *The Pearl Oyster*, Elsevier, Amsterdam, 2008).

Recently, we received two yellowish brown samples (both ~8 mm in diameter; e.g., figure 20) for identification. Microradiography revealed centrally positioned beads that were noticeably more transparent to X-rays than typical freshwater shell nuclei. The beads appeared to have distinct

Figure 19. In this UV-Vis-NIR absorption spectrum (here, of the 0.47 ct sample), the unusual shaded region represents the strong emission of NV$^-$ centers, which contribute to the pink bodycolor. In most natural-color pink diamonds, this region normally shows the absorption indicated by the blue dotted line.

UV-VIS-NIR ABSORPTION SPECTRUM

575
595
637

ABSORBANCE →

WAVELENGTH (nm)
400 500 600 700 800 900 1000

Figure 20. This cultured pearl from Pteria sterna (left, ~8 mm in diameter) proved to have a plastic bead. X-ray computed microtomography of a similar sample (center) showed the presence of a near-X-ray-transparent bead as well as a drill hole. When the first sample was sawn in half (right), a white plastic bead was revealed inside.

uniform edges and drill holes, although the cultured pearls themselves were not drilled. One had a slight exterior depression apparently corresponding to one end of the drill hole.

Further gemological testing (UV fluorescence, UV-Vis reflectance spectroscopy, and EDXRF analysis) indicated that these samples were from the saltwater mollusk Pteria sterna, a species native to the Sea of Cortez in Mexico. Although we have occasionally seen cultured pearls with near-X-ray-transparent beads, and reported on some of them in the Lab Notes section (e.g., Summer 1988, pp. 114–115; Spring 1994, p. 45), we decided to acquire the samples from the client in order to investigate further and identify the material that was used.

One of the two samples was examined using X-ray computed microtomography to obtain more detailed images of its internal structure (figure 20, center). The resulting images confirmed, with more detail, a distinct uniform bead outline and drill hole. The second sample was cut in half for visual observation and Raman spectroscopic analysis. The exposed bead was semitranslucent, white, with a plastic-like appearance (figure 20, right), and was easily scratched using a metal probe. Raman spectroscopy showed a dominant peak at 997 cm^{-1}, which corresponded to predominantly aromatic functional groups of possible polystyrene materials.

This is the first time we have reported on plastic beads used in *Pteria*

sterna mollusks. Whether this atypical bead material is becoming more prevalent is unknown.

[Note: Though we have used the term *cultured pearl* in this note for simplicity, we recognize that in this instance the usage may not be in agreement with recognized definitions, e.g., the CIBJO *Pearl Book*.]

Chunhui Zhou and Akira Hyatt

Large Conch Pearl

Pearls from the Queen conch, *Strombus gigas*, have long been collectors' items, prized for their unique and attractive color and surface structure. Conch pearls come in a range of colors from white to yellow to brown, but the most desirable is pink.

Recently, a large conch pearl mounted in a pendant (figure 21) was submitted to the New York laboratory for identification. The baroque-shaped light pink to white specimen measured 35.20 × 21.65 × 16.33 mm, weighed approximately 100 ct, and showed a very fine flame structure (figure 22). X-radiography revealed an unusually large number of layered natural growth structures, which corresponded to the contours of the pearl's surface.

Raman and UV-Vis reflectance spectra were collected from both the light pink and white regions of the pearl. Raman spectroscopy of the pink area with 514 nm excitation showed two small peaks at 1520 and 1130 cm^{-1}, which are characteristic of the pigments responsible for pink color in

Figure 21. The very large conch pearl in the pendant weighs approximately 100 ct. By comparison, most conch pearls (left, 8.04 ct, 13.53 × 10.65 × 7.95 mm) are much smaller, as are South Sea (second from right, 13.00 mm) and akoya cultured pearls (right, 6.75 mm).

Figure 22. The large conch pearl in figure 21 displayed a very fine flame structure. Magnified 100×.
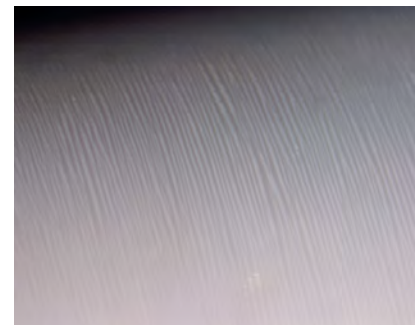
conch pearls. These peaks were barely visible in the spectrum of the white area. The UV-Vis reflectance spectrum of the pink area also showed stronger absorption between 480 and 560 nm than did that of the white area; this absorption in the green region of the spectrum is responsible for the pink color. All of these results suggested that the pink color was natural and not the result of treatment.

Though most conch pearls are small (see E. Fritsch and E. B. Misiorowski, "The history and gemology of Queen conch 'pearls,'" Winter 1987 *G&G*, pp. 208–221), large ones have been reported. The 2005 "Allure of Pearls" exhibit at the Smithsonian Museum of Natural History (www.mnh.si.edu/exhibits/Pearls/index2.htm) featured two loose pink conch pearls belonging to collector Susan Hendrickson that weighed 17.70 and 22.40 ct, as well as the Queen Mary Brooch set with two pink conch pearls weighing 24.90 and 28.10 ct. We reported on another large conch pearl in 2008 (125.26 ct; Spring 2008 Lab Notes, p. 72); though that baroque specimen was somewhat larger than this pearl, the bodycolor was a mix of pink, orange, and white. Most conch pearls are far smaller (again, see figure 21), making this specimen a true rarity, in both size and quality.

JaeWon Chang and Akira Hyatt

SAPPHIRE

Natural and Synthetic Green Sapphires with Similar Color but Remarkably Different Chromophores

Recently, two green gems were submitted to the New York laboratory. One stone (12.80 × 10.90 × 8.75 mm; figure 23, left), mounted in a ring with numerous transparent near-colorless stones, was easily identified as a natural sapphire by its inclusions and trace-element content measured by LA-ICP-MS. The other gem (2.07 ct; 7.77 × 6.09 × 4.93 mm) had no readily apparent inclusions (figure 23, center). Careful examination of the latter gem in immersion revealed faint curved color banding,

indicative of a melt-grown synthetic. LA-ICP-MS analysis confirmed that it was synthetic sapphire, as cobalt was the only trace element detected (average 25 ppma). Previous reports on cobalt-doped melt-grown synthetic sapphires were published in Spring 1996 Lab Notes (p. 51), Spring 2001 Gem News International (pp. 75–77), and Spring 2008 Lab Notes (pp. 72–73).

Sapphires—whether natural or synthetic—with such a distinct green coloration are rarely seen in the lab, and it is quite interesting that two very different compositions produced such a similar coloration. UV-Vis-NIR spectroscopy of the natural sapphire showed an absorption spectrum typical of corundum with a high iron content: strong lines at 450, 388, and 377 nm from Fe^{3+}, and broad bands at 580 and 700 nm due to Fe^{2+}-Ti^{4+} intervalence charge transfer (figure 24). In addition, the 1050–1075 nm band (due to Fe^{3+}) was surprisingly strong. It is well known that a high content of Fe^{3+} induces a yellow coloration in sapphire, and even small concentrations of Fe^{2+}-Ti^{4+} pairs contribute a blue color component. The resulting green color of this sapphire, which had an average Fe content of 1155 ppma, is quite consistent with its composition.

Polarized UV-Vis-NIR spectra of

the synthetic sapphire showed only two broad bands centered at 450 and 660 nm, which have been attributed to Co^{3+} substituting for octahedral Al^{3+} (e.g., R. Müller and Hs. H. Günthard, "Spectroscopic study of the reduction of nickel and cobalt ions in sapphire," *Journal of Chemical Physics*, Vol. 44, No. 1, 1966, pp. 365–373, http://dx.doi.org/10.1063/1.1726471). The two band positions were virtually identical for the ordinary and extraordinary rays, but the intensity of the 660 nm band was greater for the ordinary ray. Furthermore, a weak sharp line at approximately 691 nm was visible in the ordinary ray spectrum. A transmission window near 500 nm in the spectra of both samples is largely responsible for their similar green coloration.

Color coordinate calculations using the spectra reported in Müller and Günthard (1966) for 2-mm-thick wafers gave L*a*b* coordinates of 81/51/20 and 86/–34/36 for the ordinary ray and extraordinary ray, respectively (again, see figure 23). These correspond to a coloration that is remarkably similar to the synthetic sapphire reported here, supporting our conclusion that its color is due to Co^{3+}.

Emily V. Dubinsky

Figure 23. The 12.80-mm-long sapphire on the left was identified as natural, with its color due to a high iron content. The 2.07 ct gem on the right is a cobalt-bearing synthetic sapphire. For comparison, color coordinates (far right) were calculated for optical spectra reported in Müller and Günthard (1966) for Verneuil synthetic sapphire containing Co^{3+} (ordinary ray, top; extraordinary ray, bottom).

UV-Vis-NIR Absorption Spectra
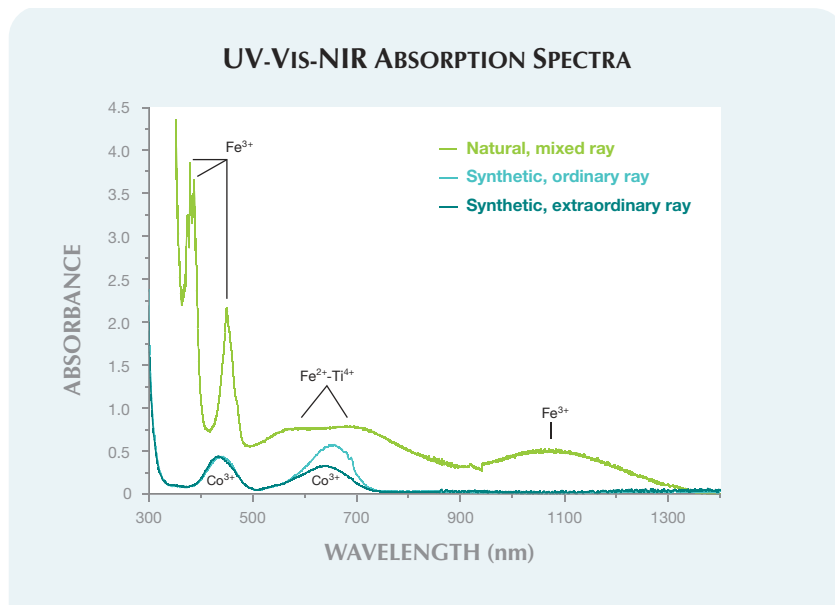
Figure 24. In these UV-Vis-NIR spectra, the natural green sapphire shows strong Fe-related features that are absent from the synthetic sample, which has bands attributed to Co^{3+}. The approximate path lengths of the beam are 9 mm for the natural stone and 5 mm for the synthetic sample.

Unusual Be-Diffused Pink Sapphire . . . A Cautionary Note

The Carlsbad laboratory recently examined a 1.40 ct pink sapphire with unusual orange color zones that was submitted for a sapphire report. Initial microscopic observation revealed numerous thermally altered light-colored crystals, some of which were surrounded by discoid "fingerprints" (fig-ure 25), an inclusion scene consistent with high-temperature heat treatment. Immersion revealed a planar orange zone near the culet and a shallow orange zone parallel to the table facet (figure 26). Orange color zones in heat-treated pink sapphires may be indicative of beryllium-diffusion treatment. However, when the stone was tested by laser–ablation inductively coupled plasma–mass spectrometry (LA-ICP-MS) in the girdle area (as is GIA's standard practice, to avoid placing an ablation spot in an area that could affect the stone's appearance), no Be was detected. This was not surprising because there was no orange color near the girdle.
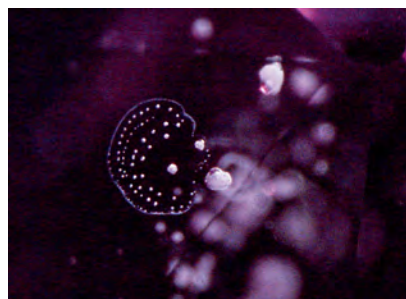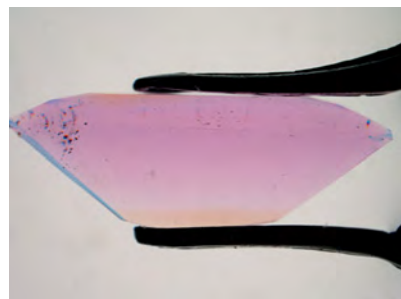
The orientation of the orange zoning in this sapphire was perpendicular to the c-axis. This is a common orientation for natural orange zones in padparadscha sapphire that are caused by trapped hole defects induced by an excess of natural magnesium (J. L. Emmett et al., "Beryllium diffusion of ruby and sapphire," Summer 2003 G&G, pp. 84–135). To rule out such orange zoning from naturally incorporated trapped hole centers, it was necessary to check for the presence of Be directly in one of the orange color zones. After obtaining permission from the client, LA-ICP-MS measurements revealed more than 35 ppma Be in an orange area, which is enough to impart significant orange color in a pink sapphire.

It was obvious from the shape and orientation of the color zones that the stone was beryllium-diffusion treated as a tabular preform or piece of rough that had sufficient sacrificial material to allow all traces of Be to be removed from the girdle area during cutting. It is difficult to say whether this was a deliberate attempt to defeat the standard practice of testing for beryllium in the girdle. Nevertheless, careful gemological observation in immersion and an understanding of color modification in corundum prevented this Be-diffused sapphire from being misidentified as a standard heated sapphire.

Nathan Renfro and Amy Cooper

Figure 25. The altered appearance of these crystals, which are probably zircon, is consistent with the high-temperature heat treatment necessary for Be diffusion of the host sapphire. Magnified 70×.

Figure 26. The orange color zones along the culet and table of this pink sapphire, as seen immersed in methylene iodide, were caused by Be-diffusion treatment. Magnified 10×.

Unusually High Beryllium in Three Blue Sapphires

Trace amounts of natural beryllium are sometimes detected in untreated sapphires, such as those from Madagascar. Typically, natural concentrations range from <1 ppma to about 4–5 ppma Be. Higher concentrations (>15 ppma) are usually associated with beryllium diffusion treatment.

Figure 27. This 3.21 ct sapphire contained relatively high levels of naturally occurring beryllium.

In addition, naturally occurring beryllium in corundum is often present with traces (usually <1 ppma) of niobium, tantalum, light rare-earth elements, and thorium (see A. Shen et al., "From the GIA Laboratory: Beryllium in corundum: The consequences for blue sapphire," *GIA Insider*, Vol. 9, No. 2, Jan. 26, 2007).

During routine testing, three blue sapphires recently submitted for identification were found to contain relatively high levels of beryllium. The three consisted of one ring-mounted stone and two loose sapphires weigh-

Figure 28. Higher concentrations of Be in this blue sapphire (values in ppma are shown next to each spot) were often associated with the presence of milky clouds. Magnified ~75×.
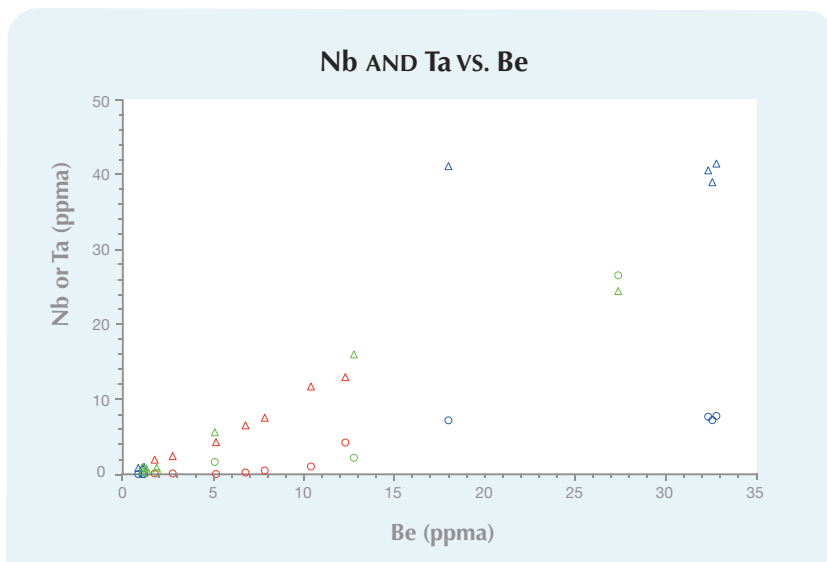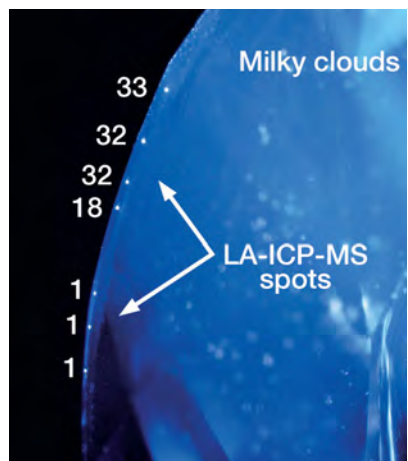
Figure 29. The concentrations of niobium (Nb, circles) and tantalum (Ta, triangles) showed an overall positive correlation to Be levels in the three sapphires (red = 3.17 ct, blue = 3.21 ct, and green = mounted sapphire). To convert to units of ppmw, the ppma values are multiplied by 0.44 for Be, 4.56 for Nb, and 8.87 for Ta.

ing 3.17 and 3.21 ct (e.g., figure 27). Two of the samples showed microscopic evidence of heating, while the other sapphire (3.17 ct) had inclusion features that proved it was unheated. The 3.21 ct stone showed a chalky blue reaction to short-wave UV radiation (consistent with its low iron content) and strong blue bands when viewed in immersion, while the other two sapphires were inert to long- and short-wave UV radiation due to their relatively high iron contents. All three stones contained milky clouds.

Trace-element analysis of all three sapphires with LA-ICP-MS showed a wide range of Be concentrations, from virtually absent up to 33 ppma (figure 28). The concentrations of Be were, in general, positively correlated to various transition metals and light rare-earth elements, including niobium, tantalum, tungsten, lanthanum, cerium, hafnium, and thorium (e.g., figure 29). Higher concentrations of all these elements, including Be, were often associated with the clouds, as documented previously in Be-bearing untreated sapphires. Magnesium also showed a positive correlation with Be, but with large

variations. Titanium showed both positive and negative correlation with Be, possibly due to Ti concentration variations in the blue zones.

The amount of Be in these sapphires is similar to or higher than that recorded in some Be-diffused stones. Their properties suggest that they came from at least two different deposits or deposit types, but their specific origins could not be determined. This is another example showing that thorough gemological and chemical analysis is necessary to identify beryllium-diffusion treatment.

Ren Lu and Andy H. Shen

DIAMONDS

Type Ib greenish brown diamonds with a color shift.
Single substitutional nitrogen causes yellow color in diamond. Therefore, type Ib diamonds are often assumed to be yellow (so-called *canary* diamonds). While this is true for type Ib synthetic diamonds, only rarely do their natural counterparts exhibit a pure yellow color. The most common color of type Ib diamonds is "olive," a mixture of green, brown-yellow, and gray. Some natural type Ib diamonds contain mixed orange and yellow colors, though often with a brownish or greenish component. In our experience, pure brown samples are by far the rarest of the type Ib diamonds, and they are seldom larger than 0.25 ct.

Recently, the GGTL laboratory received two greenish brown diamonds (1.22 and 3.01 ct) for analysis that were reportedly purchased directly from the mines in Simi, Sierra Leone. FTIR spectroscopy showed they were pure type Ib, with approximately 3.6 and 8 ppm, respectively, of single substitutional nitrogen. In daylight-equivalent illumination, the two diamonds were color graded Fancy Dark greenish brown and Fancy yellowish greenish brown. However, they showed a distinctly different coloration under incandescent light, where they appeared Fancy Dark orangy brown and Fancy orangy yellowish brown (figure 1).

When exposed to the 310–410 nm broadband illumination of our fluorescence microscope, both diamonds exhibited very distinct, rather homogenously distributed reddish orange luminescence. Exposure to standard UV radiation gave similar fluorescence reactions: orange to long-wave and a less intense orange to short-wave UV. Low-tempera-

ture (77 K) PL spectroscopy, using 405 and 532 nm excitation, identified the cause of the diamonds' luminescence as the NV^0 center (575 nm), which dominated their spectra (e.g., figure 2). In addition, the NV^- emission (637 nm) was detected with 532 nm excitation (figure 2, bottom).

The diamonds' UV-Vis-NIR spectra, obtained at 77 K inside an integrating sphere under intense incandescent illumination, showed the NV^0 and NV^- emissions were superimposed on the absorption continuum typical of brown diamonds. Intense incandescent light efficiently excited the NV^0 and NV^- fluorescence, influencing the apparent color of the diamonds.

It is important to note that the color grading of fancy-color diamonds actually includes the effect of fluorescence. For instance, purely yellow diamonds with strong green luminescence can receive green color grades, even though they do not have a greenish bodycolor. (However,

Figure 1. These 1.22 ct (top) and 3.01 ct (bottom) greenish brown type Ib diamonds, seen under daylight-equivalent illumination (left), become distinctly orangy brown under incandescent light (right). Photos by T. Hainschwang.
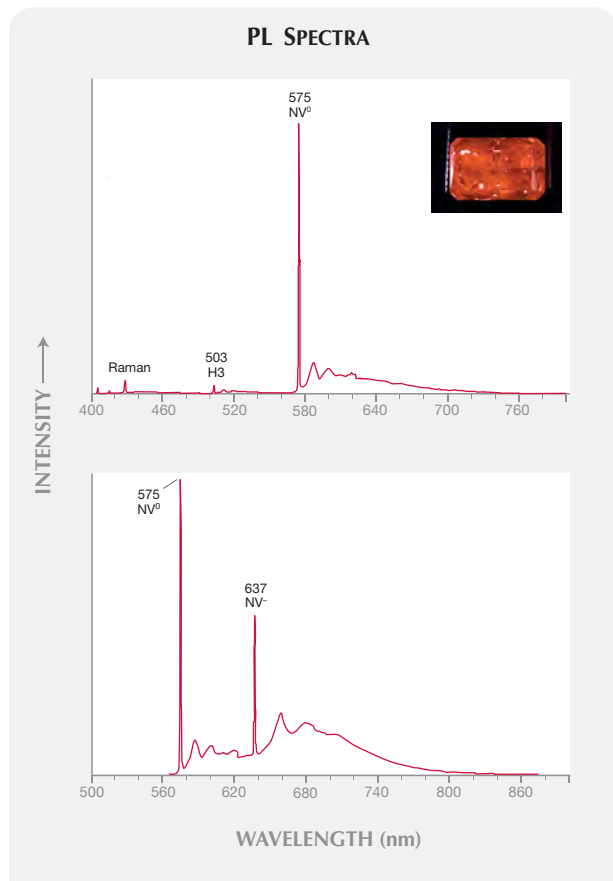
PL SPECTRA

Figure 2. The low-temperature photoluminescence spectra of the 1.22 ct diamond at 405 nm (top) and 532 nm excitation (bottom) show that the orange luminescence (inset, photographed under 310–410 nm broadband excitation) is caused by the NV^0 defect. Inset photo by T. Hainschwang.

near-colorless diamonds with extremely strong blue fluorescence are not color graded blue.) A notable example of a diamond with this type of fluorescence-related color change is the light brown Tavernier diamond, which appears light pink in incandescent light (Y. Liu et al., "The alexandrite effect of the Tavernier diamond caused by fluorescence," *Color Research and Application*, Vol. 23, No. 5, 1998, pp. 323–327, http://dx.doi.org/10.1002/(SICI)1520-6378(199810)23:5<323::AID-COL8>3.0.CO;2-Y). However, the Tavernier is not considered a fancy-color diamond since it belongs to the D-to-Z range.

We informed the client of the observed color shift shown by the diamonds and noted the phenomenon on their reports, with a comment stating that it was related to fluorescence.

Thomas Hainschwang
(thomas.hainschwang@gemlab.net)
and Franck Notari
GGTL Gemlab–Gemtechlab Laboratory
Balzers, Liechtenstein, and Geneva, Switzerland

Emmanuel Fritsch

COLORED STONES AND ORGANIC MATERIALS

Gem-quality afghanite from Afghanistan. At the 2011 Tucson gem shows, Dudley Blauwet (Dudley Blauwet Gems, Louisville, Colorado) exhibited several hundred afghanites with a light blue color similar to that of aquamarine (e.g., figure 3). Mr. Blauwet purchased his first rough piece of this material during a December 2009 trip to Peshawar, Pakistan. His supplier was not certain of the stone's identity, only that it came from a group of mines near the well-known Lajuar Madan lapis lazuli deposit in the Sar-e-Sang district of Afghanistan's Badakhshan Province. The crystal yielded a clean 1.16 ct trilliant.

On a return visit in November 2010, Mr. Blauwet purchased two additional lots of the material, 96 g in all, from a former partner of the original supplier. These were sold to him as afghanite, an identity confirmed by electron microprobe analysis (performed by Cannon Microprobe, Seattle, Washington) of two crystals. They exhibited hexagonal pyramidal terminations, which is typical of afghanite. From this rough parcel, about 45 carats of clean
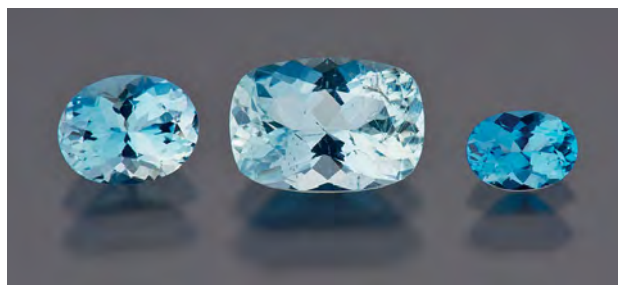
Figure 3. These light blue afghanites (0.50, 1.16, and 0.23 ct) were faceted from material reportedly found recently in Afghanistan's Badakhshan Province. Photo by Robert Weldon.

stones were cut, the two largest weighing 1.16 and 1.18 ct. Later in November, Mr. Blauwet returned to Peshawar and obtained another 320 g of rough sorted into four lots of various qualities. Some of these pieces also displayed the distinctive hexagonal pyramidal terminations. The two better lots, which totaled about 65 g, featured clean facet-grade material, including one piece that may eventually yield a 3.5 ct gem. Most of the lesser-quality rough was translucent, with some appearing silky.

Afghanite typically has a dark blue color, and gem-quality stones are considered very rare (see Spring 2008 GNI, pp. 79–80). Mr. Blauwet noted a strong demand for this brightly colored afghanite in Tucson.

Stuart D. Overlin (soverlin@gia.edu)
GIA, Carlsbad

Iridescent ammonite from Madagascar. At the 2011 Tucson Gem shows, Marco Campos Venuti (Seville, Spain) had iri-

Figure 4. Ammonite from Madagascar showing attractive iridescence is now being cut into cabochons, in addition to the polished fossils seen previously. The specimens shown here range from 2.8 to 6.4 cm long. Photo by Jeff Scovil.

descent fossil ammonites from southern Madagascar as whole polished pieces as well as cabochons (figure 4). Although this type of ammonite has been known for more than a decade (see, e.g., Fall 2000 GNI, pp. 267–268), this was the first time that this author has seen it fashioned into cabochons for jewelry use. Mr. Campos Venuti marketed this material as "Madammolite," and had about 50 cabochons that were cut into various shapes, as well as 100 matched pairs, ranging from 15 to 40 mm in longest dimension. He stated that the outer surface of the fossil must be polished off to reveal the underlying iridescence; no stabilization or other treatments are performed on the material. All of the pieces displayed red-orange iridescence, and small areas of green and blue also were seen in a few cabochons. The iridescent layer was very thin (<1 mm), and was better developed on one side of the fossil than the other, which created difficulty in cutting matched pairs. Fractures in the material created an additional challenges for shaping the cabochons. The iridescent patterns ranged from smooth and homogenous to a pleasing ridged appearance.

The availability in a variety of shapes and matched pairs gives designers interesting opportunities to incorporate these iridescent gems into jewelry, provided they are properly protected from scratching or impacts that could break the thin nacreous layer.

Brendan M. Laurs

Aquamarine from Thanh Hoa Province, Vietnam: Mining update. In May 2011, this contributor visited the aquamarine deposits on the west side of Thanh Hoa Province in northern Vietnam (see L. T.-T. Huong et al., "Aquamarine from the Thuong Xuan District, Thanh Hoa Province, Vietnam," Spring 2011 *G&G*, pp. 42–48, http://dx.doi.org/10.5741/GEMS.47.1.42). The journey started in Hanoi, the home of Mr. Lai Duy, a close friend and guide for the trip. We drove south on the main highway for about five hours to Thanh Hoa city. Continuing on narrow side roads, we passed lush rice fields and beautiful karst (weathered lime-

stone) landscapes en route to the remote mountains that host the aquamarine-bearing granitic pegmatites. From the village of Xuan Le, motorbikes were used to traverse the final 7–8 km to the base of the mountains, along a narrow dirt track that crossed several streams on rickety 1-m-wide wooden bridges.

A steep slippery footpath led from Lang Ben village up to the mining area. After climbing slowly in the tropical heat for about 1 hour and 40 minutes—and passing an area that reportedly was mined for topaz—the trail emerged from the jungle into an area containing dozens of shallow pits mined for the aquamarine (e.g., figure 5). The workings were sporadically distributed over a distance of ~400 m, extending from an elevation of 592 m (1,943 ft) to 621 m (2,039 ft). The pegmatites dipped almost vertically and were highly decomposed. The shafts reached depths up to 15 m (figure 6), and horizontal tunnels were present at the bottom of some shafts. There were no timbers or other supports, but the tunnels did not appear in danger of collapsing. No pumps or any other mechanized equipment were present, probably due to the difficulty of the climb, and the fact that hand tools were sufficient for digging through the

Figure 5. Aquamarine workings in Vietnam's Thanh Hoa Province consist of small pits surrounded by dense jungle. Photo by D. Blauwet.
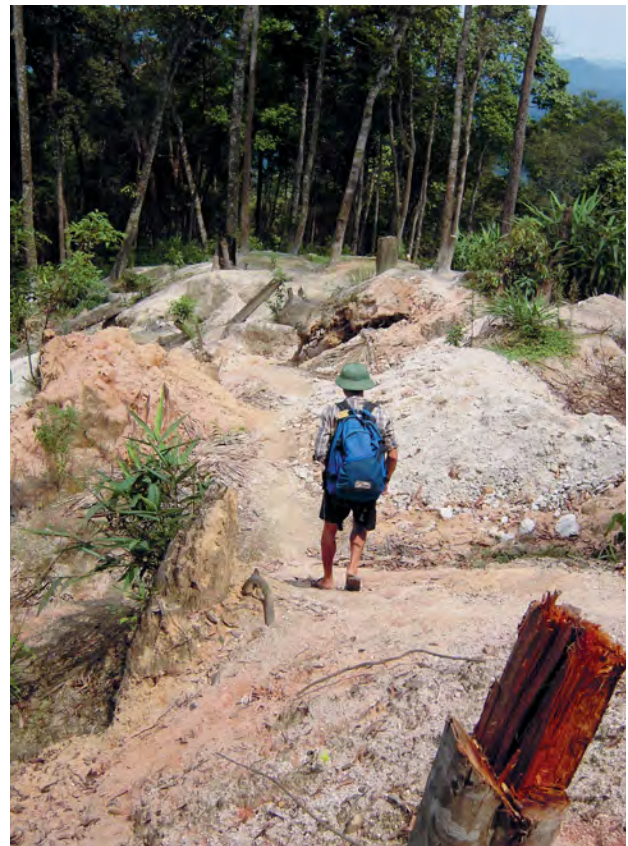
Figure 6. At the Thanh Hoa deposits, ropes are used to hoist aquamarine-bearing material from shafts (left). Some of the shafts reach depths of ~15 m (right). Photos by D. Blauwet.

weathered deposit. According to a local miner, this area had been worked for about four years, producing an estimated 50–60 kg annually of mixed-grade aquamarine.

Climbing higher up the mountain to an elevation of 811 m (2,661 ft; coordinates 19°50.7′ N, 105°09.7′ E) revealed an area that was actively being mined for aquamarine and topaz. These workings consisted of larger tunnels that penetrated deeper (15–20 m) into the hillside but at shallow angles. These pegmatites contained much more quartz, with broken fragments up to ~20 cm seen in the mine dumps. The quartz was generally opaque, white to light smoky, and partially crystallized. Approximately a dozen miners were active in this area, and they offered small parcels consisting of broken fragments (1–3 g) and a few complete crystals (up to ~7 cm long; figure 7) of attractive blue aquamarine. The crystals commonly had small fractures along their length that would restrict the cutting of clean stones to relatively small sizes but with good color saturation (again, see figure 7). Colorless topaz was occasionally found as small lustrous transparent crystals. The miners indicated this area had been worked for several months.

This fascinating—and arduous—expedition provided a first-hand view of these little-known aquamarine deposits, which appear to have good potential for producing gem- and specimen-quality material for many years to come.

Dudley Blauwet (mtnmin@q.com)
Dudley Blauwet Gems, Louisville, Colorado

Purplish blue and red-brown chalcedony from Peru. While chalcedony often occurs in light blue hues, saturated blue specimens are known from just a few localities, such as Ysterputz in Namibia and Chikwawa in Malawi. Blue chalcedony was found in Peru several years ago, but the quality was not high and the material was only used locally. The exact locality is not publicly known, though initially it was believed to lie in the vicinity of Huachocolpa in the Huancavelica region. This contributor was recently informed by a reliable local dealer, who visited the locality, that the material comes from a site called Yanacodo, about 30 km west of the city of Huancavelica. Recent production from this deposit (since 2010) is comparable to the finest blue chalcedony from other sources (e.g., figure 8). While in Lima in February 2011, this contributor saw several hundred kilograms of rough and at least 50 cabochons

measuring up to 4 cm across.

Ten pieces of rough and five cabochons were examined by this contributor for this report. All were purplish blue, and many displayed agate-like zoning. The samples had a spot refractive index of 1.54 and a specific gravity of 2.60–2.61, consistent with published values for chalcedony, and no features were seen with the hand spectroscope. As expected, the material showed an aggregate reaction in the polariscope, which confirmed its fibrous structure. The chalcedony was inert to UV radiation, although a few pieces contained veinlets that fluoresced white to both long- and short-wave UV radiation.

Another unusual chalcedony from Peru appeared in February 2011. It is reportedly from the vicinity of Santa Ana village, about 30 km southeast of Huancavelica. The chalcedony is red-brown and therefore can be described as sard or carnelian. It contains small cavities that are usually filled by colorless chalcedony. Although carnelian normally occurs as concretions in sedimentary rocks, here it forms crusts and rarely even stalactites up to 3 cm long (e.g., figure 9) within cavities hosted by volcanic rocks. From a study of three pieces of rough and three table cuts, its gemological properties were the same as for the blue variety, except that it fluoresced green to long-wave UV—particularly in lighter colored areas.

Jaroslav Hyršl (hyrsl@kuryr.cz)
Prague, Czech Republic

Figure 7. These Vietnamese aquamarines range from 1.5 to 7.1 cm long (crystals) and 1.34 to 6.96 ct (cut stones). Photo by Robert Weldon.

Figure 8. Fine blue chalcedony such as these pieces (6.1 and 4.0 cm wide) became available from Peru in 2010. Gift of J. Hyršl, GIA Collection nos. 38420 and 38421; photo by Robert Weldon.

Update on emerald mining in Afghanistan. In May 2011, author VP traveled to Afghanistan to collect reference samples for GIA's laboratory. Unfortunately, due to the security situation in parts of Afghanistan, it was impossible to visit the ruby mining area near Jegdalek or the various deposits in Badakhshan. However, the authors spent three days in the emerald mining area near the village of Khenj in the Panjshir Valley (see, e.g., G. W. Bowersox et al., "Emeralds of the Panjshir Valley, Afghanistan," Spring 1991 *G&G*, pp. 26–39, http://dx.doi.org/10.5741/GEMS.27.1.26).

We witnessed about 400 miners working in the Khenj area. Mining is performed by groups of up to 20 people, some working in day/night shifts. The most active site was Kamar Safeed (figure 10), situated on cliffs at an elevation of 3,000 m. Up to 300 miners were working this site.

Figure 9. Carnelian from Santa Ana, Peru (here, 10.5 cm wide), rarely displays finger-like formations. Photo by J. Hyršl.

Small groups were also active at Koskanda, Norola, Siakolo, Habal, and Batak. The Michalak area, where several hundred miners were said to be active in 2010, was practically abandoned. The Tartah and Dalnow deposits have reportedly been exhausted. Security concerns prevented a visit to the emerald mining areas in the Panjshir Valley located outside of the Khenj area (Dach Te Rivaat and Mukeni), where operations are reportedly limited.

All of the mining activities witnessed at Khenj were underground, in a maze of tunnels reaching 200 m deep. Because conventional explosives cannot be legally obtained in Afghanistan, miners were fabricating their own by mixing fertilizer with the contents of old unexploded Soviet military ordnance (figure 11). These mixtures are too powerful for gem mining, and many fine stones are consequently broken or fractured by the blasts.

Dealers in Kabul reported that emerald production had been good during the past few months, and this was confirmed by miners in Khenj. The emerald parcels were said to be exported to Pakistan or Dubai for faceting. The gems were typically light green to deep green, often with very good transparency. While most of the rough stones were small (less than 1 g), we also saw several large fine emerald crystals up to 6 g, as well as some attractive mineral specimens. A preliminary study of the emeralds obtained from the Khenj area (e.g., figure 12) revealed that their inclusions mirror those normally seen in Colombian emeralds.

The situation at the emerald mines has improved since VP's previous visit in 2006. Khenj can now be reached in three hours from Kabul using a new road. Small hydroelectric power stations have brought electricity to the valley, and the miners are using generators to light and ventilate the tunnels. While working the Panjshir emerald mines remains very difficult, the high-quality stones can provide good income.

Figure 10. Situated on steep cliffs, Kamar Safeed is the most active emerald mining area near Khenj, a village in the Panjshir Valley of Afghanistan. Photo by V. Pardieu.

Figure 11. Afghan emerald miners mix fertilizer with old Soviet military explosives for blasting purposes, which often damages the fragile crystals. Photo by V. Pardieu.

The Afghan government faces many challenges, one of which is replacing a complicated and inefficient rough stone export system. According to one government official, the tax value of a parcel for export must be negotiated and a 15% tariff paid, then another 9% is levied at the airport. In addition, several papers must be obtained from the Ministry of Mines and the Afghan Chamber of Commerce

Figure 12. These emerald samples are from the Khenj area of the Panjshir Valley. The cut stones weigh ~1.5–2 ct. Photo by V. Pardieu.

and Industry. The whole process takes anywhere from three days to a week. Streamlining the export process would encourage legal exports, benefiting the local gem industry and the country as a whole.

Vincent Pardieu (vpardieu@gia.edu)
GIA, Bangkok

Guy Clutterbuck
CGM Ltd., Dublin

A deep green fuchsite-rich rock. The Ricerche e Analisi Gemmologiche (RAG) laboratory in Turin, Italy, received for identification three samples of a deep green material that resembled jadeite or nephrite (figure 13). No information was provided on the samples' source. The material consisted of thin slabs no more than a few millimeters thick, with a fine granular structure characterized by a deep green matrix and some very small white spots.

Figure 13. This polished slab (~32 mm long), resembling jadeite or nephrite, proved to be a rock composed of fuchsite, albite, and sphene. Photo by R. Navone.

The samples' RI, measured with a refractometer using the distant observation technique, was between 1.53 and 1.56. The SG was 2.78 and the Mohs hardness was 5–5½. The material was inert to long- and short-wave UV radiation, and the handheld spectroscope showed general absorption in the deep red region of the spectrum. The samples had a fairly even color distribution and no apparent cleavage. At first glance, they could have been either natural or artificial, as they resembled a compressed powder with some type of hardening media.

With the permission of the client, we cut a thin section from one of the slabs for examination with a polarizing microscope (figure 14). The matrix consisted of a colorless to green foliated aggregate with low relief and low-order interference colors, consistent with a mica-group mineral. The thin section was also studied at the University of Turin's mineralogy department with a Cambridge S-360 scanning electron microscope equipped with an Oxford INCA energy-dispersive spectrometer. SEM-EDS spectroscopy identified the material as fuchsite, the green chromium-bearing variety of muscovite (in this case,
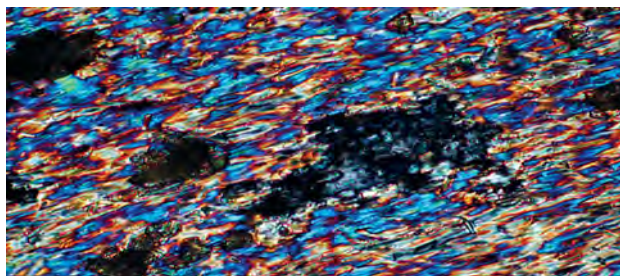
Figure 14. Viewed in cross-polarized light, this thin section of one of the slabs shows bright interference colors corresponding to Cr-bearing muscovite, gray low-relief areas of albite (center), and high-relief grains with high-order interference colors that are sphene. Photomicrograph by E. Costa; image width ~0.5 mm.
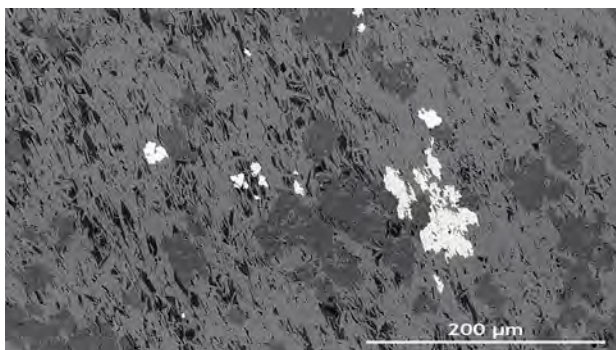
Figure 15. The texture of the green rock is well displayed in this backscattered electron image of the thin section in figure 14, which shows Cr-bearing muscovite (light gray), albite (dark gray), and sphene (white). The black areas are microscopic pores in the rock. Image by E. Costa.

1.0–1.5 wt.% Cr_2O_3). Also present was an anhedral gray to white mineral with low relief; it was shown to be albite. Finally, there were a number of high-relief inclusions, deep yellow to brown and brownish black, with high-order interference colors; these were identified as sphene.

Figure 15 shows an SEM backscattered electron image of the thin section, in which the gray tone is proportional to the mean atomic number of the phase. The light gray–appearing matrix is the Cr-bearing muscovite, the dark gray areas are albite, and the white portions represent sphene.

We detected no dyes, polymers, or other foreign media, and the texture of the minerals demonstrated the material's natural origin. We concluded that the slabs were cut and polished from a fine-grained metamorphic rock consisting predominantly of fuchsite. The material had an attractive green color and could be used for cabochons or carving, although with caution due to its relatively low hardness. Cabochons consisting of fuchsite aggregates have been seen previously (as emerald imitations; see Summer 2002 Gem News International [GNI], pp. 183–184), but those were more translucent than the material documented here, and they also contained inclusions of rutile and dolomite, rather than the albite and sphene impurities in the present samples.

Emanuele Costa (emanuele.costa@unito.it)
Department of Mineralogy and Petrology
University of Turin, Italy

Raffaella Navone
RAG Gemological Laboratory, Turin

Color-change garnet from Nandagala, Tanzania. Mark Saul (Swala Gem Traders, Arusha, Tanzania) recently informed GIA's Bangkok lab about a new deposit of color-change garnet near Nandagala village, Lindi Province, southern Tanzania. According to Mr. Saul, the stones were believed to be alexandrite when first discovered in January 2011, resulting in a minor gem rush and several dealers overpaying for rough. The garnet comes from two diggings: A primary deposit where small (typically <0.2 g) dark-colored stones are found, and a nearby alluvial deposit that produces somewhat lighter pieces up to ~2 g. One large (>5 g) clean stone from the alluvial deposit was faceted into the 11.81 ct gem in figure 16. The alluvial deposit also produces clean but nonphenomenal brownish orange garnets, some of which exceed 20 g.

The five rough samples in figure 16 were purchased by GIA, and four were polished with parallel windows and examined for this report. Their color change was distinct, showing greenish blue in fluorescent light and purplish red or red in incandescent light. They had RI and SG values of 1.762 and 3.89, which are typical for color-change pyrope-spessartine (e.g., D. V. Manson and C. M. Stockton, "Pyrope-spessartine garnets with unusual color behavior," Winter 1984 *G&G*, pp. 200–207, http://dx.doi.org/10.5741/GEMS.20.4.200). They were inert to long- and short-wave UV radiation. With the desk-model spectroscope, the

Figure 16. Pyrope-spessartine from Nandagala, Tanzania, shows a distinct color change between daylight-equivalent fluorescent (left) and incandescent (right) light. The faceted stone weighs 11.81 ct and the rough pieces are 0.4–1.2 g. Photos by V. Pardieu.
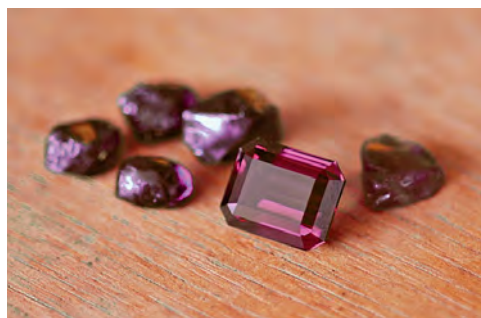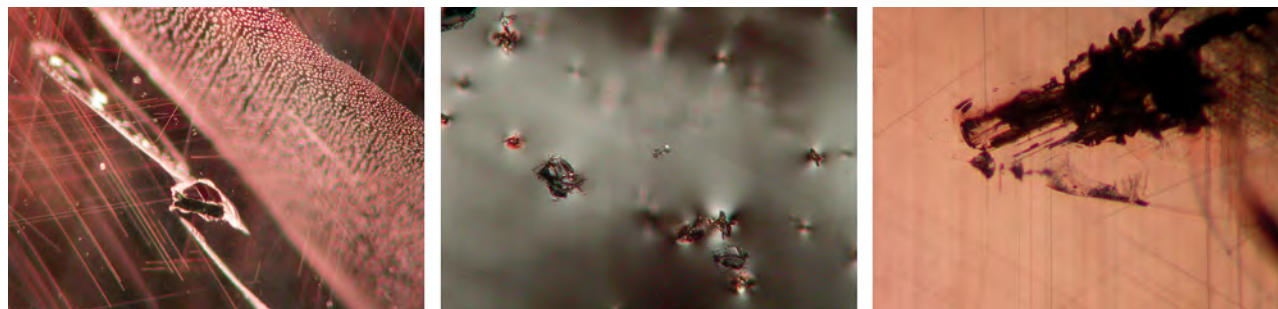
Figure 17. Partially healed fissures, needles, and black grains formed a typical inclusion scene in the color-change garnet samples (left). Also present were zircon-like crystals (center; cross-polarized light) and another type of dark reddish brown crystalline inclusion (right). Photomicrographs by V. Pardieu; magnified 40×.

darkest sample showed a band at ~400 nm and a broad absorption at ~570 nm; the latter feature was less obvious for lighter stones with a weaker color change. The inclusion scene (figure 17) was dominated by needles, zircon-like crystals, partially healed fissures, and negative crystals. We also saw some black opaque, reddish brown, and elongated greenish crystals. Unfortunately, the inclusions were too deep in the samples to be identified with Raman spectroscopy.

Chemical composition was measured using EDXRF spectroscopy and a Thermo X Series II LA-ICP-MS. The garnets had an average composition of $Pyp_{51}Sps_{40}$-$Grs_{3.5}Alm_3Gol_2Uva_{0.5}$ (with 7300 ppm V and 1100 ppm Cr). This was very similar to that reported for color-change garnets from Bekily, Madagascar (K. Schmetzer and H. J. Bernhardt, "Garnets from Madagascar with a color change of blue green to purple," Winter 1999 *G&G*, pp. 196–201, http://dx.doi.org/10.5741/GEMS.35.4.196).

UV-Vis absorption spectra were collected using a PerkinElmer Lambda 950 spectrometer. A strong absorption band at ~570 nm (due to V^{3+} and Cr^{3+}) dominated the spectra of all samples (e.g., figure 18). This band created two

Figure 18. This UV-Vis spectrum of a light-colored Nandagala garnet (3.3 mm thick) shows a broad absorption at ~570 nm due to V^{3+} and Cr^{3+}, creating transmission windows in the blue-green and red regions.
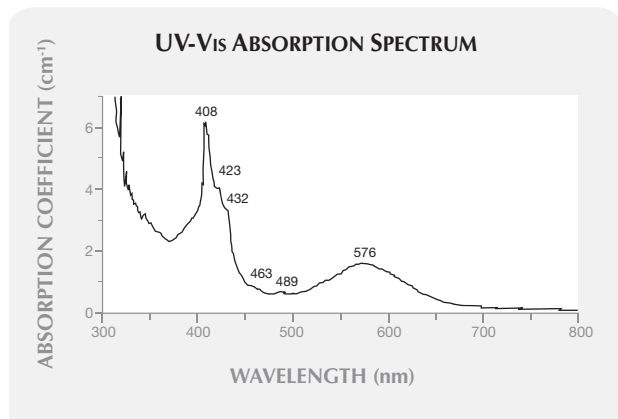
transmission windows, in the blue-green (~480 nm) and red (700 nm) regions, which are responsible for the color change. The darkest sample showed a cutoff at ~440 nm, while the lighter stones had a cutoff at ~310 nm and also showed absorptions due to Mn^{2+} (408, 423, and 489 nm), Fe^{3+} (432 nm), and Fe^{2+} (463 nm; see P. G. Manning, "The optical absorption spectra of the garnets almandine-pyrope, pyrope and spessartine and some structural interpretations of mineralogical significance," *Canadian Mineralogist*, Vol. 9, 1967, pp. 237–251).

This new Tanzanian deposit joins Kenya and Madagascar as another source of color-change garnet in the East African region.

Vincent Pardieu, Kamolwan Thirangoon, and
Sudarat Saeseaw
GIA, Bangkok

An examination of some colorless gems from Myanmar. This contributor recently had the opportunity to examine rough and cut samples of four colorless gems—phenakite, petalite, pollucite, and goshenite beryl—recovered from granitic pegmatites located near Molo village in Momeik township, northern Shan State, Myanmar. At this locality, pegmatite dikes intrude a peridotite body that is hosted by gneiss, marble, and calc-silicate rocks of the Mogok Group. The pegmatites primarily produce gem-quality pink tourmaline, along with other minerals such as topaz, beryl, hambergite, quartz, and the colorless gems listed above (see, e.g., figure 19 and U H. Kyi et al., "The pegmatitic gem deposits of Molo [Momeik] and Sakhan-gyi [Mogok]," *Australian Gemmologist*, Vol. 22, No. 7, 2005, pp. 303–309).

The phenakite (Be_2SiO_4) crystals were distorted and some were twinned. They showed etch marks on their prism faces. The faceted gems usually weigh <1 ct. Inclusions consisted of small growth tubes and tiny irregular solid crystals.

The petalite ($LiAlSi_4O_{10}$) crystals showed etched cleavages with deep channels. The material is transparent in a range of sizes, yielding finished gems of 3–50 ct. Small solid colorless rounded inclusions were present.

The rough pollucite ($CsAlSi_2O_6 \cdot nH_2O$) did not show any crystal faces, and its surfaces were cracked, pitted, and

UV-Vis Absorption Spectrum

Figure 19. These samples of phenakite (2.5 ct), goshenite (4.9 ct), and pollucite (1.0 ct) are from the Momeik area near Mogok, Myanmar. Photo by U T. Hlaing.

Figure 20. These samples of Nuummite (an aggregate of iridescent orthoamphibole) from Mauritania weigh 9.20–16.03 ct and illustrate the variation in color of this material. Photo by, and gift of, G. Scott Davies; GIA Collection nos. 38384–38386.

iron stained. Cut gems generally range from 3 to 6 ct. Parallel lath-like solid inclusions and spiky crystals were seen.

The goshenite crystals were tabular and typically yield finished gems of 0.85–2.0 ct. The material was quite included, with internal features consisting of two-phase "fingerprints," distorted needle-shaped crystals in random orientations, and white opaque solids.

The gemological properties recorded from the phenakite, petalite, pollucite, and goshenite samples were within reported ranges. They can be differentiated from one another by their standard gemological properties (e.g., RI and/or SG values) and sometimes by their morphologic characteristics. The Burmese petalite is tabular to elongated with prominent cleavage, phenakite forms isolated prismatic crystals with rhombohedral terminations, goshenite typically consists of short prismatic crystals, and pollucite is recovered as broken pieces without any crystal faces.

U Tin Hlaing
Dept. of Geology (retired)
Panglong University, Myanmar

Nuummite from Mauritania. Iridescent orthoamphibole (anthophyllite-gedrite) as a gem material was first reported from Greenland nearly 25 years ago (P. W. Uitterdijk Appel and A. Jensen, "A new gem material from Greenland: Iridescent orthoamphibole," Spring 1987 G&G, pp. 36–42, http://dx.doi.org/10.5741/GEMS.23.1.36). Until fairly recently, this was the only known locality for this gem, called *Nuummite*. The Greenland material is notable for its golden iridescence, though blue iridescence has also been seen (Spring 2000 GNI, pp. 73–74).

In 2009, a new source of gem-quality iridescent orthoamphibole was discovered in the Sahara Desert of central Mauritania (see T. Kobayashi, "Iridescent Nuumite," *Gemmology*, Vol. 41, No. 486, Issue 3, pp. 14–15 [in Japanese]). Three faceted stones and a piece of rough were donated to GIA by G. Scott Davies (American-Thai Trading, Bangkok). His company has cut more than 3,000 carats of this Nuummite, showing iridescence that is mostly bluish green, although some stones appear golden yellow and a small percentage are a highly desirable pure blue (e.g.,

figure 20). Finished stones are typically cut to between 10 and 20 mm, corresponding to a weight range of ~8–20 ct in cabochon or faceted form. This size range is preferable because the iridescence is not apparent in smaller stones, and larger pieces can show an uneven color distribution.

Raman spectra of the iridescent laths were consistent with anthophyllite and gedrite, which are orthorhombic members in the magnesium-iron-manganese-lithium amphibole group. The samples had RI measurements between 1.649 and 1.669, consistent with the Raman identification. A second shadow edge also was noted at 1.54, due to an additional mineral component in the rock. Brassy metallic mineral grains, presumably pyrite, were also seen in the samples. Hydrostatic SG was 2.98 ± 0.05, and all three stones were inert to long- and short-wave UV radiation. With magnification, the iridescent phenomenon closely resembled that of labradorite. It therefore seems likely that the iridescence is caused by a lamellar structure

Figure 21. These Nuummite orthoamphibole laths show blue iridescence on the outer perimeter that shifts to greenish yellow toward the interior, suggesting a chemical variation within the crystal. Photomicrograph by N. Renfro; magnified 20×.
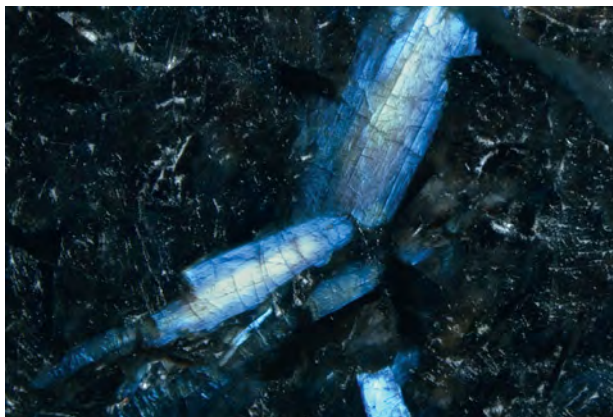
Figure 22. Mechanized mining is once again producing blue opal from Sinaloa, Mexico (left). The opal is hosted by rhyolite, and the adjacent matrix is commonly silicified into perlite (right). Courtesy of Blue Opal Light Co.

of the orthoamphibole mineral grains. The iridescence displayed color zoning from blue to greenish yellow toward the core of the crystals (figure 21). This type of concentric zoning suggests a chemical variation in the amphibole.

This new find of iridescent orthoamphibole makes for an interesting and unusual gem. This material has also been offered by online dealers as spheres several centimeters in diameter.

Nathan Renfro (nrefro@gia.edu)
GIA, Carlsbad

Blue opal showing play-of-color from Sinaloa, Mexico. Mexican opal is known mainly from Querétaro and Jalisco States, which are most recognized for producing "fire" and "crystal" varieties. Recently the owners of an opal mine in Sinaloa State (Bertha Almaral, Marco Reyes, and Juan Vital) showed this contributor a number of specimens that displayed a blue bodycolor and an attractive play-of-color.

The volcanic-hosted deposit is located near the town of Cosalá, approximately 137 km (85 miles) north of Mazatlan. Although the site was discovered 25 years ago, mining activity has been sporadic and limited to hand methods. Under the ownership of Blue Opal Light Co. since April 2011, operations have become mechanized. A backhoe fitted with a hydraulic hammer is used to break up the host rhyolite in search of opal concentrations (figure 22, left). This opal forms nodules and infillings in a rhyolite lava flow, and is commonly surrounded by perlite (figure 22, right). The owners estimate that only 10% of the deposit has been mined.

Two cabochons (one loose and one mounted) were briefly examined at GIA, and they had spot RI values of 1.46 and 1.47. The hydrostatic SG of the unmounted sample was 2.32, but this value is not reliable due to the presence of some matrix material in the cabochon. Both samples—as well as several rough pieces—showed interesting UV fluorescence: They were inert to long-wave but luminesced strong green to short-wave UV, with no phosphorescence.

The opals (figure 23) are reportedly stable, as pieces discovered two decades ago have not shown any crazing. The material will be marketed as Lightning Blue Opal, starting in late 2011.

Stuart D. Overlin

Pallasite pendants. Bob and Carol Falls of Rock Falls Designs (Colorado Springs, Colorado) recently showed GIA some interesting pendants (e.g., figure 24) set with pallasite from the Esquel meteorite. Pallasite is a rare type of stony iron meteorite containing inclusions of transparent crystalline olivine (peridot) in an iron-nickel matrix (for more information on pallasitic peridot, see the article by A. Shen et al. on pp. 208–213 of this issue). Faceted pallasitic peridot, though rare, has seen jewelry use in the past. These pendants were unusual in that they combined polished pieces of pallasite with mother-of-pearl to create an attractive optical effect.

According to Mr. Falls, slices of pallasite were selected based on the characteristics of the olivine crystals, which need to be sufficiently large and transparent. These were then polished and mounted on top of iridescent slabs of mother-of-pearl, which were selected based on the pattern and positioning of the iridescent areas. The sheen from the mother-of-pearl helps to reflect light back through the olivine crystals; the backs of the pendants also are left open to allow light in from behind.

Mr. Falls reported that five of these pendants have been produced to date, ranging from 2 to 5 cm long. They plan to continue production as long as sufficient Esquel material is available.

Thomas W. Overton (toverton@gia.edu)
GIA, Carlsbad

Figure 23. These opals from Sinaloa represent higher-quality material from the deposit. The loose cabochon weighs 30.41 ct, and the matrix specimen is 8.7 cm long. The earrings in the inset contain opals measuring 21 × 12 mm. Samples courtesy of Blue Opal Light Co.; photos by Robert Weldon.

Figure 24. This unusual pendant (2.5 × 3.0 cm) is mounted with polished pallasite over mother-of-pearl. Photo by Robert Weldon.

Figure 25. These Chinese freshwater cultured pearls (17–21 mm long) proved to be beaded by baroque cultured pearls. Photo by E. Strack.

Chinese freshwater cultured pearls beaded with baroque freshwater cultured pearls. This contributor recently examined a strand of Chinese freshwater cultured pearls loaned by Jeremy Shepherd of Pearl Paradise, Los Angeles, California. According to Mr. Shepherd, they were produced at the same farm in Jiangsu Province that was the source of the so-called "Soufflé pearls" ("beaded" with mud) that began appearing on the market in September 2009 (see Spring 2010 GNI, pp. 61–63).

The strand (figure 25) originally consisted of 23 cultured pearls weighing a total of 66.8 g; two were subsequently sacrificed for destructive testing (see below). They were of baroque shape, ranging from 17.0 × 12.0 mm to 21.0 × 13.6 mm. Colors varied from white with a distinct purplish green overtone to light purple, purplish green, orange, and bronze with varying overtones. The five cultured pearls with a white bodycolor all showed strong blue fluorescence to long-wave UV radiation; the others were inert. All displayed a pronounced metallic luster (again, see figure 25).

Thirteen of the 23 cultured pearls were examined by X-radiography. Strangely, all the X-radiographs showed beads with an off-round shape (figure 26, left). In particular, the internal features of the beads strongly suggested that non-beaded freshwater cultured pearls had been used. To further investigate this possibility, one sample was sawn in half (figure 26, center), revealing a concentric structure surrounded by an outer rim of nacre. The rim was clearly distinguishable from the inner portions and appeared more yellowish with a uniform color distribution; its thickness varied from 0.6 to 1.2 mm. A second sample was broken apart with a jeweler's hammer, confirming that a white freshwater cultured pearl of baroque shape had been used as a bead (figure 26, right).

According to Mr. Shepherd, these cultured pearls were produced using the same type of mussel as the "Soufflés," which some believe to be a hybrid of the Chinese *Hyriopsis cumingii* and the Japanese *Hyriopsis schlegelii*, though it may be a local variety of *H. cumingii*. This mussel shell shows a strange curvature on its outer rim that

Figure 26. The X-radiograph of the cultured pearls (left) revealed off-round beads displaying concentric growth structures that were clearly visible when one sample was cut in half (center, 15.7 × 12.5 mm). When another sample was broken apart (right, originally 17 × 12 mm), a baroque freshwater cultured pearl bead was exposed. Photos by E. Strack.

Figure 27. *The alleged hybrid of* Hyriopsis cumingii *and* Hyriopsis schlegelii *used to produce these cultured pearls shows an unexplained curvature at the rim (see arrow) and intense iridescence. The shell (13 × 19 cm) contains a blister pearl on the left (26.3 mm long), and is shown with an assortment of mostly "Soufflé pearls" that are 10–17 mm long. Photo by Jeremy Shepherd.*

lacks explanation so far (figure 27). Similar curvatures have been observed in old European pearl mussel shells (*Margaritifera margaritifera*). It is also interesting to note that the interior of the shell shows an array of intense spectral colors. The cause of these metallic colors, which are also visible in the resulting cultured pearls, has not yet been determined. It is highly probable that both the "Soufflé pearls" and the "pearl-beaded" samples described here are produced inside the mantle, probably in a later growth phase, by making use of existing pearl sacks that stemmed from a previous harvest.

Elisabeth Strack (info@strack-gih.de)
Gemmologisches Institut Hamburg, Germany

Quartz with spessartine inclusions. Brazil's Navegadora mine (Lavra da Navegadora) in the Conselheiro Pena area of Minas Gerais State has been an important producer of spessartine, mainly as etched crystals that are sought by mineral collectors (e.g., J. S. White, "Spessartine from the

Navegadora mine, Minas Gerais, Brazil," *Rocks & Minerals*, Vol. 84, No. 1, 2009, pp. 42–45, http://dx.doi.org/10.3200/RMIN.84.1.42-45). The mine has also produced attractive quartz with inclusions of spessartine, as displayed at the 2011 Tucson gem shows by Luciana Barbosa (Gemological Center, Los Angeles). She indicated that the material has been sporadically produced, but became significantly more available between 2009 and 2010. She obtained enough rough material to cut and polish about 15–20 pieces. This quartz has been worked into a wide range of products (e.g., figure 28), ranging from 5 ct gems to faceted stones in the 100 ct range and large polished crystal points and spheres.

Although euhedral syngenetic spessartine has been reported previously as inclusions in quartz (e.g., E. J. Gübelin and J. I. Koivula, *Photoatlas of Inclusions in Gemstones*, ABC Edition, Zurich, Switzerland, 1986, p. 159), the availability of this material in significant quantities and sizes is notable.

Brendan M. Laurs

Pink cat's-eye quartz, with color and chatoyancy caused by tourmaline needles. Chatoyant quartz is widely available in gray, yellow, and green, and it is often misrepresented as chatoyant chrysoberyl. Recently, this contributor examined a pink cat's-eye quartz that proved interesting because of the unusual cause of the color and chatoyancy.

The 34.65 ct specimen (figure 29) displayed a broad but distinct chatoyant band with a dull vitreous luster. At first glance, it was reminiscent of chatoyant tourmaline because of its color. Closer examination with the unaided eye showed color concentrations in various areas, especially toward the sides. This suggested the presence of a dye along the growth tubes/surface breaks. The specimen appeared anisotropic under crossed polarizers, with some interference colors perpendicular to the chatoyant band or along the direction of the needles. This suggested a uniaxial mineral, although a clear optic figure could not be resolved due to the dense inclusions. Spot RI and hydro-

Figure 28. *These quartz specimens from Brazil contain well-formed inclusions of spessartine. The faceted stone weighs 18.60 ct (photo by Robert Weldon) and the cabochon weighs 25.60 ct (photo by Luciana Barbosa).*

Figure 29. This 34.65 ct quartz specimen, despite its resemblance to rose quartz, owes its pink color and distinct chatoyant band to the presence of tourmaline needles. Photo by G. Choudhary.

static SG were measured at approximately 1.54 and 2.68, respectively. The sample displayed no reaction to UV radiation, and no features were seen with the desk-model spectroscope. These properties indicated quartz, but further analysis was required.

With magnification, the sample displayed long tube or needle-like inclusions (figure 30). From the side, some pink color was observed along these tubes, which again raised suspicion regarding the cause of color. The cross-section of the tubes was even darker. At higher magnification, some appeared perfectly triangular (figure 31), a feature typically associated with trigonal minerals such as tourmaline. This was further supported by the color of the tubes and the absorption along the c-axis: The inclusions appeared darker when viewed in cross-section. Hence, the bodycolor of the sample was colorless but appeared pink due to the colored inclusions.

IR transmission spectra were obtained both parallel and perpendicular to the needles. In the parallel direction,

Figure 30. Viewed with magnification, the needles appeared pink while the rest of the sample was colorless. This suggested that the quartz's pink appearance was due to these inclusions. Photomicrograph by G. Choudhary; magnified 48×.
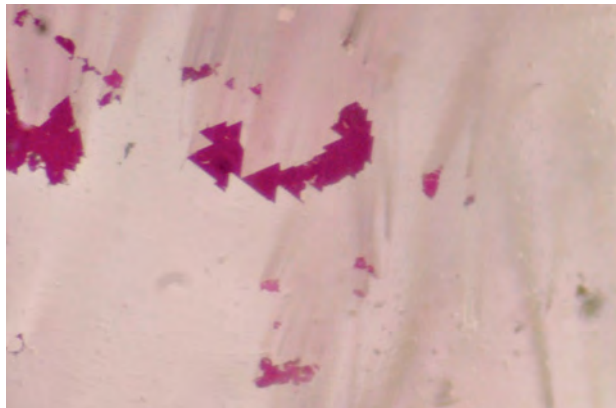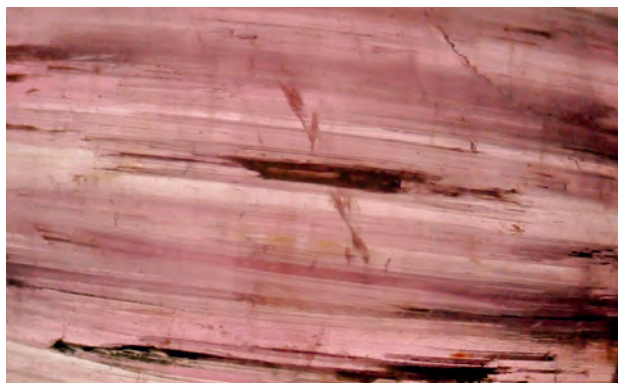
Figure 31. The cross-section of the needles in figure 30 displayed a perfect triangular shape typically associated with minerals belonging to the trigonal system, such as tourmaline. Photomicrograph by G. Choudhary; magnified 64×.

two sets of distinct peaks were seen: in the 4800–4200 cm^{-1} region (4594, 4534, 4438, and 4343 cm^{-1}) and in the 3700–3000 cm^{-1} region (3585, 3563, 3480, 3379, 3300, and 3197 cm^{-1}). According to our database and past studies (see, e.g., L. T. M. Oanh et al., "Classification of natural tourmalines using near-infrared absorption spectroscopy," *VNU Journal of Science: Mathematics – Physics*, Vol. 26, 2010, pp. 207–212; G. Choudhary and S. Fernandes, "Spectroscopic examination of commercially available quartz varieties: A gemological perspective," Summer 2011 *G&G*, pp. 146–147), the first set of peaks is similar to those seen in tourmaline, while the second corresponds to those seen in quartz. In the perpendicular direction, only a broad absorption band was observed in the 3700–3000 cm^{-1} region, due to the lower degree of transmission in that orientation.

On the basis of microscopic examination and the infrared spectra, we identified this sample as quartz with inclusions of pink tourmaline. Tourmaline is a common mineral inclusion in quartz, but typically it is randomly oriented. Thus, this sample was interesting and unusual because of its pink color (though it was not rose quartz) and chatoyancy. Both were caused by the presence of parallel tourmaline needles.

Gagan Choudhary (gtl@gjepcindia.com)
Gem Testing Laboratory, Jaipur, India

An exceptional rhodochrosite carving. Rhodochrosite, a manganese carbonate mineral known for its classic "rose"-red color, is often found as massive pink opaque or translucent specimens. Such material is available in large sizes and typically fashioned into ornamental carvings, beads, and cabochons. Transparent specimens, however, are relatively rare.

The Gem Testing Laboratory of Jaipur, India, recently tested a carved specimen (figure 32, left) that was remarkable for its size and fair degree of transparency. The color was uneven, ranging from brownish red to reddish brown to brownish pink. The specimen weighed 10.875 kg and measured approximately 21.60 × 20.50 × 15.60 cm. It was carved

Figure 32. This carved rhodochrosite is exceptional for its size (10.875 kg), rich brownish red color, transparency, and artistic quality. Photos by M. B. Vyas.

in the form of Lord Mahaveera, one of the ancient Indian sages who established the tenets of Jain Dharma. The piece was also noteworthy for the fine artistic work on the back, which is unusual (figure 32, right).

Although the bodycolor clearly suggested rhodochrosite, we conducted gemological tests to establish the identity. However, the carving's large size impeded our ability to measure all the properties. Its relatively dull luster indicated a low hardness, which was confirmed by scratching an inconspicuous spot on the base with fluorite. The spot RI of around 1.60 displayed a large birefringence blink, typically associated with carbonate minerals. A weak red reaction was visible with long- and short-wave UV radiation, and the handheld spectroscope showed strong absorption bands centered at ~460 and 550 nm. We could not measure the carving's specific gravity, but its heft indicated a somewhat high SG value. Examination with strong fiber-optic light and a loupe in relatively transparent areas revealed three directions of cleavage (figure 33), a feature associated with calcite-group minerals such as rhodochrosite. In addition, some portions on the back had rhodochrosite's characteristic irregular to wavy concentric banding patterns (figure 34).

Identifying this specimen was not particularly difficult, even though its size did not allow the measurement of all

gemological properties. Encountering such a large and finely carved rhodochrosite with attractive color and transparency was truly a pleasure.

Gagan Choudhary and Meenu Brijesh Vyas
Gem Testing Laboratory, Jaipur, India

Sapphire and zircon from Ethiopia. In March 2010, Farooq Hashmi (Intimate Gems, Glen Cove, New York) loaned GIA several rough and faceted sapphires that he obtained on a buying trip to Ethiopia. According to Mr. Hashmi, the stones came from Yabelo in southern Ethiopia, 185 km northwest of the Moyale border with Kenya. The sapphires (figure 35) are associated with reddish brown zircon (figure 36) in secondary deposits. He reported that the rough zircon was generally available in the 0.5–3 g range, and that production of better-quality sapphire and zircon typically has been about 1 kg per month.

The sapphires ranged from yellow to brownish green to blue, and many of the rough pieces showed strong yellow and blue color zones. The four faceted sapphires examined (0.34–1.32 ct) were cut as round brilliants with the optic axis oriented approximately perpendicular to the table. They yielded the following properties: RI—n_o = 1.765, n_e = 1.775; birefringence—0.010; SG—3.95–4.03, with the more reliable values

Figure 33. Relatively transparent areas of the carving displayed the three directions of cleavage that are associated with the calcite group of minerals. Photo by M. B. Vyas.

Figure 34. Areas of the carving showed rhodochrosite's characteristic wavy to irregular growth banding. Photo by G. Choudhary.
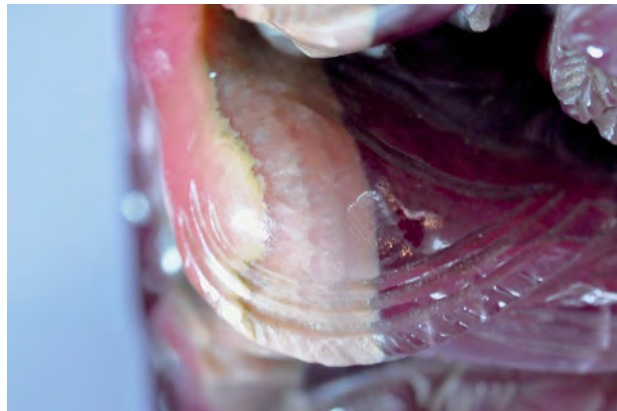
Figure 35. These sapphires are from a new deposit in Ethiopia. The four faceted samples (cut by Matt Dunkle, Aztec, New Mexico) range from 0.34 to 1.32 ct; the largest rough stone is 12.06 ct. Photo by Robert Weldon.

Figure 37. The faceted dark blue-green sapphire in figure 35 contained needles (probably rutile), clouds, and equatorial thin films. Photomicrograph by D. Beaton; image width 1.0 mm.

of 3.99 and 4.00 coming from the larger specimens; UV fluorescence—inert to both long- and short-wave UV radiation, except for one yellow stone that fluoresced very weak orange to long-wave UV; and bands at 450, 460, and 470 nm seen with the desk-model spectroscope. Microscopic examination (figure 37) revealed sparse long needles, dense clouds of short needles and particles, equatorial thin films, and reddish brown platelets of hematite (identified by Raman spectroscopy). Unidirectional twinning was also seen in one rough specimen.

UV-Vis-NIR spectroscopy of the sapphires confirmed the Fe^{3+} absorption features at 450 (very strong), 460, and 470 nm, as well as strong peaks at 376 and 386 nm attributed to Fe^{2+}-Ti^{4+} intervalence charge transfer. In addition, the blue to green stones exhibited a broad intervalence charge transfer absorption due to iron in the 800–900 nm range.

The trace-element composition of three representative sapphires measured by EDXRF spectroscopy showed relatively high levels of Fe in all colors, small amounts of Ga and Ti, no detectable V, and no Cr except in the yellow stone (table 1). These properties are consistent with sapphires of magmatic origin.

A 13.01 ct zircon (again, see figure 36) was also exam-

ined for this report. Its RI was >1.81, SG was 4.70, and it fluoresced weak orange with yellow chalkiness to short-wave UV radiation. Magnification revealed strong doubling and wispy stringers of reflective particles. Its properties are consistent with "high"-type (non-metamict) unheated zircon.

Donna Beaton (donna.beaton@gia.edu)
GIA, New York

TABLE 1. Chemical composition of sapphires from Yabelo, Ethiopia.

Oxide (wt.%)	Olive green	Yellow	Dark blue-green
TiO_2	0.009	0.002	0.004
Cr_2O_3	nd[a]	0.001	nd
Fe_2O_3	1.438	1.037	0.928
Ga_2O_3	0.011	0.010	0.010

[a] nd = not detected.

Update on sapphire mining in Sri Lanka. In March–April 2011, this contributor visited several sapphire deposits in Sri Lanka to gather information and collect samples for the GIA laboratory reference collection. The trip assistants included recent graduates from GIA's Bangkok campus (Andrea Heather Go of Canada and Afsaneh Tazari of Iran), David Goubert of Switzerland, and Jeremy Brian and Jonathan Muyal of France. Our work was facilitated by ICA members Armil Samoon (Sapphire Cutters Ltd., Colombo) and Gamini Zoysa (Institute of Gemmological Sciences, Colombo).

The region around Ratnapura continues to be the most active gem mining area. We saw 14 mechanized operations in the area (e.g., figure 38), quite an increase compared to the author's previous visit in 2005 when only one such mine was working. Most of the operations use water

Figure 36. Reddish brown zircon is mined with sapphire in the Ethiopian deposit. This unheated 13.01 ct oval brilliant was cut by Hassan Z. Hamza (Noble Gems Enterprises, Dar es Salaam, Tanzania) from the largest piece of rough seen by Mr. Hashmi. Photo by Robert Weldon.
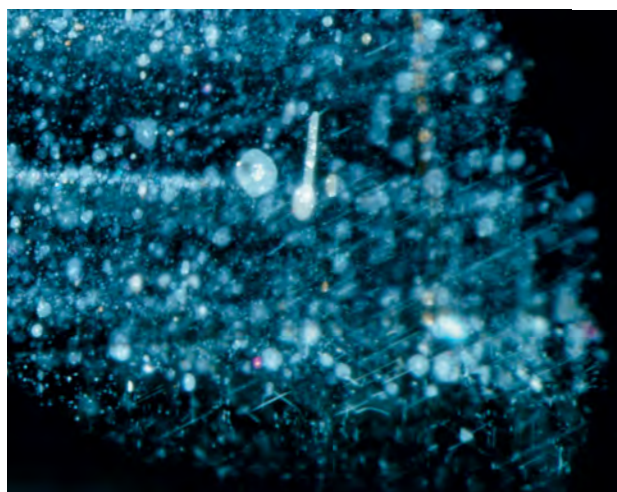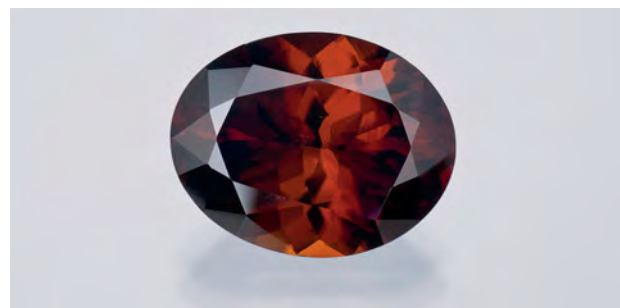
Figure 38. Several mechanized mines are active in Sri Lanka, including this operation at Kuruwita near Ratnapura. Photo by V. Pardieu.

Figure 39. Artisanal hillside mining in Sri Lanka involves digging shallow pits to reach gem-bearing horizons, as shown here near Balangoda, about 35 km east of Ratnapura. Photo by V. Pardieu.

cannons and gravel pumps inside the pits, and some use an excavator to bring the gem-bearing gravels (*illam*) to trommels and jigs for processing. We also witnessed traditional pit mining in paddy fields and rivers, and well as hillside mining that takes place where the gem-bearing layers are very close to the surface (figure 39). The area produces mainly blue (typically with some yellowish zones), yellow, pink, and geuda sapphires (e.g., figure 40). Gem mining and trading around Ratnapura is well regulated. Most operations possess mining licenses, and the production is usually sold through an auction system. The region hosts several busy gem markets, as well as cutting and treating centers. A number of treaters are active using both modern and traditional heating methods.

The second most active mining area is near Elahera (especially the Matale District). We visited nine mechanized operations scattered over a large area. Activities were somewhat limited due to early rains, and we were informed that 20–30 excavators are expected to be working in the area after seasonal agricultural activities are completed. In addition, several hundred small-scale traditional mines are anticipated. Unfortunately, a dam project near Elahera is expected to flood some potentially rich sapphire prospects, raising concerns among miners. This region is drier than Ratnapura and the gem gravels are not as deep. The miners usually dig during the dry season, stockpile the gem gravel, and then wash it during the rainy season. Production includes sapphire, ruby, garnet, tourmaline, zircon, chrysoberyl, and many other gems. The sapphires are mainly blue, geuda, and yellow; pink is least common. The blue sapphires can be extremely fine and are usually more evenly colored than those found around Ratnapura. The rubies (very rare) are usually pinkish with some blue zoning.

Our next stop was Hasalaka to the south in the highlands. There was little activity, reportedly due to the rice harvest; up to 3,000 people were said to be active there recently. We saw sapphires that were yellow, *ottu* type (blue on the surface with a colorless or yellowish core), and geuda; most had very good crystal shape.

Further southeast, we visited a large mechanized mine near Bibile where several excavators were being used to recover mainly geuda and yellow sapphires. The operation reportedly started about one year ago and was similar to the other large pits we saw near Ratnapura.

Continuing south, we documented some mechanized operations in paddy fields to the north of Passara. The production consisted mainly of yellow, geuda, pink, padparadscha, and some blue sapphires; most of the crystals were well formed. Further south toward the coast we visited Okkampitiya and Kataragama. Although we saw some evidence of mining in these areas, there was little activity due to heavy rains.

Vincent Pardieu

Green cat's-eye spodumene from Brazil. At the 2011 Tucson gem shows, Luciana Barbosa showed this contributor some green spodumene that displayed chatoyancy (e.g., figure 41). The material was reportedly mined from

Figure 40. These sapphires were seen near Niwitigala in the Ratnapura area. Photo by V. Pardieu.

Figure 41. This green spodumene from Brazil (4.35 and 6.15 ct) shows chatoyancy. Photo by Robert Weldon.

Figure 42. This 27.38 ct topaz shows unusual color zoning, with a pattern resembling that seen in sapphire. Photo by G. Choudhary.

the Neves pegmatite in the Araçuaí area of Minas Gerais State. Although the deposit has been a source of facet-grade green spodumene for years, Ms. Barbosa first saw small parcels of the chatoyant material in 2010; only about 5% of the production shows this effect, yielding enough rough material to polish about 25 cabochons. While clean faceted stones may reach 20+ ct, the cat's-eyes tend to be smaller, typically as cabochons weighing 5–8 ct. The material is reportedly not treated in any way.

Although GIA has seen several examples of cat's-eye kunzite, green spodumene showing chatoyancy is much more unusual (S. F. McClure, pers. comm., 2011). Chatoyant kunzite has been reported previously ("Kunzit-katzenaugen aus Brasilien [Kunzite cat's-eye from Brazil]," *Gemmologie: Zeitschrift der Deutschen Gemmologischen Gesellschaft*, Vol. 46, No. 2, 1997, pp. 64–65, and references therein), but this is the first time that green material has been documented in the literature, to this author's knowledge.

Brendan M. Laurs

A color-zoned topaz. The Gem Testing Laboratory in Jaipur, India, received for identification a transparent yellowish to greenish brown specimen that was striking for its unusual color zoning. The oval mixed cut (figure 42) weighed 27.38 ct and measured 21.18 × 16.39 × 9.64 mm. The specimen initially appeared to be a sapphire because

of the pattern of its color zoning, but the luster and brilliance were lower than would be expected.

The stone had refractive indices of 1.621–1.629, with a birefringence of 0.008 and a biaxial positive optic sign. The hydrostatic SG was 3.57, and moderate greenish brown to brown pleochroism was observed. The sample was inert to long-wave ultraviolet radiation and displayed a weak green reaction to short-wave UV. No absorption features were observed with the desk-model spectroscope. The RI and SG values were consistent with topaz; the RIs indicated an intermediate OH/F composition, while the SG was consistent with F-rich topaz (R. Webster, *Gems*, 5th ed., rev. by P. G. Read, Butterworth-Heinemann, Oxford, UK, 1994, pp. 150–163).

When the topaz was immersed in bromoform, the color zones became sharper and more prominent (figure 43), and they were still reminiscent of those seen in sapphire. The angles formed by the zones varied with viewing direction. Viewed from the table, the angles were approximately 40°/140° (figure 43, left); from the side, they were 70°/110° (figure 43, right). These angles are different from those seen in corundum (60°/120°). We were unable to find any reference in the literature to such angles formed by the crystal faces of topaz; the pyramidal faces {111} and {1$\bar{1}$1} only form an angle of 39° (E. S. Dana, *Mineralogy*, 4th ed., rev. by W. E. Ford, Wiley Eastern Ltd., New Delhi, 1949, pp. 613–615). The intersection of the color zones did
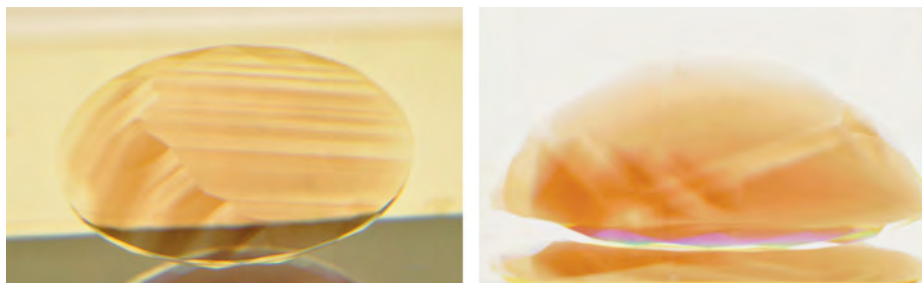

Figure 43. The angles formed by the color zones in the topaz were different when viewed from the table (left) and the side (right). Also note the planes of intersection, which form a zigzag pattern. Photos by G. Choudhary.
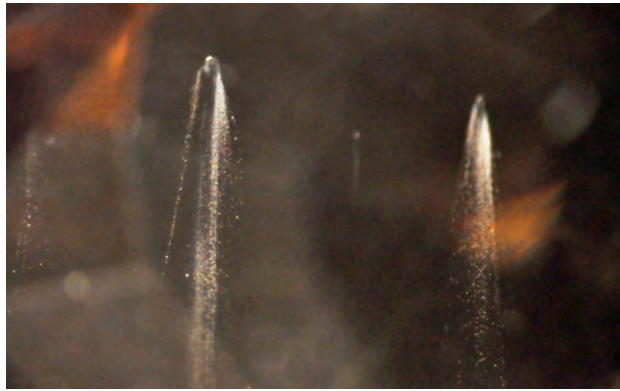
Figure 44. The topaz contained tiny transparent crystal inclusions associated with streams of fine pinpoints, forming "comet-tail" patterns. Photomicrograph by G. Choudhary; magnified 45×.

not form a smooth plane but rather a zigzag pattern (again, see figure 43, left). Therefore, the exact orientation of these color zones is unknown and can only be assumed to be aligned with the pyramidal faces.

With magnification, the sample was mostly clean, except for a few tiny transparent crystals associated with streams of fine pinpoints that formed comet-like patterns (figure 44). Similar inclusions were documented in topaz by E. J. Gübelin and J. I. Koivula (*Photoatlas of Inclusions in Gemstones*, Vol. 2, Opinio Publishers, Basel, Switzerland, 2005, pp. 751–752).

This is the first time this contributor has encountered topaz with a distinct color zoning pattern.

Gagan Choudhary

Variscite from Peru. Green variscite is a popular ornamental material that is best known for the attractive nodules from Clay Canyon, Utah (W. E. Wilson, "Famous mineral localities: The Clay Canyon variscite mine, Fairfield, Utah," *Mineralogical Record*, Vol. 41, No. 4, 2010, pp. 321–349). More recently, gem-quality variscite was found in the Meekatharra District in Western Australia (Spring 2007 GNI, pp. 63–64).

In 2009, a new find of variscite was discovered in Peru. The material was initially thought to be green turquoise, and its locality was kept secret. An abundance of rough came to market in early 2011, reportedly from the vicinity of Yauli, 20 km east of the city of Huancavelica and ~200 km southeast of Lima. The geological position of the find is not known, but variscite normally originates near the earth's surface from the interaction of Al-rich rocks with meteoric phosphate-bearing waters. The Peruvian rough forms veins rather than nodules, and is usually light green or rarely gray-green (figure 45). It typically contains hollow cavities, which can be up to 2 cm long; these diminish a specimen's value. Nevertheless, cabochons can be quite attractive. Some of the gray-green material shows a lamellar agate-like structure (see the stone on the right in figure 45). While in Lima in February 2011, this contributor saw

at least 100 kg of rough, although much more material has probably been produced since then.

Ten rough pieces and six cabochons (up to 4 cm across) were examined for this report. All were identified as variscite by X-ray diffraction, regardless of their color. The cabochons yielded the following gemological properties: spot RI—1.55–1.56; SG—2.12–2.23 (lower for material with cavities); Mohs hardness—3½–4; streak—colorless; UV fluorescence—weak green-yellow reaction to long-wave and inert to short-wave UV; and no features seen with the hand spectroscope. While these samples were not treated, polymers can enhance variscite's durability and utility for jewelry.

Jaroslav Hyršl

SYNTHETICS AND SIMULANTS

An accidental corundum and lead glass triplet? In December 2010, one of these contributors (P-YC) acquired a parcel of six oval black cabochons—sold as star sapphires—through several dealers from Chanthaburi, Thailand via eBay. Since the Gemmological Association of All Japan (GAAJ) laboratory had described black star sapphires treated with lead glass ("Lead glass filled black star sapphire," *Gemmology*, Vol. 39, No. 470, issue 11, 2008, p. 2), the parcel was inspected carefully, and one cabochon exhibited an unusual feature. At 10× magnification, the 6.01 ct stone appeared to have a thin transparent section through the center, roughly parallel to its base and ~0.5 mm thick at its widest point (figure 46). Standard gemological testing gave the expected spot RI of ~1.76 and a hydrostatic specific gravity of 4.00. Some fractures contained a foreign material with an RI close to that of corundum, as evidenced by their similar luster in reflected light. The unusual transparent layer appeared yellow and con-

Figure 45. These variscites are from a new find in Peru. The pear-shape cabochon is 14.76 ct and the oval is 9.81 ct. Gift of J. Hyršl, GIA Collection nos. 38422 and 38423; photo by Robert Weldon.
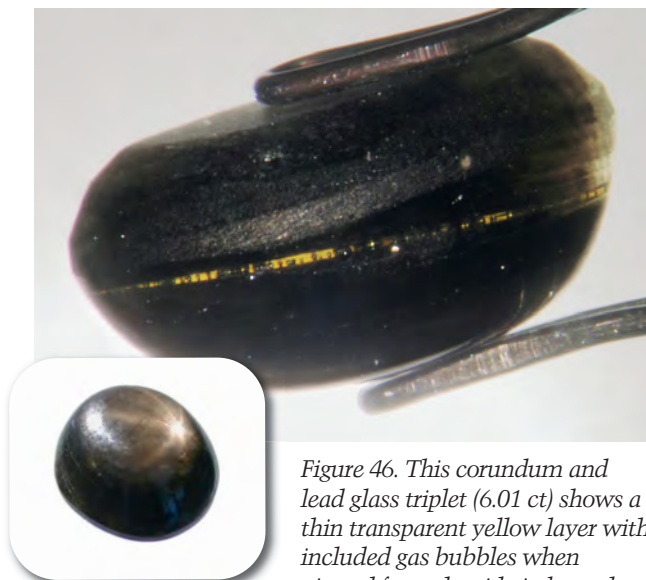
Figure 46. This corundum and lead glass triplet (6.01 ct) shows a thin transparent yellow layer with included gas bubbles when viewed from the side in benzyl benzoate immersion. The cabochon's general appearance is typical of black star sapphires from Thailand (inset). Photos by E. Fritsch and B. Rondeau (inset).

tained numerous gas bubbles, suggesting a glass. Some of the bubbles reached the surface, creating cavities.

The stone was examined with a JEOL 5800 scanning electron microscope. The transparent section showed a

Figure 47. In this backscattered electron micrograph, the transparent layer in the black star sapphire shows a light tone indicative of a high atomic number, consistent with a high lead content. A surface-reaching bubble is seen in the center; note that the two sides of the fracture do not correspond in shape. Image by E. Fritsch.

contrasting tone, even in secondary electron imagery. The contrast was even more pronounced in a backscattered electron image (figure 47), which is sensitive to atomic number. Chemical analysis with a PGT IMIX secondary X-ray detector indicated that the transparent layer was composed of Pb, Si, Al, and O, strongly suggesting a lead-based glass. The matrix was clearly corundum—containing only aluminum and oxygen—but elsewhere in the stone the lead-based substance could be found in narrow fractures, mostly parallel to the base.

Because the top and bottom edges of the transparent layer did not correspond in shape (again see figure 47), it was not a fracture filling in a single crystal. The relative crystallographic orientation of the two halves, examined using strong lateral fiber-optic illumination to reveal growth zones, also differed. The upper half showed a typical dark brown chevron, with one side roughly parallel to the long axis of the stone, while the bottom half had stripes that were nearly parallel to the short axis. This meant that both sections shared roughly the same optic axis plane, but were rotated ~30° from one another.

The two halves of this cabochon were likely treated with lead glass as part of a larger parcel of black star sapphire rough. By chance, two crystals showed parting perpendicular to the c-axis, and those two parting surfaces, both approximately flat, came in contact during the treatment. When the molten lead glass solidified, the two halves were fused together and cut into a cabochon, leaving a thin layer of lead glass between them. This cabochon, then, would be most properly described as a corundum-glass-corundum triplet.

Emmanuel Fritsch

Pierre-Yves Chatagnier
Centre de Recherches Gemmologiques, Nantes, France

Benjamin Rondeau
CNRS, Team 6112, Laboratoire de Planétologie
et Géodynamique, University of Nantes, France

Stefanos Karampelas
Gübelin Gem Lab, Lucerne, Switzerland

Eloïse Gaillou
Carnegie Institution, Washington, DC

Glass triplet resembling coated "mystic topaz." Recently these contributors received from India a 10.32 ct oval mixed cut that had been purchased as a coated "mystic topaz." However, when viewed from the side, the sample's true nature as a triplet became apparent (figure 48). A thin iridescent layer ran through its center, between colorless top and bottom halves, and the "mystic" effect was reflected throughout the specimen. When placed in an immersion cell with water, the triplet lost most of its colorful appearance.

Both the top and bottom were singly refractive with an RI of 1.581, and the hydrostatic SG was ~2.47. In the polariscope, it displayed anomalous double refraction when

Figure 48. The two halves of this colorful glass triplet (12.28 × 17.33 × 7.92 mm) are easily visible to the naked eye. The junction between them is seen within the frosted girdle. Photo by O. Segura.

viewed from the side. We saw no internal characteristics with magnification, only some rounded facet junctions. All of these features are consistent with glass.

Energy-dispersive chemical analysis using an EDAX instrument revealed Si and K as major components, with impurities of Ti, Fe, Zn, and Zr. This composition is typical of glass, and has been seen previously in other glass imitations, although the Ti might be attributed to the layer creating the iridescent effect.

"Mystic topaz" was first introduced in 1998 by Azotic Coating Technology (Rochester, Minnesota) as an enhancement of colorless topaz with a thin-film coating of undisclosed material. Today, many firms worldwide use the same process with topaz, quartz, and glass. Although the coating is quite resistant, it can be scratched or damaged by abrasives, chemicals, or an ultrasonic cleaner. Thus, coated gems cannot be recut or repolished. Placing the iridescent

Figure 49. Viewed face up, the internal iridescent layer in the glass triplet reflects scratches on the table. Photo by O. Segura.

layer inside a triplet creates a much more durable multicolor effect. However, since the coating is parallel to the table, it reflects and colors any surface scratches and breaks (figure 49), thus making these defects far more visible than on externally coated stones. Although such a triplet is not particularly difficult to design and produce, this is the first example we have seen.

Olivier Segura (o.segura@bjop.fr)
Laboratoire Français de Gemmologie, Paris, France

Emmanuel Fritsch

CONFERENCE REPORTS

ICA Congress 2011. Fair trade certification is not yet available for gemstones, but it is clear that the movement is gaining grassroots support. Fair trade, corporate social responsibility, and supply chain issues were central topics at the 14th biennial International Colored Gemstone Association (ICA) Congress in Rio de Janeiro, May 1–4. In the more than 20 presentations delivered at the conference, industry leaders urged ICA's international delegates, which include miners, gem wholesalers, and gemstone dealers, not to ignore these issues in the colored stone industry. Highlights of some of the presentations are given below.

Eli Izhakoff of the World Diamond Council, New York, a key player in developing the Kimberly Process certification scheme for diamonds, urged delegates to recognize problems and develop defensive strategies, much like the WDC does to stay ahead of issues with "conflict diamonds." **Andy Lucas** of GIA in Carlsbad used video examples of how rural communities develop skills through education and training, which he said leads to social sustainability and poverty alleviation in mining areas. He highlighted GIA's efforts at developing educational programs to meet those needs. **Vincent Pardieu** of GIA in Bangkok suggested that remote gem locales develop partnerships with existing civic groups, such as those protecting game reserves and national parks, to advance social and environmental responsibility. **This contributor** noted that in the absence of a fair trade label for gemstones, there are many things that small- and medium-scale miners can do to alleviate poverty, protect the environment, and ensure the supply chain from mine to market. Some miners and gem dealers are already creating a blueprint for "doing the right thing" in the gem business, such as Eric Braunwart of Columbia Gem House, who asks his suppliers, employees, and other stakeholders to sign and uphold a series of Quality Assurance and Fair Trade Gems Protocols.

Congress attendees also heard from other segments of the industry, including policy makers and gem miners. **Dr. Gaetano Cavalieri** of the World Jewellery Confederation (CIBJO), Milan, Italy, discussed the CIBJO Blue Books, which promote standards for nomenclature and disclosure codes for gem treatments. He described CIBJO's commit-

ment to social and economic responsibility through the development of the World Jewelry Confederation Education Foundation under the auspices of the United Nations Millennium Development Goals. **Ian Harebottle**, CEO of Gemfields, London, which mines for emerald in Zambia, noted that his company focuses on social sustainability by supporting local schools, medical clinics, and farming projects, as well as working in partnership with other stakeholders. Gemfields sells off old equipment rather than discarding it, plants trees in waste dumps, and fills nonworking pits with water and stocks them with fish. He pointed out that such efforts also need to be economically sustainable: They are only made possible by mining consistent supplies of rough gems, investing in key resources, and developing marketing campaigns to ensure stable market prices.

Representatives from two laboratories pointed to their efforts in determining gemstone country of origin, which goes to the heart of supply chain issues, particularly in areas of conflict. **Dr. Dietmar Schwarz** of the Gübelin Gem Lab, Lucerne, Switzerland, spoke about global sources of corundum, while **Thomas Hainschwang** of GGTL Laboratories, Balzers, Lichtenstein, discussed their efforts to trace emeralds through observation, chemical composition, and spectroscopy.

Copies of some of the presentations delivered at the conference are available on the ICA website (visit www.gemstone.org, and click on "ICA Congress 2011" under Quick Links).

Robert Weldon (rweldon@gia.edu)
GIA, Carlsbad

Scottish Gemmological Conference 2011. This four-day SGA event was held in Perth, Scotland, on April 29–May 2 with more than 50 delegates in attendance. The first lecture, by **Dr. Marcia Pointon** (University of Manchester, U.K.), addressed the depiction of geologic features and mineral specimens by 19th century British artists.

Two lectures on alexandrite were given by **Dr. Karl Schmetzer** (Petershausen, Germany). The legend of alexandrite being discovered the same day that Russian crown prince Alexander came of age seems to be false, as records show it was found a year earlier. Historically, alexandrite production in Russia was a byproduct of emerald mining, and the gem was not considered important. The color change of alexandrite is best described as going from bluish green to purplish red. Stones showing a color change without a red component should simply be described as color-change chrysoberyl.

Alan Hodgkinson (SGA president, Edinburgh), discussed issues surrounding specific gravity testing. Traditional heavy liquids such as bromoform, methylene iodide, and Clerici solution are all toxic. A safer and more versatile liquid is sodium polytungstate (SG 2.9), which is water-soluble and also has a specific gravity that corresponds directly to its refractive index. Thus, if the liquid is adjusted so that a stone remains suspended, a drop of that liquid can be placed on a refractometer to determine the stone's RI. When working with mounted stones, RI can be determined from the point at which a stone "disappears" in the liquid. With traditional hydrostatic weighing, the use of pure water at 4°C and taking readings to at least two places to the right of the decimal point are important.

Dominic Mok (Asian Gemmological Institute & Laboratory, Hong Kong) discussed the laboratory situation in the Far East. There are now more than 20 labs in Hong Kong, as well as increased competition from China. Prices for services have fallen substantially, and customers are insisting that more advanced testing such as EDXRF analysis be shown on reports. Due to insurance considerations, more-expensive items cannot be kept overnight, so same-day service is required.

Market trends were addressed by **Stuart Robertson** (Gemworld International, Glenview, Illinois). Economic recovery is slow in the U.S. and Europe, while the Far East markets continue to be strong. Blue sapphire is still the best seller, with ruby drawing very high prices for extra fine color, and the emerald market is improving as a result of greater consumer acceptance of treatments and an increase in supply. Color substitutions are commonly being used to provide lower-cost alternatives (e.g., rubellite tourmaline and spinel instead of ruby, and apatite instead of Paraíba tourmaline). Treatments are creating a category best described as "Fashion Accessories," and such stones cannot be promoted as rare.

David Callaghan (retired jeweler, London) discussed the use of nature motifs in jewelry. He showed examples of flowers, insects, and animals that were depicted with gemstones or materials such as enamel and Bakelite.

In the closing two days, delegates had the option to attend various workshops and tour the mineral collection on display at the National Museum of Scotland in Edinburgh.

Douglas Kennedy (douglas@gialondon.co.uk)
GIA, London

Sinkankas Diamond Symposium 2011—Diamond. The ninth annual symposium in honor of John Sinkankas took place April 16 at GIA in Carlsbad. Co-hosted by GIA and the San Diego Mineral and Gem Society, the sold-out event was attended by 132 people.

After opening remarks by convener **Roger Merk** (Merk's Jade, San Diego, California), **Scott Sucher** (The Stonecutter, Tijeras, New Mexico) reviewed the fascinating history of diamond cutting up to 1750. The first record of diamond being "made" was in 1280 AD, when stones were "point cut" by grinding them on an iron plate with diamond grit. Major breakthroughs came with the development of the scaife in the 1400s and wire saws in the 1600s. **Al Gilbertson** (GIA, Carlsbad) continued with diamond cutting after 1750, following the development of the brilliant cut with contributions by John Mawe, Henry Morse, and Marcel Tolkowsky. In contemporary times, we

have seen the development of laser cutting, proportion viewers, and automated scanners that provide a variety of possibilities for cutting rough into various fancy shapes.

Dr. James Shigley (GIA, Carlsbad) reviewed the geology and exploration of diamond deposits. An economic kimberlite pipe typically has a grade of only one part diamond per 1 million parts host rock (0.0001% by volume). **Dr. William "Skip" Simmons** (University of New Orleans) focused on diamond's crystal structure and mineralogy. Due to its high density, diamond has the highest RI of any natural colorless transparent material.

Dr. Sally Eaton-Magaña (GIA, Carlsbad) reviewed the production of synthetic diamond by chemical vapor deposition (CVD) and high pressure, high temperature (HPHT) growth techniques. For the latter process, it takes about 80 hours to grow a 3.5 ct crystal. **Dr. Christopher (Mike) Breeding** (GIA, Carlsbad) explained how treatments such as irradiation and heating (with or without accompanying high pressure)—and various combinations thereof—can change the color of diamond based on the characteristics of the starting material. For example, HPHT processing of type Ia pale yellow starting material containing nitrogen pairs can form defects consisting of isolated nitrogen atoms that are then irradiated and annealed to produce NV centers, which give rise to red coloration. **Dr. George Rossman** (California Institute of Technology, Pasadena) examined the causes of coloration in diamond. While the mechanisms involved in producing the color of yellow, blue, green, brown, and black stones are known, the color origin of blue-gray-violet, red-pink, and "chameleon" diamonds is not well understood.

Meg Berry (Mega Gem, Fallbrook, California) described her experience with diamond drills for processing and carving gem materials. She favors a 0.75-mm-diameter bit that is sintered with diamond particles, rather than being CVD coated. **John Koivula** (GIA, Carlsbad) illustrated the "microworld" of diamond, and emphasized that mineral inclusions are actually quite rare, with fissures/feathers and graphite being much more common. Certain mineral inclusions are indicative of a diamond's source rock, such as chromite (peridotite), omphacite (eclogite), and moissanite (deep mantle paragenesis).

Each attendee received a two-volume handout with presentation summaries as well as outside contributions; additional copies are available from Mr. Merk ($25 + shipping; merksjade@cox.net). Next year's Sinkankas symposium will take place April 21, and the theme will be topaz.

Brendan M. Laurs

MISCELLANEOUS

A jewel that survived 9/11. September 11, 2011, marked the 10-year anniversary of the terrorist attacks on New York and Washington, DC. In the aftermath of the New York attacks, a nine-story office building adjacent to the twin towers, 5 World Trade Center, partially collapsed but remained standing. The structure was ulti-mately demolished in January 2002. Buried under tons of rubble inside the building were 2,500 safety deposit boxes in the vault of a JPMorgan Chase branch. The vault sustained severe damage from the fires that burned for several days after the attacks.

The melted and semi-fused safety deposit boxes were subsequently moved as a unit to the basement of One Chase Manhattan Plaza. In early 2002, the bank began meeting with box owners to return any remaining contents. Charles Maikish, a JPMorgan Chase official, told the *New York Daily News* that workers had found mostly ashes in the boxes: "The only thing that would have survived was metal or stone."

Los Angeles gem specialist Robin Silvers recently brought to this contributor's attention a piece of jewelry that survived the disaster in one of these deposit boxes, a 1950s-era 14K white gold ribbon bow brooch (figure 50). A client of hers was hoping to restore the brooch. The client's father had recovered it with a few other jewelry articles during the very last appointment for retrieving possessions. The insurer had an appraisal done and returned the jewelry six months later.

This contributor's examination showed the following: The brooch measured 49.85 × 31.00 mm and contained 75 diamonds (2.78 carats estimated total weight) in a variety of cuts and settings, consisting of eight prong-set round brilliants, 41 bead-set round single cuts, seven prong-set marquise cuts, and 19 channel-set baguettes. It was missing one diamond (apparently lost before the terrorist attack). The metalwork was blackened, but remarkably the diamonds were in good condition and did not show any significant signs of degradation.

The client ultimately decided not to restore the piece, preferring instead to keep the brooch in its present condition so people can reflect on the ironic beauty of this blackened jewel that survived the tragic September 11 attacks.

David Humphrey (dhjewels@earthlink.net)
Gallery of Rare Jewels, Pacific Palisades, California

Update on Myanmar gem sales and production. The Myanma Gem Emporium conducted a special sale of jadeite, cultured pearls, and other gems July 3–13, 2011. According to an article in *Working People's Daily* (July 15, 2011, pp. 9, 16), a total of 22,317 lots of jade were offered, of which 17,449 sold. Of those, 17,222 lots sold by tender and 227 by competitive bidding. Attendance and buying, especially from China, was up from previous sales. On average, jade lots sold at 343% of reserve prices. A total of 38 lots of other gems were sold, and cultured pearls also were popular among buyers.

Production of jadeite in Myanmar remains strong, while figures reported for other gem materials show variable trends (see table 1).

U Tin Hlaing
Dept. of Geology (retired)
Panglong University, Myanmar

Figure 50. This white gold and diamond brooch (49.85 × 31.00 mm) was recovered from a melted safety deposit box at the World Trade Center site that was devastated by the September 11, 2001, terrorist attacks. The metalwork is blackened, but the diamonds are in good condition. Photo by Robert Weldon.

TABLE 1. Production of jadeite and other gems in Myanmar, 2005–2010.

Year	Jadeite (tons)	Ruby (carats)	Sapphire (carats)	Spinel (carats)	Peridot (carats)
2005–2006	20,005	2,298,413	428,891	–	125,755
2006–2007	20,458	1,555,596	715,160	833,218	344,471
2007–2008	20,266	1,518,854	308,642	925,050	732,442
2008–2009	32,921	1,821,085	1,234,596	363,260	583,215
2009–2010	25,795	1,692,587	1,081,773	429,312	21,160

ERRATA

Gems & Gemology regrets two incorrect figure captions in the Summer 2011 Symposium Proceedings issue.

1. In the abstract by C. P. Smith, "Natural-color tanzanite" (p. 119), the caption should have read as follows:

Heating of zoisite produced little to no change in V^{3+} absorptions. A shift in the absorption edge was recorded along the alpha pleochroic direction, while additionally along the beta direction a band at 375 nm became apparent. The most significant change took place along the gamma direction, where the shift in the absorption edge revealed another band at ~380 nm, and the combined removal of the 455 nm band created a transmission window in the blue region of the spectrum. This caused the pleochroic hue to change dramatically from a brown-yellow or brownish greenish yellow to slightly greenish blue.

2. In the abstract by S. Gumpesberger, "Extreme conoscopy" (p. 147), the caption should have read as follows:

An array of mini-sized spheres shows multiple uniaxial figures across the entire surface of the twinned amethyst slab on the left. The ametrine slab on the right exhibits typical uniaxial figures in Brazil law-twinned zones as well as uniaxial bull's-eye figures in untwinned areas. Amethyst can also exhibit twinned and untwinned zones in the same crystal. Photo by S. M. Gumpesberger; specimens courtesy of the Royal Ontario Museum, Toronto, Canada.

We thank Mr. Smith and Ms. Gumpesberger for bringing these corrections to our attention.

For online access to all issues of *GEMS & GEMOLOGY* from 1981 to the present, visit:

store.gia.edu

The Book Reviews and Gemological Abstracts sections are provided in the online (PDF) version of the journal. Below are the titles of the books and articles reviewed, with the reviewers' names indicated in brackets. These sections are available free of charge both on the *G&G* website (gia.edu/gandg) and as part of *G&G* Online (gia.metapress.com), and are paginated separately from the rest of the issue.

Book Reviews

Living Jewels: Masterpieces from Nature. By Ruth Peltason, 2010 [*Delphine A. Leblanc*]

The Extraordinary World of Diamonds. By Nick Norman, 2010 [*A. J. A. "Bram" Janse*]

The Workbench Guide to Jewelry Techniques. By Anastasia Young, 2010 [*Doug Canivet*]

World Hallmarks, Volume I: Europe, 19 th to 21 st Centuries, 2nd ed. By William Whetstone et al., 2010 [*Jo Ellen Cole*]

Mineral Treasures of the World. By The Geological Museum of China and The Collector's Edge Minerals, 2010 [*Michael T. Evans*]

Gemological Abstracts

COLORED STONES AND ORGANIC MATERIALS

A survey of Mn-rich yellow tourmaline from worldwide localities and implications for the petrogenesis of granitic pegmatites. By W. B. Simmons et al. [*James E. Shigley**]

DIAMONDS

Alluvial diamond resource potential and production capacity assessment of the Central African Republic. By P. G. Chirico et al. [*James E. Shigley**]

Alluvial diamond resource potential and production capacity assessment of Ghana. By P. G. Chirico et al. [*James E. Shigley**]

Alluvial diamond resource potential and production capacity assessment of Mali. By P. G. Chirico et al. [*James E. Shigley**]

Brown diamonds from an eclogite xenolith from Udachnaya kimberlite, Yakutia, Russia. By A. S. Stepanov et al. [*Guy Lalous**]

Spectroscopic and microscopic characterization of color lamellae in natural pink diamonds. By E. Gaillou et al. [*James E. Shigley**]

Trace-element patterns of fibrous and monocrystalline diamonds: Insight into mantle fluids. By S. Rege et al. [*Kyaw Soe Moe**]

GEM LOCALITIES

Geochemical and geological controls on the genesis of gem-quality "Paraíba tourmaline" in granitic pegmatites from northeastern Brazil. By H. Beurlen et al. [*James E. Shigley**]

The history of kunzite and the California connection. By M. Mauthner [*Keith A. Mychaluk**]

L'opale du Wollo, Ethiopie: Des mines de gisement! [Opal from Wollo Ethiopia: A source of mining capacity!] By F. Mazzero et al. [*Guy Lalous**]

Prediction of exploration target areas for gem deposits in Mogok Stone Tract, northern Myanmar, by integrating remote sensing and geoscience data. By T. K. Oo [*James E. Shigley**]

Rubis et saphirs de Marosely, Madagascar [Ruby and sapphire from Marosely, Madagascar]. By L. E. Cartier [*Guy Lalous**]

Sapphires from Sri Lanka. By T. Waltham [*Annette Buckley**]

INSTRUMENTS AND TECHNIQUES

Test visuel sur l'attraction magnétique des matières gemmes [Visual test of the magnetic attraction of gemstone materials]. By T. Pradat and J.-P. Gauthier [*Rolf Tatje**]

Three-dimensional X-ray radiography. By T. Hainschwang [*Kyaw Soe Moe**]

JEWELRY HISTORY

Brazilian colored gemstones in historical jewelry. By R. Galopim de Carvalho [*Jo Ellen Cole**]

Hippologie arabe et archéogemmologie sur un harnachement mameluk, 2ème Partie [Arab hippology and archaeological gemology on a Mamluk harness – Part 2]. By E. Gonthier et al. [*Guy Lalous**]

Hippologie arabe et archéogemmologie sur un harnachement mameluk, 3ème Partie. By E. Gonthier et al. [*Guy Lalous**]

Gemme da Vigna Barberini (Colle Palatino, Roma) [Gemstones from Vigna Barberini (Palatine Hill, Rome)]. By E. Gliozzo et al. [*Rolf Tatje**]

Non-destructive analysis of amber artefacts from the prehistoric Cioclovina hoard (Romania). By E. S. Teodor [*Edward R. Blomgren**]

SYNTHETICS AND SIMULANTS

Crystal growth and perfection of large octahedral synthetic diamonds. By A. F. Khokhryakov et al. [*Jennifer Stone-Sundberg**]

Developments of elemental technologies to produce inch-size single-crystal diamond wafers. By H. Yamada et al. [*Jennifer Stone-Sundberg**]

TREATMENTS

Discrimination between natural and HPHT-treated type IIa diamonds using photoluminescence spectroscopy. By H. J. Lim et al. [*James E. Shigley**]

Nouvelle absorption utile à la détection des diamants traités par irradiation et chauffage: Le triplet à 6021, 6070 et 6139 cm^{-1} [New absorption useful in detecting diamond irradiation and annealing treatment: A triplet at 6021, 6070 and 6139 cm^{-1}]. By A. Respinger [*Guy Lalous**]

MISCELLANEOUS

2010: Year of replenishment, speculation and recycling. By C. Even-Zohar [*Edward Johnson**]

Blood diamonds: International policy options for conflict resolution. By S. Lahiri [*Russell Shor**]

Diamonds without borders: An assessment of the challenges of implementing and enforcing the KP Certification Scheme. By Partnership Africa Canada [*Edward Johnson**]

Environmental stewardship in gemstone mining: Quo vadis? By L. Cartier [*Edward R. Blomgren**]

Gemstone mining as a development cluster: A study of Brazil's emerald mines. By J. Puppim de Oliveira and S. Ali [*Edward R. Blomgren**]

The geoheritage significance of crystals. By M. Brocx and V. Semeniuk [*Edward R. Blomgren**]

The Tucson mineral show and the market for collector minerals: The potential for artisanal and small scale miners. By B. Ross et al. [*Michele Kelley**]

---

* Member of the Gemological Abstracts Review Board

G&G Online Book Reviews

Living Jewels: Masterpieces from Nature

By Ruth Peltason, 224 pp., illus., publ. by The Vendome Press [www.vendomepress.com], New York, 2010. US$50.00

In a time of skyrocketing gold prices, it is interesting to see organic materials such as leather, wood, amber, and feather making a strong comeback in the jewelry industry. Yet this "new" trend is as old as jewelry itself. Peltason takes the reader on a thematic journey to explore the variety of "living jewels," traditional as well as exotic. Organic materials are just as challenging as minerals for gemologists, whether it concerns identification, treatment detection, disclosure, or ultimately valuation. This book is intended for jewelry amateurs and professional dealers interested in estate pieces, as well as jewelry designers.

Lavishly embellished with more than 350 color illustrations, *Living Jewels* presents a vast selection chosen according to three main criteria: originality, historical importance, and the aesthetic prominence of the organic material. It is therefore a subjective selection comprising famous jewelry houses such as Van Cleef & Arpels, Cartier, Tiffany, Boivin, Belperron, Verdura, and Grima, while also spotlighting contemporary jewelers such as Marguerite Stix, Patricia Van Musulin, Ted Muelhing, and Jennifer Trask. The book is well organized by material: amber, coral, horn, ivory, pearls, shell, tortoise shell, wood, and "exotica."

Among the most noteworthy elements is a detailed 40-page section on pearls. It features classical pearl jewelry such as Victorian fringe necklaces as well as the most contemporary pieces such as the "Queen Anne's lace" pin by Ted Muehling. Also in this section are coveted pearl treasures, including the late Elizabeth Taylor's Peregrina pearl and the so-called Baroda pearl necklace by Cartier. Non-nacreous pearls such as melo and conch are also discussed.

Two other sections of particular interest deal with wood and exotica. The wood section shows how this versatile material, so prominent in the decorative arts, is used by jewelers. A most welcome glossary on selected varieties of wood provides simple and useful descriptions for identification. After highlighting Art Deco and 1970s pieces, Peltason reviews interesting works of contemporary studio artists such as Noma Copley, Christine J. Brandt, Liv Blåvarp, and Anthony Roussel. She features Lee Hale and Kiff Slemmons, who use reclaimed everyday materials such as pencils and rulers. Equally interesting is the exoticas section, which displays the use of scarabs, butterflies, feathers, teeth, animal skins (snakeskin and stingray), and even various type of hair (elephant and human). She also rekindles the memory of Harry Emanuel, an English Victorian jeweler remembered for his exquisite hummingbird ear pendants.

Peltason's elegant writing style is one of the book's main assets. One might hope, however, for more content on this rich topic. For instance, the materials are presented very succinctly, with room for more detailed gemological content. The antique jewels come with very little contextual information on art period, manufacturing techniques, and provenance. Some of the jewelry in the exotica section warrants more detailed ethnological explanation. The photos are obviously of various sources and reproduction quality, with different magnifications often on the same page. Unfortunately, this makes it more difficult to evaluate the rarity and quality of an individual piece. This becomes particularly evident in the pearl section, where assessing the actual size of the jewelry and gemstones is a challenge, some pieces being magnified and others minimized. Jewelry size information isn't noted either.

Nevertheless, *Living Jewels* is an elegant and interesting book for antique jewelry enthusiasts, one that explores a rich topic with a wide scope of interest from 19th century jewelry to the most cutting-edge creations.

DELPHINE A. LEBLANC
Hoboken, New Jersey

The Extraordinary World of Diamonds

By Nick Norman, 302 pp., illus., publ. by Janaca Media [janaca.co.za], Auckland Park, South Africa, 2010. R199.96

The world of diamond is an extraordinary one indeed. The author has made a brave attempt to outline this world in 300 pages. The book is illustrated with many well-chosen archival and contemporary photographs acquired from the Brentwood Library in Johannesburg, De Beers, and various diamond mining companies.

The first 40 pages give a summary overview of where diamonds are found, a history of their discoveries, prospecting and mining methods, and cutting and polishing. The next 150 pages discuss in greater detail the development of discoveries from ancient India, Brazil, and Venezuela,

to more recent times in South Africa and the rest of the continent, Russia, Canada, and Australia. Earlier narratives such as Legrand's 1980 book *Diamonds: Myth, Magic and Reality* are used extensively, but for recent developments the author has drawn upon firsthand accounts from known experts. Included are discussions of the recently discovered diamond mines in Canada, the Bunder prospect in India, and the Argyle mine in Australia.

The next 60 pages present a more detailed account of modern exploration and mining, beginning with criteria for area selection, defining drill targets, and conducting feasibility studies. Also included are case histories of the alluvial deposits at Oena in the lower Orange River, Verneukpan in Namaqualand, coastal and offshore deposits along the Atlantic, and kimberlites in Botswana and Canada. There is also a discussion of Clifford's rule, kimberlite indicator minerals (e.g., G10 garnet and the Gurney Cr/Ca diagram), and the distribution of carbon in the mantle and subducted crust. This is followed by a discussion of microdiamonds formed by meteorite impact (exemplified by Popigai in northern Siberia), microdiamonds found in meteorites, graphitized diamonds in the Ronda ultrabasic massif in southern Spain, and a possible cosmic origin of carbonado.

This is followed by a chapter on diamond deposits along the Atlantic coast of South Africa and Namibia, and how the diamonds traveled from inland kimberlite deposits. This chapter seems a bit misplaced, as its content really belongs in the section on case histories. A final chapter on the supply chain discusses the Central Selling Organisation and the breakup of its "single-channel marketing pipeline" in the wake of conflict diamonds and new mines in Australia and Canada that were outside De Beers's control.

The author effectively uses text boxes to present short biographies and specific subjects, and he tells the story in clear language. There are some lapses, though. In the glossary, for instance, a *diamantaire* should be defined as a trader in diamonds, not just a cutter. The case history for the discovery of Orapa should have linked Gavin Lamont with Manfred Marx, the young De Beers geologist who actually discovered the mine by collecting soil samples on the site and noting the large numbers of garnets in them. And while the Popigai and Ronda occurrences are mentioned, the very large source of microdiamonds near Kokchetav in northern Kazakhstan is omitted. There, diamonds are contained in Cambrian metasediments that were deeply buried and subsequently uplifted. In contrast to Ronda, however, the tiny diamonds were enclosed in garnet and zircon crystals and thereby preserved from graphitization.

It is the maps, which appear to have been adapted from a simple atlas, that let the book down. All nine maps contain some mistakes—misplaced symbols, misnamed or omitted occurrences, and inconsistent terminology in the captions.

Overall, this is an interesting story that should have been edited more tightly, as the sequence of subjects jumps around and parts are repetitive (beach and offshore mining are discussed in three different sections in the book). The first 40 pages are spent summarizing the rest of the book, and a detailed discussion of the subject matter doesn't begin until page 60. In a book that tries to cover the whole world of diamonds in 300 pages, that seems a waste of space. The book is written as a story rather than a scientific text, so it falls between two stools. It is not up to the standard of a textbook on diamond geology, but at the same time it is sometimes too detailed for the interested layman who would have to be well versed in geology and geography to fully appreciate the text. Otherwise, it is a well-told story and a reasonably priced book.

A. J. A. (BRAM) JANSE
Archon Exploration
Carine, Western Australia

The Workbench Guide to Jewelry Techniques

By Anastasia Young, 320 pp., illus., publ. by Interweave Books [www.interweave.com], Loveland, CO, 2010. $34.95

In this meticulously prepared work, Anastasia Young presents over a hundred jewelry making processes and techniques, organized in a bench reference style. The book opens with a contents section that goes beyond a simple listing of topics and page numbers. There is a "technique file" that numbers all the methods described and the relevant page numbers, making it simple to quickly locate a specific topic. There are also mini-indexes called "finders" strategically placed throughout the book. As a result of this well-considered structure, navigating the book is a pleasure.

The first chapter opens with a short piece on how to set up a small workshop. The rest of the chapter is about the tools and materials used to make jewelry. As an unreformed toolaholic, I was delighted with this section. Each item was represented by a small high-quality photograph of each tool, the techniques it is used for, and how it is used. I particularly liked the fact that the author noted the skill level required for each tool. Essential tools for beginning goldsmiths were also identified by a symbol to help novices assemble a tool kit. The materials section of the chapter gives a broad overview of both traditional and nontraditional materials used in modern jewelry, ranging from gold to concrete.

The second chapter is the heart of the book. It begins with essential techniques that must be mastered, including sawing, filing, soldering, sanding, and polishing; these become more advanced as you go farther into the chapter. Each technique is described in some detail and then illustrated using three or four photographs accompanied by captions. The method is effective in conveying a basic understanding. Jewelers who have

mastered the core techniques should be able to incorporate the more advanced techniques into their own projects using the examples provided.

Given the broad range of techniques the author describes, it would be unfair to expect a lot of detailed or highly technical information. The section on chasing and repoussé is typical of her approach. Its four pages cover three techniques, well described and illustrated, with three excellent photos of jewelry made using the techniques and about a dozen paragraphs discussing materials, tools, and the basic operations involved. While she mentions that chasing tools can be handmade by the craftsman, she does not go into the details of annealing, shaping, hardening, and tempering them, although she does point out the necessity of these steps. Clearly, if you want to master one of these techniques, you will need to look beyond this book. On the other hand, if you would like to try some of them out and see how they apply to your work, it is a great starting point.

The chapter ends with a section on outwork. This section discusses the kinds of work that might be contracted out to someone with advanced expertise or specialized equipment. Many books written about our field mistakenly give the impression that the craftsman should master every technique and "do it all." The fact is that there have *always* been specialists, and it is perfectly appropriate to send out work to someone who can do it faster or better. The jewelry industry is seeing the rapid development of many highly technical and expensive processes, and none of us has the time or capital required to master it all. This section discusses the kind of jobs that might be outsourced and contains many common-sense suggestions about how to work with subcontractors to achieve good results.

The third chapter is a brief 10 pages on design, including inspiration and where to find it, sketching, and technical drawing. I particularly liked the Design Checklist and the notion of a "brief" to define and give structure to a project. The last section, Design Realization, shows how to convert drawings and concepts into finished items. The idea of using models or 3-D sketches made from inexpensive or easily worked materials such as paper or modeling clay to work out final shapes and solve assembly problems is excellent. I was impressed with the author's emphasis on keeping detailed notes and drawings so that the sequence for constructing the piece has been worked out before expensive materials and labor are applied.

Next, the Going into Business chapter covers a topic often omitted in books of this type. In today's global market, understanding the business side of our craft has become more important than ever. The first half of the chapter covers photography and promoting one's work. The author has included a technique file that shows how software can improve an image, plus a brief discussion of the difficulty in getting quality images of jewelry. Her section on promotional material is only one page, but it is full of great ideas for communicating a clear identity or brand to the world. The balance of the chapter deals with pricing jewelry and deciding where to sell it and how to display it.

This book is very attractive; almost every page has a photograph of jewelry that relates to the text on that page. The layout is pleasing and user friendly, the text well written and packed with good information. This is a valuable book for students and beginning goldsmiths, who will discover the broad range of techniques and materials available today. Professional designers and goldsmiths who seek innovative techniques or materials to meet the changing demands of today's jewelry market will also find plenty of inspiration here.

DOUG CANIVET
Gemological Institute of America
Carlsbad, California

World Hallmarks, Volume I: Europe, 19th to 21st Centuries, 2nd ed.

By William Whetstone, Danusia Niklewicz, and Lindy Matula, illus., publ. by Hallmark Research Institute [www.hallmarkresearch.com], San Francisco, 2010. $228

This is a wonderfully organized volume that has long been needed by appraisers, collectors, and museums. The authors have a gift for taking this very complex subject and making it easily understandable.

The book's "5S" approach to identifying hallmarks stands for Strike, Shape, Style, Standard, and System. Strike is the actual stamping of an impression onto a tested metal and the resulting placement and quality of that impression. The shape of the mark is its outline, while the style refers to its design and imagery. Standard marks indicate the fineness of a particular metal. Lastly, the System of sequential hallmarks involves the mark image and the existence of a surrounding frame with specific shape and fineness numbers, sometimes with a date number or letter.

The fifth S, System, also includes four subcategories: Implied, Symbolic, Inclusive, and Sequential (ISIS). In this methodology, an implied hallmark is recognized by the core image and/or frame shape. These alone can indicate type of metal, metal fineness, and country or location of assay. A symbolic hallmark uses a formal or national symbol representing the assaying country but provides little other information. A hallmark with letters and numbers added to a core image is considered an inclusive hallmark. The most informative and easily read hallmarks are sequential hallmarks, consisting of a series of marks in a line or cluster.

The chapters that follow give a brief history of the European hallmarking systems by country. The 5S system is applied, and a timeline of precious metal use in each country is provided. Additional hallmarks, along with ancillary marks that serve a spe-

cific purpose, are described with assay office marks and identification symbols.

In the back of the book is an analytical index containing a convenient listing of hallmark images. Although this image index does not include all hallmarks, its orderly arrangement makes looking for the image less overwhelming than one might suppose. A historical timeline illustrates various periods of political transition for the countries that once formed the Austro-Hungarian Empire, the Russian Empire and the USSR, and Yugoslavia. The glossary of hallmark terms is helpful in reading this book, and an extensive bibliography completes the work. Companion volumes featuring hallmarks of other countries are in the works.

JO ELLEN COLE
Vista, California

Mineral Treasures of the World

By The Geological Museum of China and The Collector's Edge Minerals Inc., 125 pp., illus., publ. by Geological Publishing House [www.gph.com.cn], Beijing, 2010. ¥286

The "Mineral Treasures of the World" exhibit opened in the summer of 2010 during China's World Fair in Shanghai. Cosponsored by the Geological Museum of China and The Collector's Edge Minerals, it showcased many of the world's greatest localities for fine minerals with very rare and exquisite examples. This book was written to accompany the exhibition, while educating readers and serving as an infomercial for The Collector's Edge.

The book's Gallery of Treasures section contains splendid color photographs of specimens from the exhibit. They are outstanding examples, worthy of the finest collections—treasures indeed! Each specimen is described with its name, chemical formula, size, and a brief narrative. Many of these are gem species.

The book's educational purpose is accomplished by the first five chapters. They cover the mining of specimens, their trimming and cleaning, identifying superb specimens, worldwide market trends, and how to start collecting fine minerals. These chapters are richly illustrated with color photographs that accentuate the subject matter. They build a strong case for collecting fine minerals, comparing them to fine works of art that justify their high prices. The effort and expense of their mining and the careful cleaning and trimming necessary to bring out their best are chronicled in the story that follows one piece from mine to mineral cabinet. The criteria of excellence are given as a general guide to help the reader recognize a fine mineral specimen and why it holds greater value.

The book extols the virtues of collecting and preserving fine minerals for their enjoyment and as an investment, while also setting out on its third purpose, to be an advertisement for The Collector's Edge Minerals as a prime source for their acquisition. In relating its care and know-how, the company makes a strong case for itself.

The Mineral Treasures of the World exhibit ended in July 2010, but this accompanying book stands as a permanent record of its excellence. Readers of *Gems & Gemology*, especially those who also collect minerals or appreciate gem species in their natural finest forms, should enjoy this book. Although it does mention that some of these specimens are affordable, it should have elaborated on this point, as most people only dream of owning such a specimen, let alone an entire collection of them. And while The Collector's Edge is a great resource, there are many other excellent dealers to choose from. With these last few points in mind, this book is highly recommended, especially for the beginner.

MICHAEL T. EVANS
*Gemological Institute of America
Carlsbad, California*

OTHER BOOKS RECEIVED

Collectors Guide to Granite Pegma-tites. *By Vandall T. King, 96 pp., illus., publ. by Schiffer Publishing [www.schifferbooks.com], Atglen, PA, 2010, US$19.95*

Collectors Guide to Silicate Crystal Structures. *By Robert J. Lauf, 96 pp., illus., publ. by Schiffer Publishing [www.schifferbooks.com], Atglen, PA, 2010, US$19.95*

These works, volumes 8 and 9 of the Schiffer Earth Science Monograph series, review the formation and mineralogy of pegmatites and the crystallography of silicates, respectively. Typical for the series, both books are aimed at the educated collector rather than the academic reader. Both are also well illustrated, though the pegmatite volume curiously features several photos of Colombian emerald and red beryl, neither of which form in pegmatites.

TWO

Gems and Gemology in Pakistan. *By Tahseenullah Khan and Allah Bakhsh Kausar, 231 pp., illus., publ. by Geological Survey of Pakistan (www.gsp.gov.pk), Quetta, 2010, Rs. 3000.* This special publication by the Geological Survey of Pakistan reviews the exploration, mining, manufacturing, and marketing of gem materials from that country.

TWO

Diamond Math. *By Kenneth A. Glasser, 451 pp., illus., publ. by Kenneth A. Glasser Co. [www.diamondmath. com], Las Vegas, 2010, US$75.00.* This pocket-sized handbook contains a set of charts allowing quick estimation of a diamond's weight based on its external measurements. Separate charts are provided for rounds and a wide variety of fancy cuts.

TWO

G&G Online Abstracts

COLORED STONES AND ORGANIC MATERIALS

A survey of Mn-rich yellow tourmaline from worldwide localities and implications for the petrogenesis of granitic pegmatites. W. B. Simmons [wsimmons@uno.edu], A. U. Falster, and B. M. Laurs, *Canadian Mineralogist*, Vol. 49, No. 1, 2011, pp. 301–319, http://dx.doi.org/10.3749/canmin.49.1.301.

While yellow is an uncommon color for tourmaline, this variety has been found in certain granitic pegmatites in several countries. The authors present electron microprobe data from more than 200 yellow to yellow-green tourmalines from Zambia, Madagascar, Russia, Mozambique, Nepal, the United States, and Democratic Republic of Congo. The material is predominantly Mn-rich elbaite and "fluor-elbaite" (>3 wt.% MnO), although rare yellow rossmanite and "fluor-rossmanite" have come from Mozambique. Among the analyzed samples, the MnO content ranged from 3.09 to 8.90 wt.%. No material that could be classified as tsilaisite (>10.71 wt.% MnO) was encountered. The analyzed samples also had higher TiO_2 contents (averaging 0.28 wt.%) than pale-color tourmalines. The yellow color is due to absorptions associated with the Mn^{2+}-Ti^{4+} intervalence charge-transfer mechanism. Yellow tourmaline is a rare late-stage magmatic to miarolitic cavity–stage mineral that requires specific conditions to form. Its presence implies that the original pegmatite-forming melt is relatively low in Fe and enriched in both Mn and B. During the early stages of melt crystallization, Fe must be removed from the system, but abundant Mn and B along with traces of Ti must still be available during the late stages of pegmatite formation for yellow tourmaline to crystallize.

JES

DIAMONDS

Alluvial diamond resource potential and production capacity assessment of the Central African Republic. P. G. Chirico [pchirico@usgs.gov], F. Barthélémy, and F. A. Ngbokoto, *U.S. Geological Survey Scientific Investigations Report 2010-5043*, Reston, Virginia, 2010, 22 pp.

Diamonds from what is now the Central African Republic (CAR) were discovered almost a century ago, and commercial production began in 1931. The diamonds are recovered along rivers that cut through sandstone formations in both the Kadéi-Mambéré-Sangha region near Berberati, and the Haute-Kotto region northeast of Bria. The country was studied as part of an ongoing effort to assess world diamond production for the Kimberley Process certification scheme. Because accurate production figures from the CAR are not available, the authors used two indirect methods to estimate diamond potential and production. The methods took into account the size and grade of the alluvial deposits, as well as the human resources engaged in artisanal mining efforts. An estimated 39 million carats of diamonds remain in these two regions, roughly twice the country's total output since 1931. Production capacity is calculated at 840,000 carats per year, twice what has been reported by the CAR government. *JES*

Alluvial diamond resource potential and production capacity assessment of Ghana. P. G. Chirico [pchirico@usgs.gov], K. C. Malpeli, S. Anum, and E. C. Phillips, *U.S. Geological Survey Scientific Investigations Report 2010-5045*, Reston, Virginia, 2010, 25 pp.

Diamonds were first found in the former Gold Coast Colony (now Ghana) in 1919 along the Birim River near the town of Abomoso, and commercial mining began shortly afterward. There are no known kimberlite occurrences in Ghana. The two major alluvial diamond mining areas are along the Bonsa River valley southwest of Tarkwa, and the Birim River valley between the towns of Akwatia and Oda. In both areas, diamonds are mined (usually by artisanal diggers) from gravel layers beneath the alluvial flood plains and adjacent terraces. Based on careful geological fieldwork, an estimated 91.6 million carats of alluvial diamonds remain in these two areas.

JES

Alluvial diamond resource potential and production capacity assessment of Mali. P. G. Chirico [pchirico@usgs.gov], F. Barthélémy, and F. Koné, *U.S. Geological Survey Scientific Investigations Report 2010-5044*, Reston, Virginia, 2010, 23 pp.

Alluvial diamond deposits occur in Mali along river systems in the southwest portion of the country between the village of Kéniéba and the border of neighboring Senegal. Some kimberlite pipes in the area have been identified, but in most cases the primary sources of these diamonds are unknown. Most have been found fortuitously by artisanal gold washers. An interesting characteristic of diamonds from the Kéniéba area is their exceptional size—nearly 15% of them weigh >15 ct. Crystals larger than 50 ct are common, and the largest reported to date weighed 232 ct. This report represents the results of a field study undertaken to assess Mali's overall diamond potential. The resource assessment focused on two alluvial mining areas, Kéniéba and the nearby Bougouni region. The authors estimate that these two regions contain approximately 2.3 million carats of diamonds. *JES*

Brown diamonds from an eclogite xenolith from Udachnaya kimberlite, Yakutia, Russia. A. S. Stepanov [aleksandr.stepanov@anu.edu.au], A. V. Korsakov, O. P. Yuryeva, V. A. Nadolinniy, M. Perraki, K. De Gussem, and P. Vandenabeele, *Spectrochimica Acta A: Molecular and Biomolecular Spectroscopy*, Vol. 80, No. 1, 2011, pp. 41–48, http://dx.doi.org/10.1016/j.saa.2011.01.006.

Brown diamonds represent a significant proportion of global diamond production, and their economic importance has encouraged intensive research on color enhancement processes. The authors performed petrographic and spectroscopic studies of brown diamonds from an eclogite xenolith from the Udachnaya pipe (Yakutia, Russia). A thick plate was cut from the middle of the xenolith, from which 19 thin sections were subsequently prepared. In addition, diamonds were extracted from the xenolith and their distribution was mapped. A polarizing microscope was used to examine both the thin sections and the diamond crystals. Brown diamonds were randomly intermixed with colorless ones in the rock, often at the grain boundaries of clinopyroxene and garnet.

Electron paramagnetic resonance, photoluminescence, infrared, and Raman spectroscopy were used to identify defects in the diamonds. The brown diamonds were characterized by a set of defects (H4, N2D, and a line at 490.7 nm), which is typical for plastically deformed diamonds and indicates that they were likely annealed for a relatively short period after deformation occurred. The Raman peak corresponding to graphite was not observed in brown regions of the diamonds, eliminating the possibility that graphite caused the coloration. Comparison with previous reports of brown diamonds from eclogites showed that the eclogitic sample had a typical structure, with no signs of apparent deformation. Two mechanisms are proposed: (1) deformation of the eclogite by external forces followed by subsequent recrystallization of silicates, or (2) deformation by local stress arising from decompression and expansion of silicates during the xenolith's ascent to surface conditions. *GL*

Spectroscopic and microscopic characterization of color lamellae in natural pink diamonds. E. Gaillou [gailloue@si.edu], J. E. Post, N. D. Bassim, A. M. Zaitsev, T. Rose, M. D. Fries, R. M. Stroud, A. Steele, and J. E. Butler, *Diamond and Related Materials*, Vol. 19, No. 10, 2010, pp. 1207–1220, http://dx.doi.org/10.1016/j.diamond.2010.06.015.

Some natural pink diamonds owe their coloration to multiple thin (~1 mm) pink lamellae oriented along octahedral planes. Gemologists refer to these parallel colored lamellae as a type of "graining." The diamond is often nearly colorless between these lamellae, and stronger pink color is associated with more numerous lamellae. Examination at high magnification shows that the lamellae consist of paired microtwins created by plastic deformation when the diamond was under stress. The color of these diamonds results from a broad absorption band centered at about 550 nm. The optical defect responsible for this broad spectral feature was not identified, but it is likely associated with plastic deformation. Different optical defects were identified spectroscopically within the lamellae (where residual stress persists) and the intervening diamond. The authors suggest that during plastic deformation, carbon-atom vacancies are created in the diamond lattice during twinning, and when these vacancies diffuse through the lattice they tend to become trapped by nitrogen impurities to form the new defect centers along the lamellae. Annealing of plastically deformed brown diamonds can result in a residual pink color that is stable under high pressure and temperature conditions. The authors conclude that the deformation responsible for the pink color in diamond occurred in the earth's mantle. Similar lamellae causing the brown color of some diamonds probably resulted from deformation during a more recent geologic event, such as a rapid ascent to the surface in kimberlitic or lamproitic eruptions.   *JES*

Trace-element patterns of fibrous and monocrystalline diamonds: Insight into mantle fluids. S. Rege, W. L. Griffin [bill.griffin@mq.edu.au], N. J. Pearson, D. Araujo, D. Zedgenizov, and S. Y. O'Reilly, *Lithos*, Vol. 118, 2010, pp. 313–337, http://dx.doi.org/ 10.1016/j.lithos.2010.05.007.

The fluids in the earth's mantle provide valuable information for understanding complex metasomatic processes. These fluids can be trapped inside a diamond during its formation in the cratonic subcontinental lithospheric mantle. The trace-element patterns of 538 fibrous and monocrystalline diamonds from deposits worldwide were measured and analyzed using LA-ICP-MS.

In the fibrous diamonds, trace-element concentrations varied irregularly within each stone, so no obvious chemical zoning was observed. There were two groups—those rich in K-Rb-Ba and those poor in Ba-Rb-K. Rock-forming elements such as Al, Ca, Mg, K, Fe, and Ti showed positive correlations with each other, although this could not be easily related to petrogenetic processes. Therefore, these elements represented the fluids trapped during diamond formation. The chemical patterns observed in the fibrous diamonds were broadly similar to those seen in kimberlites and carbonatites.

Peridotitic monocrystalline diamonds were classified into two groups. The first showed a higher trace-element content but a negative anomaly in Ce, Y, and Sr. The second group had lower trace-element concentrations, while Yb, Lu, Ba, and Rb were below the limit of detection. Chalcophile elements, such as Pb, Cu, Zn, Co, and Ni also were detected, representing submicroscopic sulfide inclusions. Eclogitic monocrystalline diamonds were also divided into two groups. The major rock-forming elements, such as Na, Fe, Mg, and Al, were present in these diamonds, while chalcophile element contents were low. Interestingly, the trace-element patterns of both peridotitic and eclogitic diamonds from a single source were similar. The authors propose the existence of immiscible high-density fluids/melts within the diamond stability field (6 GPa and 1200–1300°C). According to this model, most peridotitic and eclogitic monocrystalline diamonds likely crystallized from fluids such as the high-density hydrous-silicic fluids related to the precipitation of fibrous diamond.

Although diamonds of subduction origin did not contain rock-forming elements, they did show similar patterns of other elements. Thus, they were formed from broadly similar high-density fluids. Diamonds of superdeep origin (from the transition zone to the lower mantle) had patterns similar to those of other monocrystalline diamonds around the world, except those from Brazil, in which Al was the only rock-forming element detected. A direct link between diamond-forming fluids and pyrope, the most important diamond indicator mineral, was also found by analyzing trace-element patterns. The diamond growth rate and environment may be closely related. In other words, diamond grows more slowly in silicate-rich fluids, and consequently fewer fluid inclusions are trapped.   *KSM*

GEM LOCALITIES

Geochemical and geological controls on the genesis of gem-quality "Paraíba tourmaline" in granitic pegmatites from northeastern Brazil. H. Beurlen [beurlen@ufpe.br], O. J. M. de Moura, D. R. Soares, M. R. R. da Silva, and D. Rhede, *Canadian Mineralogist*, Vol. 49, No. 1, 2011, pp. 277–300, http://dx.doi.org/10.3749/canmin.49.1.277.

Brazil's famous "neon" blue Cu-bearing elbaite tourmalines occur in only four deposits of zoned and highly fractionated granitic pegmatites of the Borborema Pegmatitic Province. Among several thousand barren pegmatites and

more than 750 Be-Li-Ta rare-metal pegmatites known in this region, it is only in these four deposits (Batalha, Capoeira, Glorious, and Quintos) that the necessary conditions were met for these tourmalines to form. The pegmatites are hosted by Fe-poor quartzite or metaconglomerate of the Equador Formation, and they are rich in Li minerals (mainly spodumene or lepidolite) and in B. Significant amounts of schorl that crystallized in the border zone helped lower the Fe and Mg contents of the pegmatite-forming melt to allow the subsequent crystallization of Fe-poor elbaite. These pegmatites also show extensive replacement of feldspar and other primary minerals by lepidolite.

The Cu-bearing tourmalines usually occur at the transition between an albite-rich inner intermediate zone and the quartz core, where they form wedge-shaped crystals arranged in fan-like, radial, or comb-textured aggregates. In some cases, they are also found in crystal-lined cavities in the center of the pegmatites. The tourmalines may be strongly color zoned, with a pink to red core, a blue intermediate portion, and a green rim. They are distinguished by relatively high Cu, Li, and F, low Mn and Mg, and near absence of Fe. They formed by direct crystallization from a pegmatite-forming melt during an early stage of formation of the quartz core. The crystals are often partially or completely replaced by lepidolite except within the quartz core. Several sources have been suggested for the copper found in these tourmalines, such as skarns and quartz veins containing Cu-sulfide minerals in the Jucurutú Formation that underlies the Equador Formation, but this question has not been fully answered.

JES

The history of kunzite and the California connection. M. Mauthner [mmauthner@gmail.com], *Rocks & Minerals*, Vol. 86, No. 2, 2011, pp. 112–131.
Facts are often lost to history, but occasionally good detective work can bring back missing details and complete an interesting story. Kunzite, the main gem variety of spodumene, is relatively new to commercial markets, dating back to the early 1900s. Yet questions remain about when, where, and by whom the "first" specimens were truly discovered. Detailed research has yielded a surprisingly intriguing history that traverses a scientific rivalry, exotic localities, and hardened prospectors. Equally noteworthy are the article's historical photographs, many of which the author has rephotographed from the originals. Although heavily weighted toward Southern California discoveries, the article provides a good summary of kunzite finds in Brazil and Madagascar. Discussion of kunzite from Afghanistan and Nigeria is limited. *KAM*

L'opale du Wollo, Ethiopie: Des mines de gisement! [Opal from Wollo Ethiopia: A source of mining capacity!] F. Mazzero, C. Désagulier, B. Rondeau, D. Ayalew, G. Ezezew, T. Cenki, and E. Bekele, *Revue de Gem-*

mologie a.f.g., No. 174, 2010, pp. 14–20 [in French].
The article investigates the geologic conditions of gem opal formation at Wegel Tena, in Ethiopia's Wollo Province. The deposit consists of a single horizontal layer of weathered ignimbrite (a volcano-sedimentary rock of rhyolitic composition, formed by the deposition of volcanic ash over a wide area) within a thick series of unaltered Oligocene ignimbrite. The opals contain very well-preserved plant fossils, which show they formed in a sedimentary environment, most likely during a pause in the volcanic succession.

Mining conditions at Wegel Tena are harsh and dangerous, and the workers have little knowledge of proper techniques. Their tools are limited to hammers, chisels, shovels, and pickaxes. Many fatal accidents occur due to collapsing tunnels or falls from cliffs. There is no shoring or ventilation in the tunnels. During their visit, the authors explained some basic safety rules to the miners and donated safety equipment. The deposit is very promising, as the opalized layer is quite extensive and shows a high gem opal content. Wegel Tena has the potential to become an important opal deposit, provided that the mining becomes more organized and professional. *GL*

Prediction of exploration target areas for gem deposits in Mogok Stone Tract, northern Myanmar, by integrating remote sensing and geoscience data. T. K. Oo, *Advances in Geosciences*, Vol. 26, 2010, pp. 181–198.
The region around Mogok in northern Myanmar has been one of the world's most famous gem-producing areas for almost 400 years. Igneous and metamorphic rocks, including granites and pegmatites, gneisses, marbles, schists, and quartzites, are the source for the ruby, sapphire, and other gems that are found in both primary and secondary deposits. Most economic gem mines are found either along certain horizons in marbles or in skarns, as well as in alluvial placers derived from these rocks. The overall geology of the area is complex, with igneous rocks intruding into preexisting metasedimentary rocks, which are folded and faulted on a regional scale. Remote sensing and geoscience data have produced a map of promising target areas for gem mineralization at locations where marbles occur. *JES*

Rubis et saphirs de Marosely, Madagascar [Ruby and sapphire from Marosely, Madagascar]. L. E. Cartier [gemlab@ssef.ch], *Revue de Gemmologie a.f.g.*, No. 175, 2011, pp. 9–13 [in French].
This article examines the eluvial corundum deposit recently discovered at Marosely, in south-central Madagascar. The material ranges from red to blue, and stones are typically zoned, giving them an overall purple color. FTIR spectra show the presence of 3160 and 3309 cm^{-1} absorptions in the untreated corundum. The relevance of these bands to the detection of heat-treated corundum is

discussed. LA-ICP-MS data for chromophores in color-zoned samples are consistent with EDXRF spectroscopy. Results for other trace-elements (i.e., concentrations of <1000 ppm) proved less revealing. Further research using other analytical methods is needed to advance the study of the corundum origin. *GL*

Sapphires from Sri Lanka. T. Waltham [tony@geophotos. co.uk], *Geology Today*, Vol. 27, No. 1, 2011, pp. 20–24.

Sri Lanka has long been famous for its sapphires, which are found scattered in the soils of the country's valley floors. Half of the world's sapphires weighing more than 100 ct hail from the Ratnapura region. Sri Lanka's gem deposits, mined for over 2,000 years, are best exploited through small-scale, nonmechanized mining. Shallow pits worked by only a few miners dot the forested area of Ratnapura, and when the pits reach bedrock, they are considered mined out. Old pits are refilled with soil from new adjacent pits. This article features excellent photos accompanying detailed descriptions of the locals' mining processes.

Once the sapphires have been mined, they enter into a low-key local trade. Buyers and miners do not sell from formal stalls but instead gather around the local clock tower to deal through trusted verbal transactions. The country also has a significant (50,000+ people) cottage industry of cutting and polishing stones.

The majority of Sri Lankan sapphires are pale, and these are heat treated to darken their color. Sapphires are far from the only gems produced in Sri Lanka; only a quarter of its 3-million-carat annual production is sapphire. Other gems include spinel, aquamarine, garnet, alexandrite, and zircon. *AB*

INSTRUMENTS AND TECHNIQUES

Test visuel sur l'attraction magnétique des matières gemmes [Visual test of the magnetic attraction of gemstone materials]. T. Pradat and J.-P. Gauthier, *Revue de Gemmologie a.f.g.*, No. 175, 2011, pp. 14–18 [in French].

Gems can show different types of magnetism (dia-, para-, ferro-, antiferro-, and ferrimagnetism) depending on their composition and the "spin" of certain elements they contain. This determines whether they are strongly or weakly attracted to a magnet, or not at all. This behavior is easily demonstrated with neodymium magnets, which are inexpensive and very strong. The authors describe three simple methods (direct application, the floating technique, and the pendulum method) for determining a gem's magnetic behavior. These can be applied as a quick test for presorting mixed lots of similar-looking stones (e.g., red garnets and spinels, as illustrated). However, magnetism alone is not sufficient for identifying a gem, and a sample's identity

must always be corroborated by standard tests. The article contains a useful, comprehensive list of gems and their magnetic characteristics. *RT*

Three-dimensional X-ray radiography. T. Hainschwang [thomas.hainschwang@ggtl-lab.org], *Gems & Jewellery*, Vol. 20, No. 1, 2011, pp. 11–14.

X-ray computed microtomography is the most sophisticated and effective method for 3D X-ray imaging, but it is very costly and time-consuming. Thus the author developed a rapid, economical analytical method. Three-dimensional X-ray radiography was conducted using a tunable X-ray tube, a digital X-ray sensor, and a high-precision rotation device.

The process involves recording multiple images to obtain 3D radiographs, and these are processed using special software for higher contrast and sharpness. Each analysis requires 20 minutes, including sample preparation and data processing. Extensive testing proved that this system could identify and quantify dense filler substances in gemstones, such as fissure-filled rubies and diamonds. It also revealed the concentric structure of a natural pearl from *Pteria penguin*, whereas conventional X-radiography usually shows indistinct structure. Unfortunately, entire pearl strands cannot be scanned by this method.

The 3D X-ray radiography system is cost-effective to operate and maintain, and it is a faster method than X-ray computed microtomography. Although its images do not have such high resolution, they are far superior to conventional X-radiographs. *KSM*

JEWELRY HISTORY

Brazilian colored gemstones in historical jewelry. R. Galopim de Carvalho, *InColor*, No. 15, Fall/Winter 2010, pp. 40–44.

Brazil is well known for its seemingly inexhaustible supply of various gems from many areas of the country. But until the discoveries of gold in Minas Gerais in the 17th century and of diamonds in the mid-1720s, little was known of Brazil's stunning mineral wealth. When diamonds were found near a town now called Diamantina, locals became more aware of the mineral riches in the riverbeds and other sedimentary deposits. During the second quarter of the 18th century, prospectors discovered what were initially termed "Brazilian rubies" in the Ouro Preto area of Minas Gerais. These turned out to be yellow, orange, pink, and orangy red topaz, and they soon proved quite popular with jewelers in Portugal, which still ruled Brazil. The trade term "Imperial" topaz is thought to have originated soon after the discovery of these deposits.

To enhance the apparent color of Brazilian gemstones, colored foil was often placed under closed-back settings. In the late 18th and early 19th centuries, colorless topaz was widely used in silver jewelry. Several methods were

employed to make it resemble diamond, including painting the culet with black ink to simulate the extinction of light in diamonds with a closed-back setting. In the late 1700s, huge quantities of colorless quartz were discovered in Brazil, and the resulting gems also were set in Portuguese silver jewelry with closed backs and painted culets. Pyrope-almandine and transparent yellow chrysoberyl were also given the foil-back treatment to present a uniform color.   *JEC*

Hippologie arabe et archéogemmologie sur un harnachement mameluk, 2ème Partie [Arab hippology and archaeological gemology on a Mamluk harness – Part 2]. E. Gonthier [gonthier@mnhn.fr], T. De-Noblet, and J.-P. Sage-Fresnay, *Revue de Gemmologie a.f.g.*, No. 174, 2010, pp. 27–30. **Hippologie arabe et archéogemmologie sur un harnachement mameluk, 3ème Partie.** E. Gonthier, T. De-Noblet, and J.-P. Sage-Fresnay, *Revue de Gemmologie a.f.g.*, No. 175, 2011, pp. 22–27 [in French].

Part 2 of this series on the Mamluk harness (see abstract of Part 1 in Spring 2011 *G&G*, p. S9) focuses on its dark blue lapis lazuli and red coral, and the meaning of these colors. Lapis was associated with the night and its myriad stars, the sacred sanctuary of the pharaohs' souls. Red coral was prized for its rarity and its symbolic and traditional values. The color red represented the desert, as well as blood, violence, and victory. The article also mentions the shipping routes that brought these stones to Egypt.

Part 3 examines the harness's turquoise and ruby. Turquoise from Persia has a more stable color than its Chinese counterpart, and the color quality of the turquoise in the harness suggests a Persian origin. The ruby is evidence of the trade ties between the Far East and North Africa. The caravans of the Silk Road brought the stones first to Turkey and then to Egypt. It is difficult to identify the exact origin of the ruby in the Mamluk harness, though it could be of Afghan or Tajik origin. In the Mamluk tradition, the role of precious metals and stones complements the relationship between man and his horse. The Arabian horse was ornately decorated not because its rider was a lord, but because this breed was considered the mount of the prophet.   *GL*

Gemme da Vigna Barberini (Colle Palatino, Roma) [Gemstones from Vigna Barberini (Palatine Hill, Rome)]. E. Gliozzo, N. Grassi, C. Meneghini, P. Bonanni, and M. A. Tomei, *Rivista Gemmologica Italiana*, Vol. 5, No. 3, 2010, pp. 185–196 [in Italian].

The authors examined 25 gemstones found in archaeological excavations of Vigna Barberini, a 1st/2nd century AD site at the Palatine Hill of Rome. Spatially resolved X-ray diffraction, Raman spectroscopy, and PIXE measurements were used to identify the stones, which included various chalcedony and jasper varieties, almandine, peridot, and lapis lazuli. In most cases, however, their geographic origin

could not be determined. The approach used in this study may help to establish discriminating criteria, which in turn would allow the reconstruction of ancient trade routes.   *RT*

Non-destructive analysis of amber artefacts from the prehistoric Cioclovina hoard (Romania). E. S. Teodor [esteo60@yahoo.co.uk], E. D. Teodor, M. Virgolici, M. Manea, G. Truica, and S. Litescu, *Journal of Archaeological Science*, Vol. 37, 2010, pp. 2386–2396, http://dx.doi.org/10.1016/j.jas.2010.04.011.

Amber is well known from the Baltic Sea and the Dominican Republic, but deposits are found around the world, including Romania (referred to as *Rumanite* or *Romanite*). The aim of this study was to determine if the samples found in a Romanian archeological hoard came from local deposits or from the shores of the Baltic Sea on the Amber Route, which crossed central Europe.

Nondestructive analytical techniques are naturally preferred for archeological artifacts. A total of 43 amber bead fragments belonging to 13 different types according to shape and color, dating from the transitional period between the Late Bronze Age and the Iron Age, were analyzed by Fourier-transform infrared spectroscopy–variable angle reflectance (FTIR-VAR) and Fourier-transform Raman spectroscopy (FT-Raman) coupled with multivariate data analysis. Raman spectroscopy has been used in the last decade to identify specific structural units or functional groups in complex mixtures of fossil resins, allowing quick and nondestructive provenance determination; this technique has also been used to identify and explain chemical degradation mechanisms of Baltic amber. The combination of the two analytical techniques used in this study increases the accuracy of either technique alone, given the great similarities between Baltic and Romanian amber.

The results strongly suggest that a large part of the amber from the hoard had its origin in the Buzău county of Romania, not in the Baltic area, and thus had no connection to the Amber Route.   *ERB*

SYNTHETICS AND SIMULANTS

Crystal growth and perfection of large octahedral synthetic diamonds. A. F. Khokhryakov [khokhr@uiggm.nsc.ru], Y. N. Palyanov, I. N. Kupriyanov, Y. M. Borzdov, A. G. Sokol, J. Hartwig, and F. Masiello, *Journal of Crystal Growth*, Vol. 317, 2011, pp. 32–38, http://dx.doi.org/10.1016/j.jcrysgro.2011.01.011.

For this study, the authors produced 30 octahedral synthetic diamonds ranging from 0.4 to 3.5 ct using a high–pressure, high-temperature (HPHT) technique. The crystals were grown using a split-sphere (BARS) apparatus and a $Ni_{0.7}Fe_{0.3}$ metal alloy catalyst. Growth conditions included a temperature of 1550°C and a pressure of 5.7 GPa. The

largest crystal produced was 3.53 ct and had a maximum width of 9 mm. Dislocation-free regions of about 58 mm^3 and some dislocation-free {111} growth sectors were typical for the larger crystals. The defects in these synthetic diamonds were studied using selective etching, double-reflection interference microscopy, infrared spectroscopy, and other techniques such as X-ray topography, cathodoluminescence, and photoluminescence.

The carbon source was located above the growth zone. Growth occurred as the carbon was deposited on the cooler central part, and convection rotated the melt upward along the hotter exterior walls. The upper {111} faces were preferred, with average growth rates of 39–45 μm per hour. The resulting crystals exhibited low birefringence and were generally inclusion-free and brownish yellow. All of the synthetic diamonds exhibited nitrogen concentrations between 100 and 200 ppm, with the nitrogen in the form of either C-centers (single substitutional atoms) or A-centers (pairs of nitrogen atoms in neighboring substitutional positions). The degree of nitrogen aggregation ranged from 5% to 60%, classifying them as types Ib+IaA and IaA+Ib. X-ray topography studies on (110) plates cut from the centers of the diamonds found that the synthetic diamonds contained less than four bunches of defects extending from the seed crystal. It was concluded that single <111> dislocations result in low, wide growth hillocks. *JS-S*

Developments of elemental technologies to produce inch-size single-crystal diamond wafers. H. Yamada [yamada-diamond@aist.go.jp], A. Chayahara, Y. Mokuno, N. Tsubouchi, S. Shikata, and N. Fujimori, *Diamond and Related Materials*, Vol. 20, 2011, pp. 616–619, http://dx.doi.org/10.1016/j.diamond.2011.01.001.

Diamond offers many advantages over other semiconductor materials, such as a wide band gap and high thermal conductivity. The availability of diamond wafers is therefore of great interest to the semiconductor industry. Currently, three main factors limit the production of these wafers: the difficulty of growing single-crystal synthetic diamond in suitable sizes at feasible growth rates, the lack of sufficiently large seed crystals, and the material's brittleness.

The authors produced 1 inch (2.5 cm) mosaic synthetic diamond wafers based on the microwave plasma CVD growth technique. Their process involved many clever steps to enlarge a seed crystal and subsequently clone it. Initially, enlargement was done by growth on various faces. A lift-off process involving ion implantation facilitated cloning. Then, six half-inch seed clones were joined to further widen the synthetic diamond wafer in the desired orientation. Finally, clones of this mosaic wafer were produced.

The mosaic wafer was examined with Raman spectroscopy at the junctions between seed crystal clones as well as in non-junction areas. It was determined that the full width at half maximum (FWHM) of the 1335 cm^{-1} absorption is about 1.5× greater at the junctions than in the non-junction areas. In all cases, the FWHM was less than 5 cm^{-1}, a value better than that of synthetic diamond grown hetero-epitaxially and near that of the HPHT-grown type Ib substrate, but worse than that of high-quality CVD-grown single-crystal synthetic diamond. The transmission of the mosaic wafers grown in this study showed the cutoff wavelength to be between that of CVD type IIa and HPHT type Ib synthetic diamond. *JS-S*

TREATMENTS

Discrimination between natural and HPHT-treated type IIa diamonds using photoluminescence spectroscopy. H. J. Lim, S. Y. Park, H. S. Cheong [hcheong@sogang.ac.kr], H. M. Choi, and Y. C. Kim, *Diamond and Related Materials*, Vol. 19, No. 10, 2010, pp. 1254–1258, http://dx.doi.org/10.1016/j.diamond.2010.06.007.

Based on a study of 71 untreated type IIa diamonds (65 D–F color, and six brown/M color) and 12 known-HPHT-treated stones, the authors presented spectroscopic criteria for distinguishing between them. Photoluminescence spectra were collected using 488 and 514.5 nm lasers, with diamonds cooled in a liquid helium cryostat. Spectra were collected on the six M-color diamonds both before and after annealing. The authors reported that the loss of brown color in these diamonds was minimal, which they attributed to the heating conditions they could achieve during the treatment (only up to 1800°C for three hours). The authors summarized changes in spectral features (peak position and width, and the occurrence of peaks with respect to one another) related to the GR1, NV, H4, and H3 defect centers in both the untreated and treated diamonds, and in the six diamonds that were annealed. They proposed a discrimination scheme based on the presence or absence of specific PL spectral features, which they claim provides strong evidence to distinguish untreated and HPHT-treated colorless type IIa diamonds. *JES*

Nouvelle absorption utile à la détection des diamants traités par irradiation et chauffage: Le triplet à 6021, 6070 et 6139 cm^{-1} [New absorption useful in detecting diamond irradiation and annealing treatment: A triplet at 6021, 6070 and 6139 cm^{-1}]. A. Respinger [axel.respinger@gemtechlab.ch], *Revue de Gemmologie a.f.g.*, No. 175, 2011, pp. 6–7 [in French].

Samples of irradiated green diamonds were heated from 300°C to 1100°C in 50° increments to observe changes in their infrared spectra. H1a, H1b, and H1c absorptions were

detected, as well as a previously undocumented triplet at 6139, 6070, and 6021 cm⁻¹. The triplet, which starts to appear at 1000°C, occurs mainly in type IaAB diamonds but also in some type IaB diamonds. The feature seems to be associated with B aggregates.   *GL*

MISCELLANEOUS

2010: Year of replenishment, speculation and recycling. C. Even-Zohar, *Idex*, Vol. 26, No. 253, 2011, pp. 65–73.

In the author's annual assessment of the diamond pipeline, 2010 was characterized by three factors: replenishment of rough supply, recycling of polished goods, and the return of diamond speculation. Due to the global economic downturn, 2009 saw the most severe financial contraction since World War II. But the trade managed it well and avoided major bankruptcies. After the supply of rough into the pipeline fell by about 50% in 2009, 2010 was a year to restock, even if consumer demand had not yet returned. Estimates for 2010 rough production were set at 125–130 million carats, valued at US$11.8–$12.2 billion. That production figure was up from 2009 but still considerably down from the 160–165 million carats produced in 2008. With a widening supply-demand deficit, rough prices rose accordingly. Meanwhile, many looked for alternatives to rough.

The year saw extensive recycling of previously owned polished diamonds back into the markets, especially from the U.S. into India. The author estimates that a global total of 5.2 billion carats of diamonds have been mined, worth about US$0.9–1.2 trillion in polished prices today, and up to half of that is in American hands. He quotes sources as using a widely accepted recycling price of 80% below Rapaport. Global recycling has become an important part of the trade, estimated to be worth US$6 billion in 2010.

The use of diamonds as an investment vehicle is once again becoming a factor, mainly because of expected supply shortages.   *EJ*

Blood diamonds: International policy options for conflict resolution. S. Lahiri [lahiri@siu.edy], *Indian Growth and Development Review*, Vol. 2, No. 1, 2010, pp. 5–20, http://dx.doi.org/10.1108/17538251011035846.

The article develops a model, based on recent hostilities, of how revenues from conflict diamonds, foreign aid, and arms sales to warring nations make such conflicts worse—especially as foreign aid goes toward recruiting soldiers and buying arms. The paper employs mathematical formulas to model how controlling these factors could affect potential conflicts. The author concludes that taxing arms shipments and limiting them by international agreement are the most effective means of reducing the severity of conflicts.   *RS*

Diamonds without borders: An assessment of the challenges of implementing and enforcing the KP Certification Scheme. Partnership Africa Canada, November 2010, www.pacweb.org/documents/ diamonds_kp/diamonds_without_borders-nov2010_ eng.pdf.

Diamonds are notoriously easy to smuggle. Israel, as chair of the Kimberley Process Certification System (KPCS) in 2010, recognized the importance of strengthening efforts to combat diamond smuggling. This report by Partnership Africa Canada, presented to the KPCS Plenary in November 2010, details the work done by Israel, Canada, and the U.S. to conduct multi-stakeholder consultations in four West African countries: Guinea, Ivory Coast, Sierra Leone, and Liberia.

Multilateral solutions were put forward such as collaboration between officials from key importing and exporting countries, and mechanisms for greater information sharing. Also emphasized were national solutions such as addressing the low prices offered to artisanal miners, which fuels the incentive to smuggle. Increased governance, including gathering of meaningful production data and the use of law enforcement to bring smugglers to justice, was also suggested.   *EJ*

Environmental stewardship in gemstone mining: Quo vadis? L. Cartier [laurent.cartier@unibas.ch], *InColor*, No. 15, Fall/Winter 2010, pp. 12–19.

This article explores some of the complex relationships between gems and the environmental ecologies from which they are extracted. Although a number of large and medium-scale companies are involved in colored stone mining, artisanal miners represent 80% of the extraction efforts. Protecting vulnerable ecologies is difficult when artisanal miners do not share the same sense of environmental responsibility as the local people who depend on the viability of the land. Just as often, regulation and other government support for sustainability is limited or nonexistent.

The author argues that all gem industry stakeholders, including government agencies and consumers, must examine and assume responsibility for the social, economic, regulatory, and environmental interrelationships that constitute a sustainable approach to gem extraction. The core sustainability question is this: Has the extraction left a viable physical and social environment that can support livelihoods in the long term once mining has ceased?

The author provides an excellent table summarizing major environmental challenges associated with gem mining. He specifies six domains (water, soil, air, flora/fauna, human, and landscape), with 18 potential

long-term consequences of mining and, most importantly, mitigation strategies. The article also discusses some of the cultural, economic, and institutional variables that undergird the continued lack of progress.

Twelve general recommendations to support responsible environmental stewardship and sustainability are offered. These include realistic, cost-effective regulatory mechanisms adapted to local realities, training, incentives, and practical assistance in cleaner production methods and the reclamation of mining sites.

ERB

Gemstone mining as a development cluster: A study of Brazil's emerald mines. J. Puppim de Oliveira and S. Ali [japo3@yahoo.com], *Resources Policy*, Vol. 36, No. 2, 2010, pp. 132–141, http://dx.doi.org/10.1016/j.resourpol.2010.10.002.

Using the concept of *clusters* and social upgrading, the authors employ the case study method to analyze six municipalities within the three most important emerald producing regions in Brazil (the states of Goias, Minas Gerais, and Bahia), in order to understand the numerous social, economic, and policy dynamics of emerald mining and its impact on local development. In this context, *clusters* are small agglomerations of economic agents working in one specific sector in one region.

Most of the value-added economic benefits of emerald mining have accrued to the top of the production chain, which generally lies outside the mining region. In fact, some specialists estimate that less than 5% of the retail price of a good emerald remains at the local level. Because most added value arises elsewhere, the local tax revenue from mining is also small. Thus, the economic benefits of emerald mining to local communities are minimal.

In many cases the mining activities also have caused significant negative social impacts: increased strain on public services and resources, greater crime, and health and safety problems. The working conditions for miners are notoriously poor: long hours, low wages, and dangerous mine conditions such as poor ventilation and extreme heat. Workers also have, at best, informal contracts and no benefits. The environmental impacts include deforestation, erosion, and soil and water pollution due, in large part, to a lack of appropriate controls and technology.

Small-scale emerald mining may potentially create favorable conditions conducive to longer-term development. Better cluster governance could harness the benefits of scale and collective efficiency to overcome the main obstacles to social development by upgrading through markets, ethical concerns, and thoughtful regulation.

ERB

The geoheritage significance of crystals. M. Brocx, [geoheritage@iinet.net.au] and V. Semeniuk, *Geology Today*, Vol. 26, No. 6, 2010, pp. 216–225, http://dx.doi.org/10.1111/j.1365-2451.2010.00773.x.

The earth can be considered a crystalline planet, with thousands of ubiquitous mineral varieties occurring in diverse geologic environments. Like larger geologic formations, these crystals are significant for deciphering Earth history. This article discusses how specific crystals are of geoheritage significance.

The principles of geoconservation and geoheritage as applied to geologic sites are reviewed in detail. The article also suggests that some crystals, because of their distinctive attributes (size, rarity, inclusions, etc.) or locality should be afforded geoheritage status, worthy of protection through geoconservation. Eight of the 15 significant geologic phenomena used to identify geoheritage and geoconservation significance apply to crystals and minerals. The authors illustrate a range of internal features (e.g., various types of zoning and inclusions) and nine crystal settings and features (e.g., veins, geodes, euhedrality, large cavities, and caves). These, and other dimensions such as arrangement of crystals (e.g., aggregations), occurrence of unique and unusual features (e.g., largest or best formed of its kind), and cultural value justify that crystals can be an important basic component in a given region for understanding the larger history of the earth, and thus are significant for geoheritage and geoconservation.

An extensive table of notable crystal and mineral sites worldwide and their significance is provided. It includes amethyst-bearing geodes, large well-formed dravite and elbaite tourmalines, large gypsum crystals in Mexico and Spain, zircon crystals from Jack Hills in Australia (the oldest crystals on Earth), well-formed pyrite in Spain, and outstanding Iceland spar (transparent calcite).

ERB

The Tucson mineral show and the market for collector minerals: The potential for artisanal and small scale miners. B. Ross [brad.ross@riotintocom], S. Dessureault, and M. Rieber, *Resources Policy*, Vol. 36, No. 2, 2011, pp. 168–177, http://dx.doi.org/10.1016/j.resourpol.2010.11.001.

During the first two weeks of February, the city of Tucson in Arizona hosts 43 gem and mineral shows, making it the largest event of its kind in the world. Six of these shows specialize primarily in collector minerals. This article focuses on the potential for artisanal and small-scale miners to compete in the collector market. The principal challenges facing them are capital requirements and intense competition. Because of these barriers, and the way the shows are managed and organized, participation is difficult or impossible for the miners. With the support of government policy makers and NGOs, alternative solutions—including the creation of a separate venue in Tucson solely for artisanal and small-scale miners—may help these individuals find success in this lucrative market.
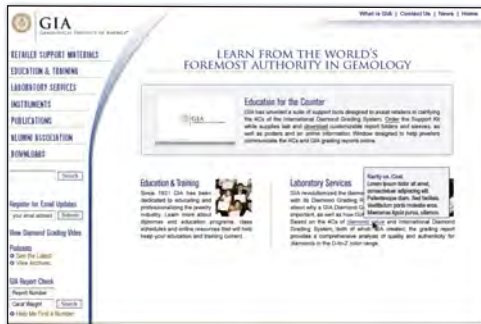
MK

BECAUSE PUBLIC EDUCATION
HAPPENS AT THE COUNTER.

GIA's RETAILER SUPPORT KIT AND WEBSITE

A $97.00 value, shipping and handling extra.

GIA's Retailer Support Kit has been developed to help sales associates educate the public about diamonds, the 4Cs, and thoroughly explain a GIA grading report. Take full advantage of all that GIA has to offer by visiting www.retailer.gia.edu

To order your FREE kit, log on to www.retailer.gia.edu

GIA®

GGW110